

A STUDY OF A SERVOVALVE CONTROLLED  
HYDRAULIC RADIAL BALL PISTON MOTOR

Alfredo Ivan Goitia Parra

A Thesis  
in  
The Faculty  
of  
Engineering.

Presented in Partial Fulfillment of the Requirements  
for the Degree of Master of Engineering at  
Concordia University  
Montréal, Québec, CANADA

December 1983

© Alfredo I. Goitia Parra, 1983.

To my mother  
Rosa

to my wife  
Daisy

and to my children  
Javier, Patricia and Eduardo

- 1 -

ABSTRACT

A STUDY OF A SERVOVALVE CONTROLLED  
HYDRAULIC RADIAL BALL PISTON MOTOR

Alfredo I. Goitia

This thesis presents a study of an electrohydraulic servovalve controlled radial ball piston motor. The design and construction of a closed-loop force servo system is described as a particular application.

The two main components of the system are: a two-stage electrohydraulic servovalve with an external electronic spool position feedback, and a fixed displacement, radial ball piston type motor.

The study of the system was carried out using a general purpose test stand specially designed, as part of the project, for testing hydraulic motors. Suitable instrumentation and drive circuits were selected.

For the evaluation of system performance, a number of steady-state and dynamic tests were programmed.

Steady-state tests allowed evaluation of important characteristics of the servovalve and motor including dead

zone of the valve-motor combination, motor leakage, motor viscous coefficient of friction, and motor static friction. The behaviour of the motor under a variety of loading conditions was also analysed.

Dynamic tests, which included step response of the system in an open-loop configuration, demonstrated the validity of a second-order model for the servovalve motor combination.

The effects of the servovalve external electronic feedback on system performance were evaluated using a closed-loop force servo system.



ACKNOWLEDGEMENT

The author wishes to express his gratitude and deep appreciation to his thesis supervisors, Dr. M. McKinnon and Dr. J. Svoboda, for their support, patient explanations and continuous guidance throughout this work.

The author appreciates the cooperation of CAE Electronics Ltd., the Fluid Power Control Research Laboratory of Concordia University and the technical assistance given. The cooperation received from Mr. W. Fitch and Mr. S. Lashier is very much appreciated.

Special thanks go to Mr. E. Prado, Mr. W. Blach and Mr. N. Krouglicof. Their help throughout this research was really invaluable.

The author would also like to thank Mr. O. Salazar and Mr. M.I. Garcia for their help, particularly for preparing the final drawings. Thanks also to Lina Palazzo, who typed the final copy.

Finally, the author wishes to express his gratitude to the Government of Venezuela ("Fundacion Gran Mariscal de Ayacucho") and the school of Mechanical Engineering at Universidad del Zulia for providing him with the necessary financial support to make this effort possible.

## TABLE OF CONTENTS

	PAGE
ABSTRACT.....	i
ACKNOWLEDGEMENTS.....	iii
LIST OF FIGURES.....	vii
LIST OF TABLES.....	xiii
NOMENCLATURE.....	xiv
CHAPTER 1 INTRODUCTION	
1.1 General.....	1
1.2 Scope of the Research Work.....	7
CHAPTER 2 DESCRIPTION OF SYSTEM COMPONENTS	
2.1 Introduction.....	11
2.2 Radial Ball Piston Motor	
2.2.1 General.....	12
2.2.2 Internal Configuration.....	21
2.2.3 Advantages of Ball Piston Units.....	24
2.2.4 Limitations of Ball Piston Units.....	28
2.3 The Electrohydraulic Servovalve	
2.3.1 Servovalve Components.....	29
2.3.2 Performance Characteristics	
2.3.2.1 Steady-State Characteristics.....	43
2.3.2.2 Dynamic Characteristics.....	47
2.4 Feedback Elements	
2.4.1 Torque Sensor.....	53
2.4.2 Differential Amplifier.....	57
2.4.3 LVDT Signal Conditioning Module.....	60
2.5 The Servocontroller.....	62
2.6 Load System	
2.6.1 Elements of the Load Torque.....	67
2.6.2 Analysis of the Loading System.....	72
CHAPTER 3 DEVELOPMENT OF EXPERIMENTAL TEST STAND	
3.1 Introduction.....	79
3.2 Test Stand Design Stage.....	87
3.3 Test Stand Assembly and Tune-Up.....	90
3.4 Test Stand for Steady-State and Dynamic Characteristics.....	93
Chapter 4 MODELLING OF A VALVE CONTROLLED MOTOR, SIMULATION OF THE OPEN-LOOP VELOCITY TRANSIENT RESPONSE	
4.1 General.....	97
4.2 Development of the Model.....	101

	4.2.1	Input Reference Signal.....	102
	4.2.2	Electrohydraulic Servovalve.....	102
	4.2.3	Conduits.....	104
	4.2.4	Hydraulic Motor.....	105
	4.2.5	Load.....	106
	4.3	MIMIC Model.....	107
	4.4	Simulation vs Experimental Results.....	107
CHAPTER	5	SERVOVALVE - MOTOR PERFORMANCE: STEADY-STATE CHARACTERISTICS	
	5.1	General.....	111
	5.2	Unloaded Valve-Motor Characteristics	
	5.2.1	Motor Shaft Angular Velocity versus Servovalve Current Characteristics...	116
	5.2.2	Viscous Damping Coefficient.....	120
	5.3	Hydraulic Motor Friction Torque.....	122
	5.4	Loaded Valve-Motor Characteristics	
	5.4.1	Angular Velocity of the Motor Shaft versus Motor Torque Characteristics..	124
	5.4.2	Angular Velocity of the Motor Shaft versus Servovalve Current Characteristics.....	126
	5.5	Summary and Discussion of Results.....	129
CHAPTER	6	SERVOVALVE-MOTOR PERFORMANCE: DYNAMIC CHARACTERISTICS	
	6.1	General.....	131
	6.2	Theoretical Analysis of Valve Controlled Motor.....	132
	6.3	Transient Response Tests.....	141
	6.4	Frequency Response Tests.....	148
	6.5	Summary and Discussion of Results.....	154
CHAPTER	7	DESIGN OF CLOSED-LOOP FORCE SERVO SYSTEM	
	7.1	Introduction.....	157
	7.2	Experimental Set-Up.....	157
	7.3	Theoretical Analysis and Block Diagram of the System.....	159
	7.4	Performance Characteristics of the System	
	7.4.1	Motor Torque versus Motor Pressure Drop Characteristics.....	165
	7.4.2	Transient Response of the System.....	168
	7.4.3	Closed loop Frequency Response of the System.....	170
	7.4.4	Effects of Servovalve Dither on Amplitude Response.....	172

	7.4.5	Effects of the Servovalve Linear Variable Differential Transformer on the System Performance Characteristics	179
	7.5	Summary and Discussion of Results.....	185
CHAPTER	8	CONCLUSIONS AND RECOMMENDATIONS.....	186
REFERENCES AND BIBLIOGRAPHY.....			191
APPENDIX	A	PEGASUS SERVOVALVE	
	A1.	Servovalve Coefficients.....	199
	A2.	Servovalve Transfer Function.....	202
	A3.	Servovalve Assembly Drawing.....	206
APPENDIX	B	MIMIC MODEL OF THE OPEN-LOOP SERVOVALVE CONTROLLED MOTOR.....	209
APPENDIX	C	AUXILIARY EQUIPMENT DESCRIPTION AND CALIBRATIONS.....	219

## LIST OF FIGURES

FIGURE		PAGE
2.1.	Schematic Diagram of the Servo Motor Circuit.....	11
2.2.	Typical Hydraulic Motors:(a)External Gear Motor, (b)Internal Piston Motor, (c)Vane Motor, (d)Radial Piston Motor, (e)Bent-Axis Piston Motor, (f)In-Line Piston Motor..... (Source: Klein, Edmund:"Hydraulic Motors").	18
2.3.	The Hydraulic Motor and its Internal Parts. (Source: Planet-Hydraulic Motors.).....	23
2.4.	Basic Ball Piston Motor.....	25
2.5.	Conventional Piston Motor.....	25
2.6.	Ball Piston Hydraulic Motor.....	26
2.7.	Pegasus Servo Valve - Sectional View (Source: Pegasus Servo Valve, Two Stage Series).....	30
2.8.	Electrical Torque Motor - Schematic Diagram (Source: Pegasus Servo Valve, Two Stage Series).....	31
2.9.	Hydraulic Amplifier - Steady State with Spool on Center. (Source: Pegasus Servo Valve, Two Stage Series).....	33
2.10.	Hydraulic Amplifier - Transient (Source: Pegasus Servo Valve, Two Stage Series).....	34
2.11.	Hydraulic Amplifier - Steady State with Spool off Center (Source: Pegasus Servo Valve, Two Stage Series).....	34
2.12.	Four Way Spool Valve - On Center (Source: Pegasus Servo Valve, Two Stage Series).....	35
2.13.	Four Way Spool Valve - Flow Out C2 (Source: Pegasus Servo Valve, Two Stage Series).....	36
2.14.	Four Way Spool Valve - Flow Out C1 (Source: Pegasus Servo Valve, Two Stage Series).....	37
2.15.	Three-Stage Servo Valve. (Source: Trends in Control Components, M. Nalecz - Editor).....	38

2.16.	LVDT Schematic and Circuit Diagram. (Source: Doebelin, Ernest: "Measurement System").....	40
2.17.	Demodulation and Filtering Stages - Schematic Diagram. (Source: Doebelin, Ernest: "Measurement System").....	41
2.18.	LVDT and its Auxiliary Equipment - Schematic Diagram.....	42
2.19.	Servo valve Flow Curve.....	44
2.20.	Experimental Set-Up for the Pressure Gain Curve....	45
2.21.	Servo valve Control Ports Blocked Pressure Sensitivity Curve.....	46
2.22.	Frequency Response for Pegasus Servo valve, Model 130AA - Experimental Values.....	49
2.23.	Torque Transducer with Built-In Slip Rings.....	55
2.24.	Torque Sensor Calibration Curve.....	56
2.25.	Differential Amplifier - Simplified Schematic.....	57
2.26.	Differential Amplifier External Connections.....	59
2.27.	LVDT Signal Conditioning Module - Actual Hardware..	60
2.28.	LVDT Signal Conditioning Module Wiring Diagram.....	61
2.29.	LVDT Output versus Servo valve Current.....	62
2.30.	Servo Control Circuit - Electronic Diagram.....	64
2.31.	Servo controller Steady-State Characteristics.....	65
2.32.	Servo controller Frequency Response. Open Loop.....	66
2.33.	Sectional View of the Steel Disc.....	67
2.34.	Schematic of Loading System.....	68
2.35.	Load Pump Sectional View.....	69
2.36.	Sectional View of MOOG Servo valve.....	70
2.37.	Flow Curve Characteristics - MOOG Servo valve.....	71

2.38.	Typical Frequency Response - MOOG ServoValve.....	71
2.39.	Block Diagram for the Load System.....	77
3.1.	Side View of Experimental Test Stand (Complete)....	81
3.2.	Top View of Experimental Test Stand (Complete).....	82
3.3.	Block Diagram of the Experimental Test Stand.....	84
3.4.	Hydraulic System Schematic Diagram.....	86
3.5.	Equipment for Balancing Inertial Masses and Transmission Shaft.....	92
3.6.	Experimental Test Stand Schematic Steady-State Characteristics - No Load.....	94
3.7.	Experimental Test Stand Schematic. Steady-State Characteristics - Load Applied.....	95
3.8.	Experimental Test Stand Schematic. Dynamic Characteristics - Inertial Load.....	96
4.1.	Simplified System Diagram for Modelling Purposes...	101
4.2.	Underlapped Spool Valve.....	103
4.3.	Velocity Transient Response for Step Functions of 18 mA and 24 mA. Experimental and Theoretical Results.....	108
4.4.	Velocity Transient Response for Step Function of 24 mA. Experimental and Theoretical Results.....	109
4.5.	Pressure Transients on the Motor Pressure Line for the same Inertial Load. Experimental and Theoretical Results.....	110
5.1.	Simplified Experimental Set-Up for Determining Steady-State Characteristics.....	113
5.2.	Unloaded Motor Speed/ServoValve Current Characteristics.....	118
5.3.	Unloaded Motor Speed/ServoValve Current Characteristics - Hysteresis Region Amplified.....	119
5.4.	Unloaded Pressure Diff. across the Motor versus Motor Speed Characteristics.....	121

5.5.	Motor Torque versus Motor Pressure Drop-Shaft Locked.....	122
5.6.	Unloaded Motor Speed/Servo valve Current Characteristics. Motor Employed to Determine the Loaded Valve - Motor Characteristics.....	124
5.7.	Motor Speed/Motor Torque Characteristics for Several Values of Servo valve Current.....	127
5.8.	Loaded Motor Speed/Servo valve Current Characteristics.....	128
6.1.	Block Diagram of Set-Up to Obtain Dynamic Characteristics of the Valve Controlled Motor.....	132
6.2.	Valve - Motor Combination.....	132
6.3.	Block Diagram for $X_v$ , $m$ , and $P_L$ .....	138
6.4.	Valve Controlled Motor Block Diagram.....	139
6.5.	Experimental Transient Motor Velocity Response of the System for Several Current Levels.....	144
6.6.	Pressure Transients on the Motor Pressure Line as Several Motor Inertia Loads are Used.....	145
6.7.	Experimental Transient Velocity Response of the System for Various Motor Inertia Loads.....	146
6.8.	Pressure Transient on the Motor Line as the Hydraulic Motor is Suddenly Stopped.....	147
6.9.	Frequency Response Tests - Servo valve Current Amplitude About Null Variable.....	150
6.10.	Frequency Response Tests - Inertia Load Variable...	151
6.11.	Frequency Response Tests - Flexible Hoses and Rigid Piping Used.....	152
6.12.	Frequency Response Tests - Amplitude Ratio of Theoretical and Experimental Results.....	153
6.13.	A Linear Actuator Filled with Liquid under Compression.....	156
7.1.	Experimental Apparatus.....	158



7.2.	Block Diagram of the Force Servo System.....	163
7.3.	Motor Torque versus Motor Pressure Drop - Motor Shaft Locked - Four Different Motor Shaft Positions.....	167
7.4.	Closed-Loop Force Servo System Transient Response - System: Stable.....	169
7.5.	Closed-Loop Force Servo System Transient Response - System: Unstable.....	169
7.6.	Force Servo System Closed-Loop Frequency Response Plot.....	171
7.7.	Output Waveform for the Closed-Loop Force Servo System at an Input Frequency Signal of 0.1 Hz. (a) No Dither Used, (b) Servo- Valve Dither Added to the System.....	174
7.8	Output Waveform for the Closed-Loop Force Servo System at an Input Frequency Signal of 4.0 Hz. (a) No Dither Used, (b) Dither Added to the System.....	175
7.9.	Effects of the Servovalve Dither on the Amplitude Response. Reference Signal Equal to +7.7 lb .....	177
7.10.	Effects of the Servovalve Dither on the Amplitude Response. Reference Signal Equal to +3.3 lb .....	178
7.11.	Block Diagram of the Force Servo System with a Secondary Feedback.....	179
7.12.	Simplified Block Diagram.....	180
7.13.	Effects of Servovalve LVDT on the Amplitude Response - Theoretical Results.....	182
7.14.	Effects of Servovalve LVDT on the Amplitude Response - Experimental Results.....	184
A1.	Servovalve Frequency Response with First and Second - Order Transfer Function Fits. (a) First Order Fit, (b) Second Order Fit.....	207
A2.	Servovalve Assembly Drawing.....	208

B1.	Motor Speed Transient Response for a Current Step Function of 18 mA and Inertial Mass of 0.003 N-m-sec <sup>2</sup> .....	213
B2.	Pressure Transient of the Motor Chambers for a Current Step Function of 18 mA and Inertial Mass of 0.003 N-m-sec <sup>2</sup> .....	214
B3.	Motor Speed Transient Response for a Current Step Function of 24 mA and Inertial Mass of 0.003 N-m-sec <sup>2</sup> .....	215
B4.	Pressure Transient of the Motor Chambers for a Current Step Function of 24 mA and Inertial Mass of 0.003 N-m-sec <sup>2</sup> .....	216
B5.	Motor Speed Transient Response for a Current Step Function of 24 mA and Inertial Mass of 0.03247 N-m-sec <sup>2</sup> .....	217
B6.	Pressure Transient of the Motor Chambers for a Current Step Function of 24 mA and Inertial Mass of 0.03247 N-m-sec <sup>2</sup> .....	218
C1.	Tachometer Calibration Curve.....	221
C2.	Differential Pressure Transducer.....	222
C3.	Pressure Transducer Indicator.....	224
C4.	Differential Pressure Transducer Calibration Curve.....	225
C5.	Force Cell and its Electrical Diagram.....	226
C6.	Force Cell Calibration Curve.....	228

LIST OF TABLES

TABLE		PAGE
1.1.	Salient Features of the Power Transmission Systems (Source: McCloy and Martin: "The Control of Fluid Power").....	4
2.1.	Comparison Chart for Gear, Vane, and Piston Motors. (Source: Klein, Edmund: "Hydraulic Motors").....	19
2.2.	Technical Specifications. Fixed-Displacement Hydraulic Ball Piston Motor. Model MF47-Type 241.....	24
2.3.	Pegasus Servo Valve Performance Characteristics.....	53
2.4.	Torque Sensor Specifications.....	55
2.5.	Differential Amplifier Specifications.....	59
2.6.	Load Pump Specifications.....	69
2.7.	Load Servo Valve Specifications.....	70
3.1.	Hydraulic Power Unit Specifications.....	86

## NOMENCLATURE

$B_m$	=	viscous damping coefficient, N-m-s
$B_p$	=	internal damping coefficient of the pump, N-m-s
$b$	=	distance between the center of the motor shaft and load cell, m
$C_d$	=	discharge coefficient
$C_l$	=	motor leakage coefficient, $(m^3/s)/(N/m^2)$
$C_{lp}$	=	internal leakage coefficient of the pump, $(m^3/s)/(N/m^2)$
$C_{TF}$	=	internal friction coefficient of motor, $m^3$
$D_m$	=	hydraulic motor displacement, $m^3/\text{rad}$
$D_p$	=	pump displacement, $m^3/\text{rad}$
$D_s$	=	spool diameter, m
$E_o$	=	differential amplifier output, mV
$F$	=	force exerted on the load cell, N
$F_i$	=	force input, N
$F_o$	=	force output, N
$I$	=	servo valve current, mA
$I_R$	=	input reference signal, mA
$J_L$	=	total inertia of motor and load, $N\text{-m}\cdot\text{s}^2$
$K_A$	=	servocontroller gain
$K_C$	=	flow-pressure gain coefficient of main servo valve $(m^3/s)/(N/m^2)$
$K_{C,1}$	=	valve flow - pressure gain coefficient, $(m^3/s)/(N/m^2)$
$K_{DA}$	=	differential amplifier gain
$K_f$	=	slope of the force cell calibration curve, mV/N
$K_L$	=	LVDT and LVDT signal conditioning module gain
$K_p$	=	servo valve pressure coefficient, $N/m^2/\text{mA}$
$K_{px}$	=	servo valve pressure/spool displacement coefficient, $N/m^2/\text{m}$

- $K_Q$  = flow gain coefficient of main servovalve,  $m^3/s/mA$
- $K_q$  = flow gain coefficient of main servovalve,  $m^3/s/m$
- $K_{q,1}$  = valve flow gain coefficient,  $m^3/s/m$
- $K_x$  = servovalve spool displacement gain,  $m/mA$
- $P_L$  = pressure drop across the load,  $N/m^2$
- $P_0$  = return line pressure,  $N/m^2$
- $P_p$  = pressure difference across the pump,  $N/m^2$
- $P_s$  = supply pressure,  $N/m^2$
- $P_1$  = motor forward pressure,  $N/m^2$
- $P_{10}$  = servovalve port 1 pressure for  $t=0.s$ ,  $N/m^2$
- $P_2$  = motor return pressure,  $N/m^2$
- $P_{20}$  = servovalve port 2 pressure for  $t=0.s$ ,  $N/m^2$
- $Q_a, Q_b$  = volumetric flows through the servovalve,  $m^3/s$
- $Q_c, Q_d$  = volumetric flows through the servovalve,  $m^3/s$
- $Q_l$  = leakage flow,  $m^3/s$
- $Q_m$  = flow through the motor,  $m^3/s$
- $Q_p$  = flow through the pump,  $m^3/s$
- $Q_v$  = flow rate through main servovalve,  $m^3/s$
- $Q_{v,1}$  = flow of servovalve,  $m^3/s$
- $Q_1, Q_2$  = flow through servovalve ports,  $m^3/s$
- $Q_L$  = load flow,  $m^3/s$
- $s$  = Laplace operator
- $T_L$  = arbitrary load torque on motor,  $N-m$
- $T_d$  = viscous friction torque of motor,  $N-m$
- $T_f$  = inertial friction torque of motor,  $N-m$

$T_m$	=	torque developed by motor, N-m
$T_p$	=	torque took up by pump; N-m
$t$	=	time, s
$V_1$	=	average contained volume of forward chamber, $m^3$
$V_2$	=	average contained volume of return chamber, $m^3$
$x_v$	=	spool displacement from neutral of main servovalve, m
$x_{v,1}$	=	spool displacement from neutral of load servovalve, m
$x_{vmax}$	=	maximum spool displacement from neutral of main servovalve, m
$x_{vo}$	=	servovalve underlap, m
$\beta_e$	=	effective bulk modulus of system, $N/m^2$
$\delta_h$	=	hydraulic damping ratio
$\xi$	=	damping ratio of main servovalve
$\rho$	=	oil density, $Kg/m^3$
$\tau_v$	=	main servovalve time constant, s
$\omega_h$	=	hydraulic undamped natural frequency, rad/s
$\omega_m$	=	motor angular velocity, rad/s
$\omega_{m0}$	=	motor angular velocity for $t=0.s$ , rad/s
$\omega_n$	=	natural frequency of main servovalve, rad/s

CHAPTER 1  
INTRODUCTION

1.1 General

The development of the present level of technology has depended on the evolution of methods for the generation, distribution and utilization of power.

The energy requirements of the domestic population and industrial sector as well as the development of the national defense in each country create an increasing demand for power. This, requires the continued development of methods for power transmission, control and utilization. Fluid power technology plays an important role in this task and promises to be even more important in the future.

The majority of contemporary power transmission systems can be classified as electrical, mechanical, or fluid systems. Fluid power systems can be further divided into pneumatic and hydraulic systems, depending on the fluid medium used to transmit force. The fluids employed in pneumatic power and control systems are gases which are characterized by high compressibility. In contrast, hydraulic fluids are relatively incompressible liquids.

Magnetic saturation, a fundamental limitation of electrical machines, limits the torque developed by an electric motor. Heat dissipation is a problem of frequent importance in electrical power transmission.

Mechanical power transmission systems employ a variety of kinematic mechanisms such as belts, chains, pulleys, gear trains, bar linkages, and cams. They are suitable for the transmission of motion and force over relatively short distances. The disadvantages of mechanical systems include lubrication problems, limited speed and torque control capabilities, and relatively large space requirements.

Pneumatic power is transmitted by the pressure and flow of compressed gases. The most commonly used gas is air. Pneumatic systems use simple equipment, have small transmission lines, and do not present a fire hazard. Disadvantages include a high fluid compressibility and a small power-to-size ratio of components. Pneumatic power systems are more elastic than mechanical systems and are very sensitive to small changes in pressure or flow. For this reason they are especially suited for pilot or control systems.



Hydraulic power is transmitted by the pressure and flow of liquids. Applications of fluid power have become virtually limitless. These include systems on machine tools, cars, earth moving and agricultural equipment, aircraft, ships, and many other areas [26].

Fluid power devices lie between electrical and mechanical power transmission devices, in respect to performance. Fluid and electrical power systems transmit power more easily over appreciable distances, compared with their mechanical counterparts. Electrical power devices are especially good in this respect at low power levels.

Table 1.1 shows a summary of the most important features of the various types of systems [26]. The final choice is a difficult one and is often influenced by the rest of the system.

One major advantage of fluid over electrical power is that the former is not so limited by physical limitations of materials. For example, the saturation limit of steel limits the performance of the electromagnet. This sort of limitation does not apply to hydraulic systems until the material strength is reached.

Property	Best	Good	Fair
Torque/inertia	H	P	M, EM
Power/weight	H, P	—	EM, M
Rigidity in steady state	H	M	F, P, EM
Friction	EM, F	H, M	P
Dirt vulnerability	E, EM, M	—	*H, F, P
Speed of response	E	F, H	P, M, EM
Compactness	E	F, H	P, M, EM
Ability to work in adverse conditions	F	P, M, H	EM, E
Relative cost	M, E, EM	H, P	F

Key: M—mechanical      EM electromechanical  
E—electronic      P —pneumatic  
F—fluidic      H —hydraulic

Table 1.1 Salient Features of the Power Transmission Systems  
(Source: McCloy and Martin: "The Control of Fluid Power")

On the other hand, fluid power devices have the following disadvantages:

- Impairment of system operation by contamination.
- Hydraulic fluid leakage.
- Fire hazard with flammable hydraulic fluids.
- Danger of burst pipes and components containing high pressure fluid, although small, is always present.

Hydraulic oils are messy if proper care is not observed.

To do work, oil flow and pressure must pass through an output device. Output devices carry the generic name of hydraulic actuators. An actuator is a device for converting hydraulic energy to mechanical energy. An actuator, or fluid motor, can be used to produce linear, rotary, or oscillatory motion.

A linear actuator or hydraulic cylinder is a fluid motor that generates linear motion. Various types are widely used in hydraulic systems because of their high force capability, ease of speed control, and high power output for a given size and weight. They are especially suitable for control systems due to their high mechanical stiffness and speed of response.

Limited-rotation motors provide an oscillating power output. A variety of such units is available, all of which consist of one or more fluid chambers and a movable surface against which fluid pressure is applied. Both vane and piston types can be used to obtain an oscillatory output.

A hydraulic motor is specified when the load must be continuously rotated, or where stroke length or accuracy requirements preclude the use of linear actuators [21]. As in linear actuators, several types of hydraulic motors are commonly employed in industrial applications.

In this research, a fixed-displacement, radial ball piston motor was chosen as the device which converts hydraulic energy into mechanical energy. A two-stage electro-hydraulic servovalve with an external electronic spool position feedback has been used to control the hydraulic motor.

Several concerns governed the choice of the hydraulic motor:

- (a) Electrohydraulic servoactuators, in general, are very expensive devices. A low-cost actuator was used in the attempt to improve system performance by using an electrohydraulic servovalve with electronic feedback.
- (b) Ball piston type motors are units with a low number of moving parts which implies easy maintenance, low wear, and high reliability.
- (c) Ball piston type motors have a low friction torque loss at starting. This feature is advantageous in applications such as robotics, automated manufacturing, and control loading.

This work is based on the study of an electrohydraulic servovalve controlled radial ball piston motor. The outline of the thesis presentation is as follows: Chapter 2 includes a detailed description of the main components which make up the servovalve controlled motor system as well as the load. The development of the experimental test stand is described in Chapter 3. The modelling of the valve controlled hydraulic motor and the digital simulation of the open-loop velocity transient response are covered in Chapter 4. Chapters 5 and 6 deal with Steady-State and Dynamic tests respectively. A particular application based on a closed-loop force servo in order to analyze the effects of the servovalve external electronic feedback on the system is presented in Chapter 7. Finally, conclusions and recommendations are presented in Chapter 8.

#### 1.2. Scope of the Research Work

The main objective of this investigation was to study the performance of an electrohydraulic servovalve controlled hydraulic motor. A two-stage electrohydraulic servovalve with external electronic spool position feedback was used to control a radial ball, fixed displacement hydraulic motor.

Experimental tests have been performed in order to derive the characteristics of the valve controlled motor. To do this, a complete test stand was designed and built so that all the steady-state and dynamic characteristics were obtained without difficulty. The design of the test stand was based on a torque feedback system which has the capability of regulating torque loading by the motor. The test stand was designed both to test the hydraulic motor used in this project, and also as a general purpose test stand suitable for testing other hydraulic motors.

A digital simulation using the MIMIC language was developed in order to select the current step size used for the dynamic tests and gain insight into the open-loop velocity transient response.

To investigate the effects of the servovalve external electronic feedback on the system, design and construction of a closed-loop force servo system was carried out. Such a system was composed of the valve-motor combination, a tension-compression load cell used as the main feedback, and the necessary electronic apparatus to carry out such an evaluation.

To accomplish the main objective outlined above, the following tasks were performed:

- (a) Selection of a fixed displacement, radial ball piston motor after reviewing commercially available alternatives.
- (b) Selection of a two-stage electrohydraulic servovalve according to the hydraulic motor technical specifications.
- (c) Design and construction of an experimental test stand to evaluate the servovalve and motor performance.
- (d) Selection of other components suitable for the valve motor system including pressure, velocity, torque and force transducers.
- (e) Selection and construction of suitable electronic circuits to obtain the required data. That includes servocontroller, LVDT's signal conditioning module, differential amplifier, differential pressure transducer indicator, XY-plotter, strip chart recorder, etc.
- (f) Preparation of a complete set of tests to investigate the performance of the servovalve controlled hydraulic motor.
- (g) Evaluation of system performance by carrying out tests on the system.

Valve controlled hydraulic servomechanisms are an important class of control systems because of their widespread use in fields requiring high performance and light weight. This work introduces the use of a two-stage electrohydraulic servovalve with external electronic spool position feedback to control a radial ball piston motor. Due to the advantages of that type of motor, such as light weight and low friction torque loss at starting, the combination of such a valve and motor can be used in applications where a minimal friction torque are required.



## CHAPTER 2

### DESCRIPTION OF SYSTEM COMPONENTS

#### 2.1 Introduction

The main elements used in the servovalve controlled motor circuit are: a two stage, four way, electrohydraulic servovalve; a fixed displacement, radial ball piston motor; and a torque transducer connected as shown in Fig. 2.1.

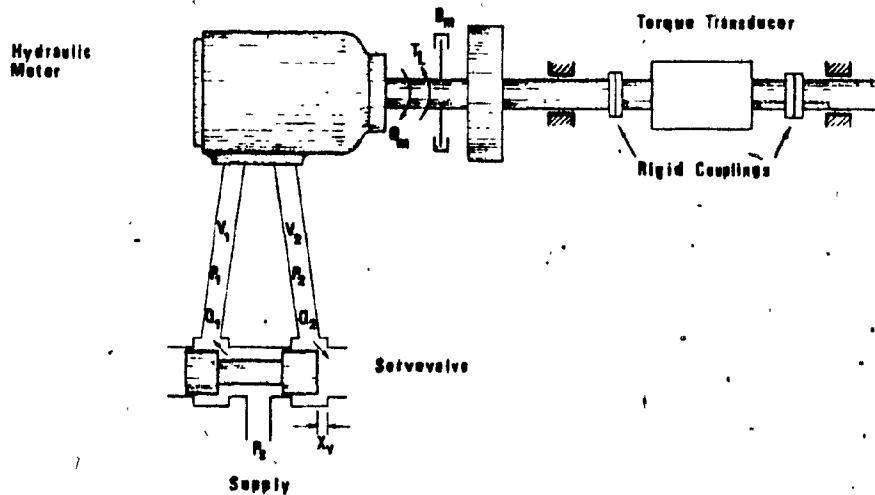


Fig. 2.1 Schematic Diagram of the Servo Motor Circuit.

In addition, a flywheel comprising a steel disc rigidly coupled to the motor shaft, and a hydraulic pump are used to provide load torque.

A controller was used for two purposes: to drive the servovalve coils in all the tests carried out, and as the control element. A proportional control mode was selected for simplicity.

Finally, a differential amplifier, an LVDT signal conditioning module, and other electronic apparatus were used to obtain the required data.

In the following pages, a detailed description of each one of these components is presented.

## 2.2. Radial Ball Piston Motor

### 2.2.1. General

A hydraulic motor converts energy transmitted through a fluid into continuous mechanical rotary motion and torque. Desirable features of rotary hydraulic motors include:

- (1) The ability to suddenly start, stop, and reverse in an easily controlled manner.
- (2) A higher horsepower-to-weight ratio than any other conventional power source.
- (3) The ability to accommodate contaminants in the fluid.

A brief description of several types of hydraulic motors commonly used in hydraulic systems follows:

(a) Gear Motors.

External gear motors, Fig. 2.2 (a) consist of a set of matched gears enclosed in a housing. Both gears have the same tooth form and are driven by fluid under pressure.

Fluid under pressure enters the housing on one side at a point where the gears mesh and causes the gears to rotate as the fluid takes the path of least resistance around the periphery of the housing. The fluid exits at the opposite side of the motor.

Internal gear motors can be divided into two groups: crescent seal and gerotor. The gerotor, Fig. 2.2 (b), consists of a pair of gear shaped elements ingeniously mated so that each tooth of the inner gear is always in sliding contact with the outer gear to form sealed pockets of fluid. Both gears rotate in the same direction at low relative speeds with the inner gear being faster. Fluid enters the chamber with increasing volume, is trapped in the spaces between the teeth, and is transported to the outlet. Frictional torques due to hydraulic unbalance restrict internal gear motors to low pressures (up to 1500 psi.). It

is not possible to vary the displacement of gear type motors.

(b) Vane motors are usually classified by the type of vane design: sliding vane, swinging vane, or rolling vane. The sliding vane machine, by far the most common design [27], Fig. 2.2 (c), has vanes which fit into slots in the rotor periphery and are held in contact with the housing by springs, centrifugal force, and/or pressure. A housing with a cam ring encloses the rotor and vanes. The inner surface of the cam ring is eccentric with respect to the rotor.

Fluid under pressure flowing to the inlet port of a vane motor is divided by internal coring and directed into chambers formed between the vanes. The fluid exerts the greatest force against the vanes extended the furthest, turning the output shaft of the motor.

The displacement of these devices can be varied by changing the rotor eccentricity, and operation is generally limited from low to medium working pressures (up to 1500 psi.) because of the basic hydrostatic unbalance.

Hydraulically balanced units are preferred for operation at higher pressures and are more efficient. The dis-

placement of hydraulically balanced machines is not variable.

Vane motors have good operating efficiencies, but not as high as those of piston motors. Vane motors generally cost less than piston motors with corresponding horsepowers.

(c) Piston motors are classified by the motion of the pistons relatively to the shaft axis as axial, bent-axis, or radial, as illustrated in Figs. 2.2 (d) to 2.2 (f).

Radial piston motors, Fig. 2.2 (d), have a cylinder barrel attached to a drive shaft, the barrel contains a number of pistons in radially oriented bores. The outer ends of the piston bear against a thrust ring held by a rotor.

The cylinder barrel is eccentric in the housing, and fluid from the pintle enters half of the cylinder barrel bores and forces the piston outward radially. However, the pistons can move radially only by revolving the cylinder barrel which then rotates the output shaft. The pistons ported by the pintle to the outlet move in a manner to decrease the chamber volume, thereby expelling fluid to the outlet.

This type of motor has a very high operating efficiency. These motors provide high torque at relatively low shaft speeds and excellent low speed operation with high efficiency, but they have limited high speed capabilities.

Axial piston motors also use reciprocating piston motion to drive the output shaft, but the motion is in the axial rather than the radial direction.

Operation of a bent-axis axial piston motor, Fig. 2.2 (e), is similar to that of a radial piston motor. Fluid under pressure flows through one of the ports in a valve plate into the bores of a cylinder block open to the port. The fluid under pressure on the pistons in these bores forces the pistons away from the valve plate. These pistons rotate the drive shaft as they move to the maximum distance from the valve plate because the piston axis is bent from that of the drive shaft. The cylinder block is driven through a universal joint shaft from the drive shaft. While some of the pistons are being driven, others are discharging flow.

An inline axial piston motor, Fig. 2.2 (f), works like a bent-axis type but differs in that the pistons reciprocate axially. Fluid under pressure entering the inlet passage into the cylinder block bores forces the

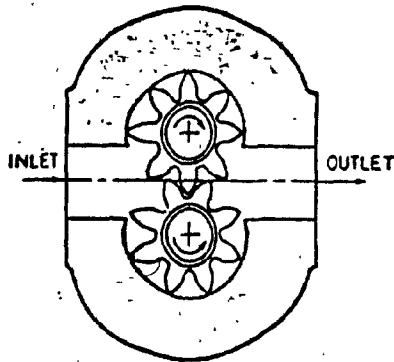
piston down the cam plate incline causing the cylinder barrel to rotate against a port plate and turn a drive shaft. As the cylinder barrel rotates, each bore in turn is exposed to the pressure inlet. Return fluid is expelled from the cylinder bores as the pistons move into the cylinder block.

Axial piston motors have high efficiencies and efficiency characteristics similar to radial piston motors. These motors cost more initially than vane or gear motors with the same horsepower. Axial piston motors have a long design life. Because of this, their higher initial cost may not truly reflect the expected life cycle operating cost [22].

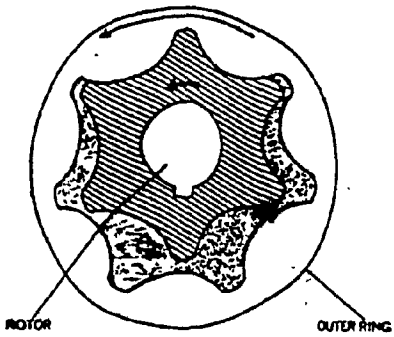
In general, axial piston motors have excellent high speed capabilities, but are difficult to control smoothly at low speed.

Of all the types of motors discussed, only the vane and piston units are capable of variable displacement.

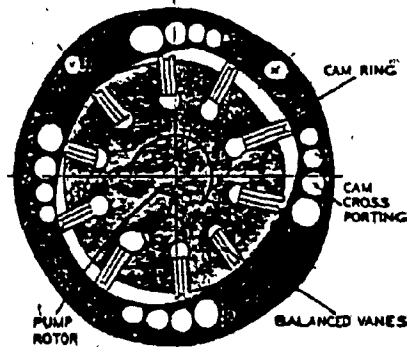
Table 2.1 presents a summary of the most important characteristics of the hydraulic motors discussed.



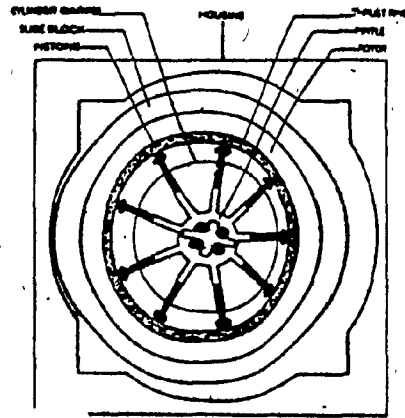
(a) External gear motors have one driving gear and one idler gear enclosed in a housing.



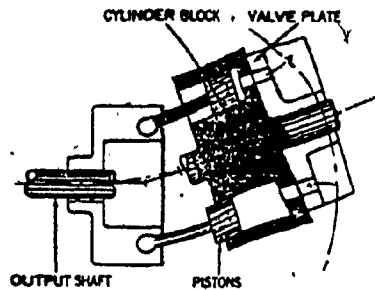
(b) Internal gear motors have a gerotor set, drive coupling, and a commutator valve, or plate.



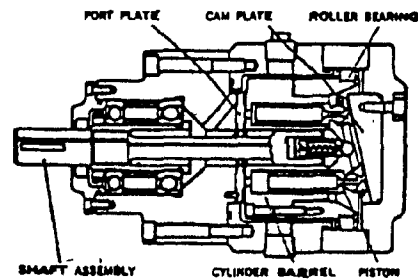
(c) Vane motors (balance type shown) have vanes in a slotted rotor mounted on a drive shaft.



(d) The pistons in radial piston motors reciprocate in a plane perpendicular to the output shaft.



(e) In bent axis, axial piston motor, pistons reciprocate in a plane parallel or inclined to output shaft.



(f) Inline axial piston motors work like a bent-axis type, but differ in that the pistons reciprocate axially.

Fig. 2.2. Typical Hydraulic Motors: (a)External Gear Motor, (b)Internal Gear Motor, (c)Vane Motor, (d)Radial Piston Motor, (e)Bent-Axis Piston Motor, (f)In-Line Piston Motor (Source: Klein, Edmund: "Hydraulic Motors" )




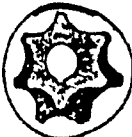
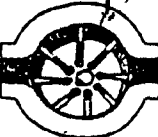

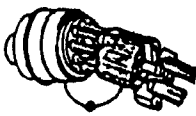
Specifications	 External Gear	 Internal Gear	 Vane	 Radial Piston	 Axial Piston
Overall Efficiency (%)	70-90	60-85	80-95	88-98	90-98
Rated Pressure (psi)	1500-3000	1000-1500	2000-3000	2000-3000	3000-5000
Rated Speed (rpm)	1200-3000	3000-4000	2000-3800	1200-2000	2000-4500
Mechanical Efficiency (%)	85-95	75-90	82-93	88-98	92-99
Displacement cu. in./rev.	2-20	1-8	2-20	To 1000	2-65
Applications	Low pressure systems Low efficiency systems			Hydraulic control systems High pressure systems High efficiency systems	

Table 2.1 Comparison Chart for Gear, Vane and Piston Motors.  
 (Source: Klein, Edmund: "Hydraulic Motors")

The use of standard ball bearing elements as pistons in hydraulic pumps and motors is a relatively old idea. It was not until 1953, however, that General Electric developed some small displacement high speed servo pumps using ball piston elements [14]. That was the first commercialization of such units. Before that, the idea of using such a method had met with relatively little success.

Hydraulic ball piston motors have been used in heavy mobile drive applications. In 1969 the Fluid Power Division of Eaton Corporation successfully commercialized two small hydrostatic transmissions using an internal pump and motor, both of the ball piston design [14].

Even though there is little available literature on hydraulic motors using ball pistons, and their use is not as popular as that of other hydraulic motors such as Gear, Vane, or Piston types, such a hydraulic motor was chosen for this project for design simplicity and a small number of parts which results in a low friction torque loss at starting. This type of motor is suitable in applications where a minimal friction torque is required, for instance: robotics, and force feel systems.

The motor used in this work is a PLANET hydraulic motor, Model MF47, reversible, ball piston type, fixed

displacement. The motor has 10 ball pistons uniformly distributed.

### 2.2.2. Internal Configuration

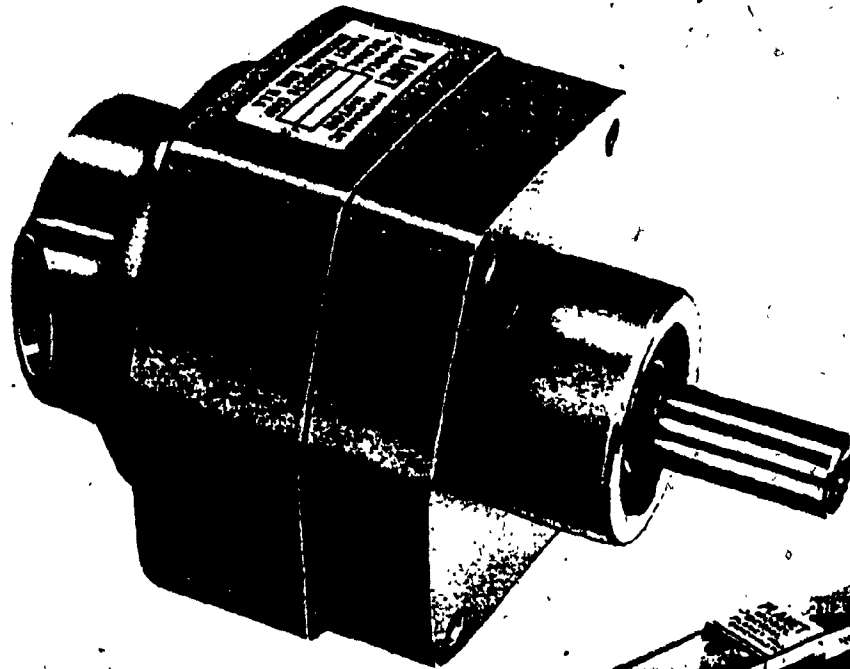
Three main functional parts make up the motor: (1) the pintle; (2) the rotor, with ball pistons; and (3) the anti-friction bearing.

(1) The Pintle provides the basic porting arrangement. It delivers fluid under pressure to the ball pistons from the motor housing pressure port, and permits return of the fluid to the motor housing return port. The pintle remains stationary with respect to the case.

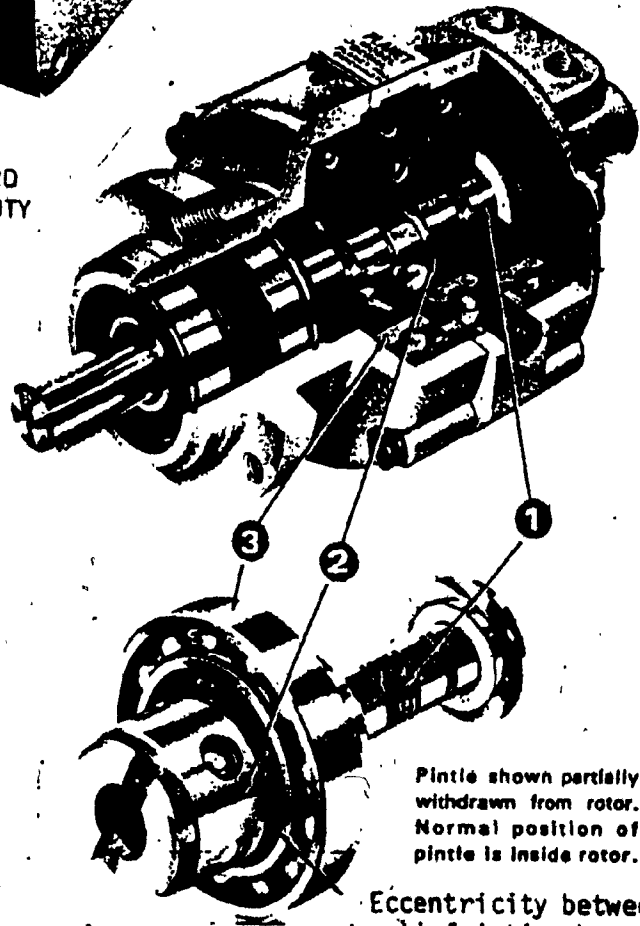
(2) The Rotor is the mechanism which converts force to torque. It is closely fitted to the pintle and contains accurately machined radial bores. Each bore holds a precisely sized ball which acts as a line contact piston in the bore.

(3) The Anti-Friction Bearing is positioned eccentric to the rotor and pintle and produces a reaction ring. This creates a displacement change in the cylinder chamber under the ball piston as the rotor revolves.

As mentioned previously, the anti-friction bearing is positioned eccentric to the motor shaft producing thus a reaction ring. Pressurized fluid from the pintle enters one half of the rotor bores and forces the piston outward radially. However, the piston can move radially only by revolving the rotor which then rotates the output shaft. The pistons ported by the pintle to the outlet move in a manner to decrease the chamber volume, thereby expelling fluid to the outlet. A sectional view of of the motor and its internal parts is shown in Fig. 2.3. Table 2.2 presents the specifications for the particular motor that has been used in this research. This model was chosen since its torque speed characteristics were compatible with typical applications in robotics or force-feel systems, and because the pressure-flow requirements were convenient for use with available test equipment.



FLANGE MOUNT  
TYPE 01-241 STANDARD  
TYPE 01-270 HEAVY DUTY



Pintle shown partially  
withdrawn from rotor.  
Normal position of  
pintle is inside rotor.

Eccentricity between  
anti-friction bearing  
and rotor.

Fig. 2.3. The Hydraulic Motor and its Internal Parts.  
(Source: PLANET-Hydraulic Motor.)

Table 2.2 Technical Specifications.  
Fixed -Displacement, Hydraulic Ball Piston Motor  
Model MF47-Type 241

Number of Pistons	10
Displacement	0.47 cu. in./rev.
Rotating Moment of Inertia	$24.5 \times 10^{-4} \text{ in.-lb-s}^2$
Torque	7 in. lbs/100 psi
Total Volume of Oil Under Compression	0.62 cu. in.
Rated Minimum Speed	5 rpm
Rated Maximum Speed	4000 rpm
Rated Pressure	1000 psi
Nominal Output at Rated Speed and Pressure	4.5 hp.
Breakaway Pressure with 1000 psi Servovalve Supply Pressure	40 psi
Flow Rate	0.20 gpm/100 rpm
External Leakage Rate @ 1000 psi	15 cu. in./min.
Hydraulic Oil	Premium Grade 75 to 300 SSU at 100°F
Maximum Operating Temperature	140°F
Degree of Filtration Recommended	10 microns

### 2.2.3. Advantages of Ball Piston Units

The ball piston motor combines the features of good hydraulic equipment design in a compact single package.

Hence, the motor is composed of less and smaller elements than a piston motor of the same rating. As a result a low moment of inertia can be maintained.

In ball piston motors, a steel ball is used as a piston. Fig. 2.4 shows such a ball which under pressurized fluid moves up against the cam rotating it. This scheme completely replaces the piston, crank shaft, wrist pin, connecting rod and associated bearing commonly found in positive displacement motors, Fig. 2.5. Expanding the basic principle of a ball piston motor, a multiple cylinder unit can be constructed as shown in Fig. 2.6.

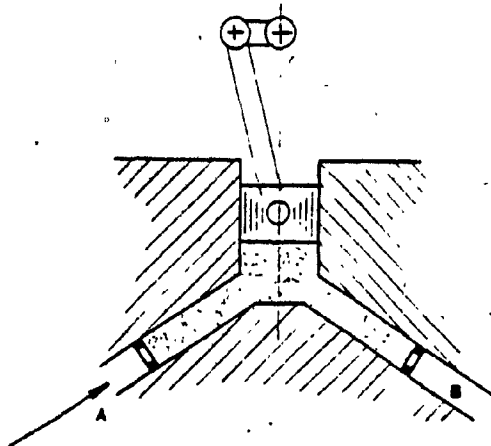
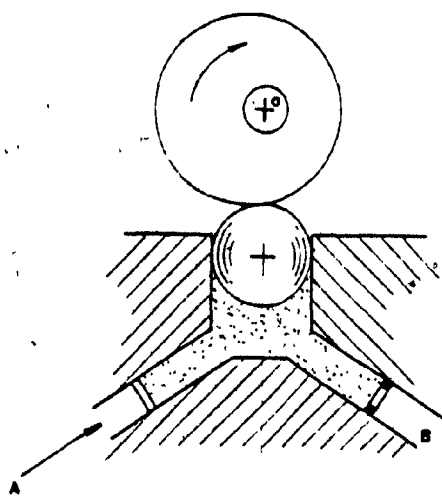


Fig. 2.4. Basic Ball Piston Motor      Fig. 2.5. Conventional Piston Motor

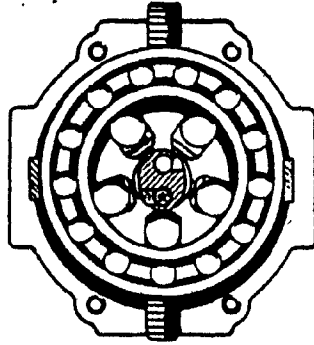


Fig. 2.6. Ball Piston Hydraulic Motor

The radial ball piston motor provides several desirable features, among them:

(a) Centrifugal force on the ball piston is sufficient to maintain contact between the ball and the race. In hydraulic motors it is necessary to have a mechanism for maintaining contact between the piston and the race. Thus, in vane motors of the sliding vane type, the vanes are held in contact with the housing by spring, centrifugal force/or pressure. For the motor which was used in this research project, the centrifugal force generated by the rotation of the motor acting on the ball piston is sufficient to maintain contact between the ball



and the race. For the motor stall position, there is no centrifugal force, however, the accuracy of the machined radial bores and the precision of the size of each ball ensure contact between the ball and the race.

(b) The stroking ring of the motor used in this work is the inner of an anti-friction bearing. In some types of motors, a profiled cam is employed as the mechanism to convert force to torque. This gives an advantage to the ball piston type motors, because a stroking ring is easier to machine than a profiled cam.

(c) The inertia of moving parts is small.

(d) Line contact between the ball and the race reduce the effective wear.

(e) The small volume of hydraulic fluid contained in the motor and cylinder chambers under the ball pistons makes a stiff system due to the limited compressibility of the fluid under pressure and thus ensuring a high resonant frequency of the motor and its inertia load.

Two other less significant advantages of ball piston units are:

(f) Radial ball piston motors do not require a mechanical piston to return the ball during the discharge cycle [14].

(g) The simple construction of the motor reduces cost.

#### 2.2.4. Limitations of Ball Piston Units

The above shows that ball piston units have design advantages; however, the problem of leakage between the ball piston and the bore wall is significant. The seal is only tangential, while with a plunger piston it extends over the length of the piston. Because of the high leakage, these units are of low volumetric efficiency; as a result, their operating pressure is also low.

Another point associated with fairly high leakage is the heat generated as the high pressure fluid passes through the small clearances around the ball. For sustained operation under high pressure, the temperature level of the complete hydraulic system may rise to such a height that external cooling may be required. Should the oil temperature exceed the operating value, the viscosity of the oil would then decrease, causing more leakage.

Oil leakage in motors is associated with the pressure drop across the motor. The total leakage through the motor can be computed by using the term  $Q_l = C_l P_L$

where  $C_l$  = leakage coefficient  
 $P_L$  = motor pressure drop.

However, the leakage characteristics in ball piston motors are also affected by the motor speed [25]. The speed effect on leakage is produced by the ball piston spinning or rotating in the bores as the rotor rotates.

### 2.3. The Electrohydraulic Servovalve

#### 2.3.1. Servovalve Components

Electrohydraulic flow control servovalves provide an output flow of hydraulic fluid proportional to an electrical input current. Hydraulic amplification feedback in a closed loop action is used to provide a stiff, accurate, spool valve motion.

The servovalve used to control the hydraulic fluid to the rotary actuator in this work was a PEGASUS Model 130 AA. It is a two-stage, four-way, critically underlapped electrohydraulic flow control valve, which uses a hydraulic-follower arrangement as internal feedback. The servovalve also includes a linear variable differential transformer (LVDT) attached to the main stage spool valve which can be used as an external feedback.

Fig. 2.7 shows a sectional view of the PEGASUS servovalve. A complete diagram including the LVDT section is presented in Appendix A.

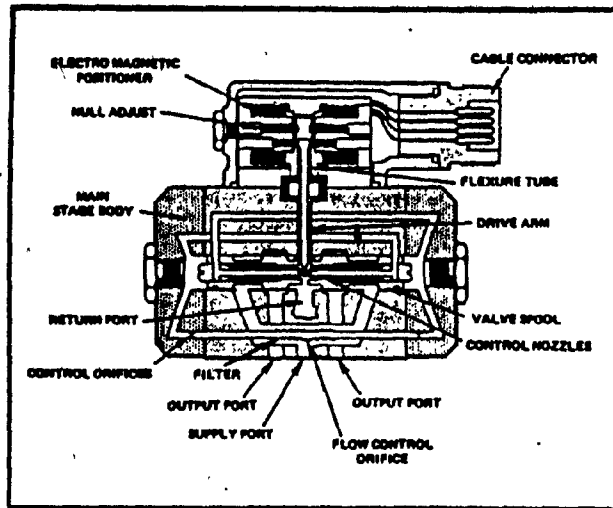


Fig. 2.7. PEGASUS Servovalve-Sectional View.  
(Source: PEGASUS Servovalve.Two  
Stage Series.)

The servovalve consists of four basic sections:

1. Electrical Torque Motor
2. Double Nozzle-Flapper Arrangement
3. Valve Spool
4. External Feedback

1. Electrical Torque Motor

The technical word "Electrical Torque Motor" has been used by most manufacturers of servovalves to describe the input stage of electrohydraulic servovalves, however, "Electromagnetic Positioner" can be used instead, to define that stage. In the Positioner an electrical current is fed to the servovalve input causing a displacement of the drive arm.

Fig. 2.8 shows a schematic diagram of the Electrical Torque or Positioner.

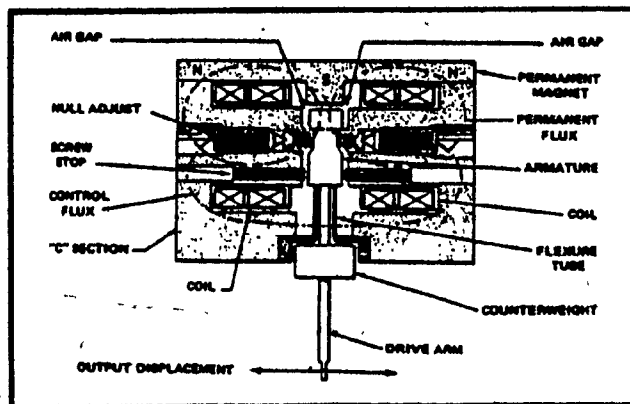


Fig. 2.8. Electrical Torque Motor-Schematic Diagram (Source: PEGASUS Servovalve. Two Stage Series.)

The input-output relationship is made linear and proportional. For positive current the drive arm will move

in one direction and for a negative current it moves in the opposite direction.

The Torque motor, as shown in Fig. 2.8, consists of two active air gaps, four separate coils which can be driven in series or parallel, at the users option, the armature, the flexure tube which performs several functions, the null adjustment mechanism whose function is to null the valve center position, and the drive arm or flapper.

## 2. Double Nozzle-Flapper Arrangement

The servovalve first stage consists of the Electrical Torque Motor and the Double Nozzle-Flapper Arrangement. The latter, also named "pilot stage", is a hydraulic amplifier which amplifies the low force level of the positioner output to the high force level required to drive the spool reliably. Because of the position internal feedback arrangement of the servovalve, the spool follows the flapper movement as if it were attached.

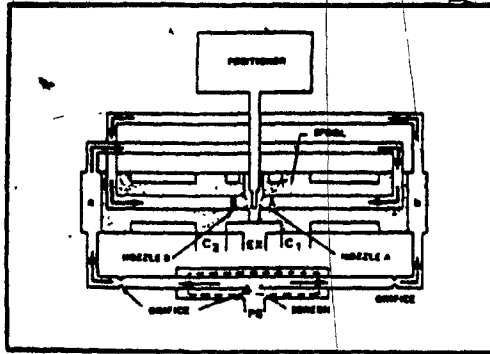


Fig. 2.9. Hydraulic Amplifier-Steady State with Spool on Center. (Source: PEGASUS Servo Valve, Two Stage Series.)

As shown in Fig. 2.9, the end of the torque motor armature forms the flapper placed between two nozzles facing each other. Note that the nozzles are located within the spool. The control orifices and nozzles are symmetrical on the two sides.

Fig. 2.9 shows the flapper centered between the nozzles, therefore the hydraulic pressures at 'A' and 'B' (also 'a' and 'b') are equal, no flapper movement is recorded because the balanced pressure on the ends of the spool. However, if an input is applied to the positioner to produce displacement 'X' at the flapper as shown in Fig. 2.10, the flow out of nozzle 'A' is more restricted than the

flow out of nozzle 'B'. As a result, the hydraulic pressure at 'A' is higher than the hydraulic pressure at 'B'. These pressure changes act on the end of spool at 'a' and 'b'. Therefore, because of the higher pressure at 'a' the spool will move in direction 'X'. Once the spool moves a distance equal to the original displacement 'X' of the flapper, as shown in Fig. 2.11, the flapper is again centered between the nozzles and pressures 'a' and 'b' are equal. At this point a balanced pressure exists on the ends of the spool and there is no further displacement of the spool. In like manner, for any other flapper displacement, the spool moves the same amount in the same direction.

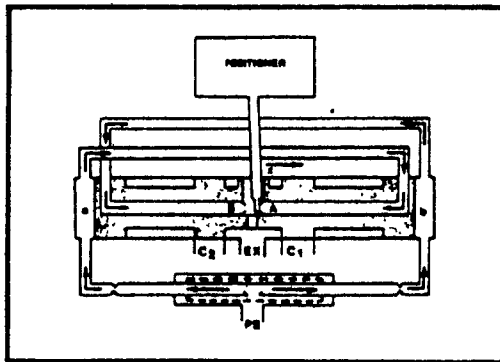


Fig. 2.10. Hydraulic Amplifier-Transient.  
(Source: PEGASUS Servo Valve Two Stage Series.)

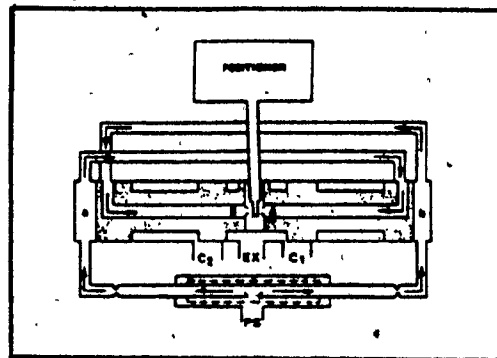


Fig. 2.11. Hydraulic Amplifier-Steady State  
with Spool off Center. (Source:  
PEGASUS Servo Valve Two Stages Series.)



### 3. Valve Spool

The output stage of the servovalve is a four-way spool valve. The valve has a pressure port, an exhaust (or tank) port, and two control ports. The four-way servovalve is designed to control flow to both control ports.

Fig. 2.12 shows a schematic diagram of the spool which is of the four-land spool type. With respect to the lap, which is the physical relationship between spool metering lands and port openings, the spool valve is critically underlapped with a specified underlapped region between 0 to  $\pm 0.5\%$  of the rated valve stroke.

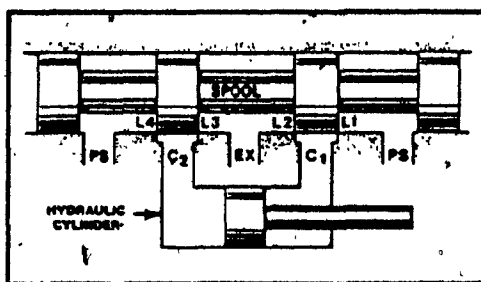


Fig. 2.12. Four Way Spool Valve-On Center.  
(Source: PEGASUS Servovalve. Two Stages Series.)

If the spool is displaced in direction 'X' as shown in Fig. 2.13, then the flow from pressure port PS to the

control port C2 drives the actuator, with the discharge oil from the control port C1 going to exhaust. The velocity of the actuator is controlled by the amount of oil metered through the metering edges L2 and L4. Therefore, the greater the spool displacement 'X', the higher the flow rate and the greater the velocity of the actuator.

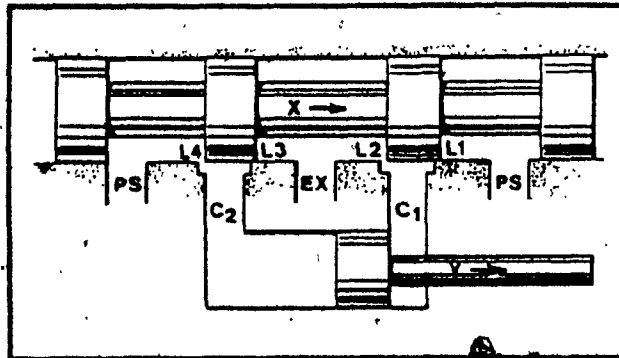


Fig. 2.13. Four Way Spool Valve-Flow out C2.  
(Source: PEGASUS Servo Valve. Two Stages Series.)

If the spool is displaced in direction 'a' as illustrated in Fig. 2.14, flow from PS to C1 drives the actuator, with the discharge oil from C2 going to tank. Therefore, the actuator moves in an opposite direction, with the velocity controlled by the amount of spool displacement.

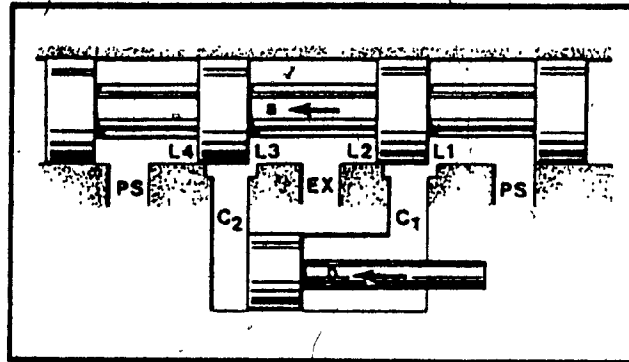


Fig. 2.14. Four Way Spool Valve-Flow out C1.  
(Source: PEGASUS Servo Valve. Two  
Stages Series.)

#### 4. External Feedback

External electronic feedback has been used in the three stage electrohydraulic servovalves to control the pilot stage. Fig. 2.15 shows an example of a three-stage servovalve. The standard two-stage flow control servovalve is used for pilot operation. The two output flows of the pilot servovalve are connected to the ends of the third stage spool. Motion of the third stage spool is fed back electronically to the servoamplifier driving the torque motor of the pilot servovalve. Therefore this is an electronic position feedback servovalve. Typically, three-stage servovalves are used for high flow control.

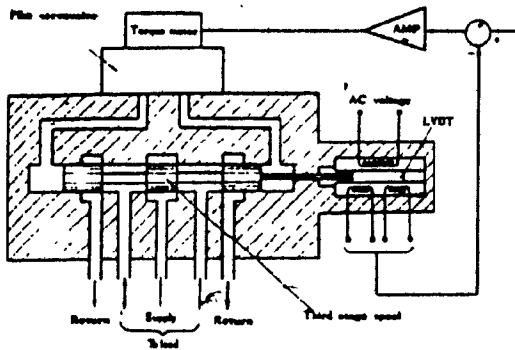


Fig. 2-15. Three-Stage Servovalve. (Source: Trends in Control Components, M. Nalecz-Editor).

External electronic feedback in two-stage electrohydraulic servovalves is a relatively new concept. It has been used in Europe, but not commonly in North America. Electronic feedback can be used to compensate for some of nonlinearities present in servovalves such as dead zone, torque motor hysteresis, spool stiction, etc.

In our case, a Linear Variable Differential Transformer (LVDT) is the external feedback device. The spool of the output stage is linked to the LVDT via a core connecting rod. Displacement of the spool valve thus causes an equivalent displacement of the LVDT core. This displacement is monitored by the LVDT coils, and the resultant electrical feedback signal sent to the servocontrol electronics which control spool position.

Fig. 2.16 shows schematic and circuit diagrams for an LVDT displacement sensor. The excitation of such a device is a sinusoidal voltage, typically between 3 to 15 volts rms amplitude and frequency of 60 to 20,000 Hz [ 5]. The two secondary coils are identical. Sinusoidal voltages as the same frequency as the excitation are induced in them, however, the amplitude varies with the position of the iron core.

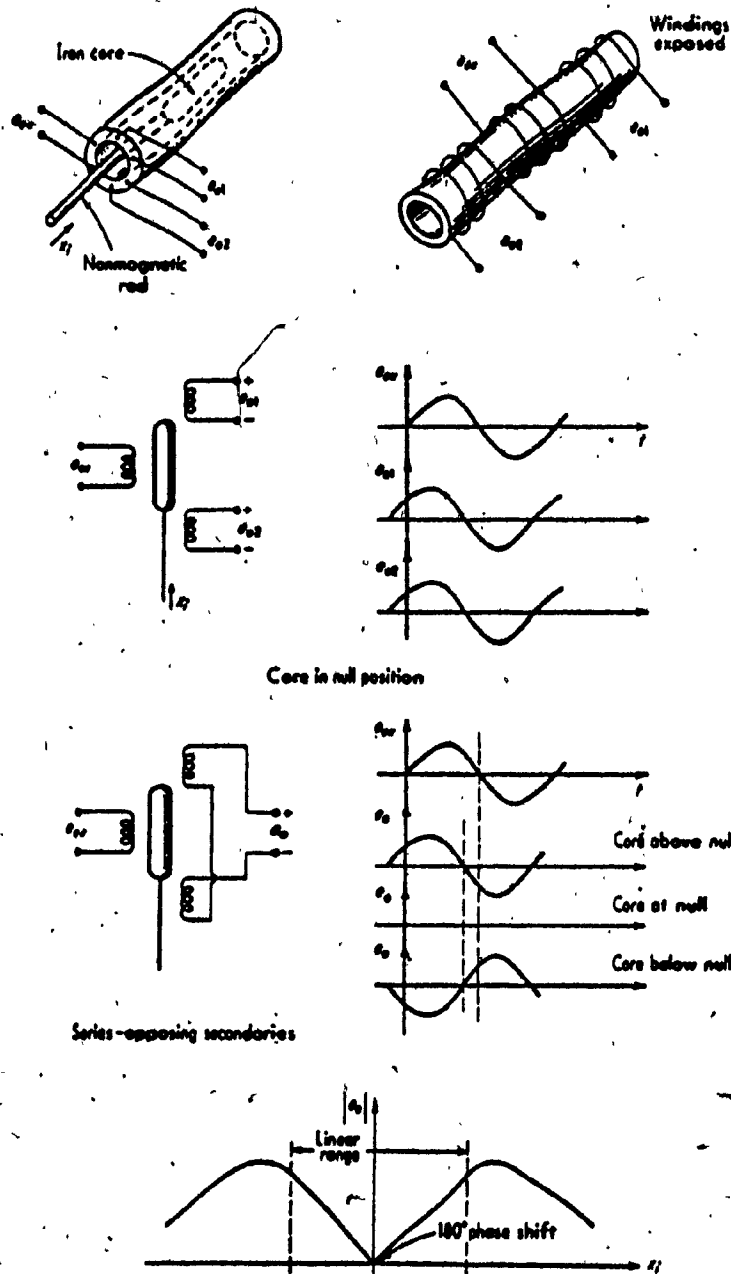


Fig. 2.16. LVDT Schematic and Circuit Diagram.  
(Source: Doebelin, Ernest: "Measurement Systems".)

Wiring connections for the two secondary coils are made in series opposition, as shown in Fig. 2.16. Thus a null position exists ( $X_1 \approx 0$ ) at which the net output,  $e_0$ , is essentially zero. The actual wave form of the output is an amplitude modulated sine wave, an undesirable form for control purposes. To have an output signal related to the mechanical motion being measured it is necessary to include a demodulation and filtering stage. The demodulation stage must be phase-sensitive to detect unambiguously the motions on both sides of null. Fig. 2.17 shows a schematic diagram of the demodulation and filtering stages.

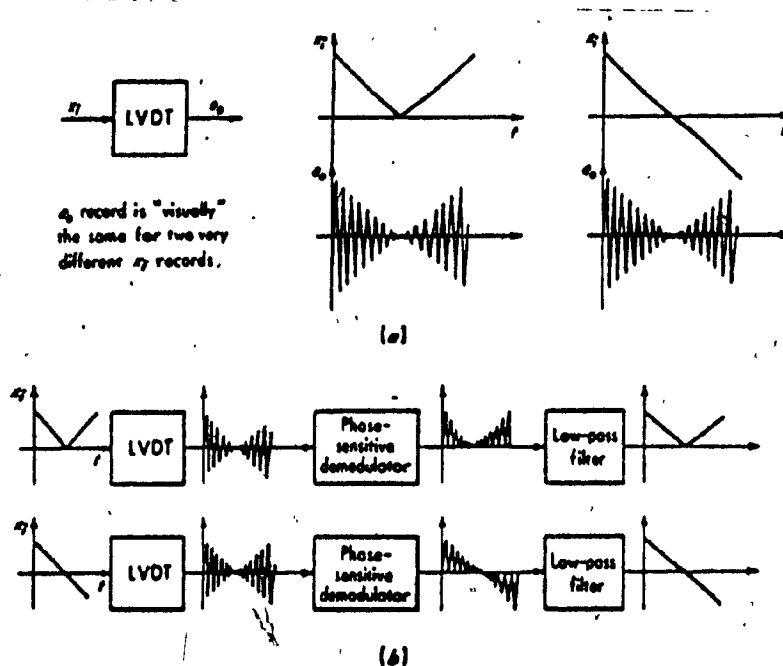


Fig. 2.17. Demodulation and Filtering Stages-Schematic Diagram. (Source: Doebelin, Ernest: "Measurement Systems")

The demodulation and signal conditioning circuit used in this work was the SMS/GPM - 108 A/ LVDT SIGNAL CONDITIONING MODULE manufactured by SCHAEVITZ Engineering. This module converts the LVDT output into a high level DC signal which can be fed to the controller input. For more details of this module, see Section 2.4.

Fig. 2.18 shows a schematic diagram of the LVDT and its associated circuitry.

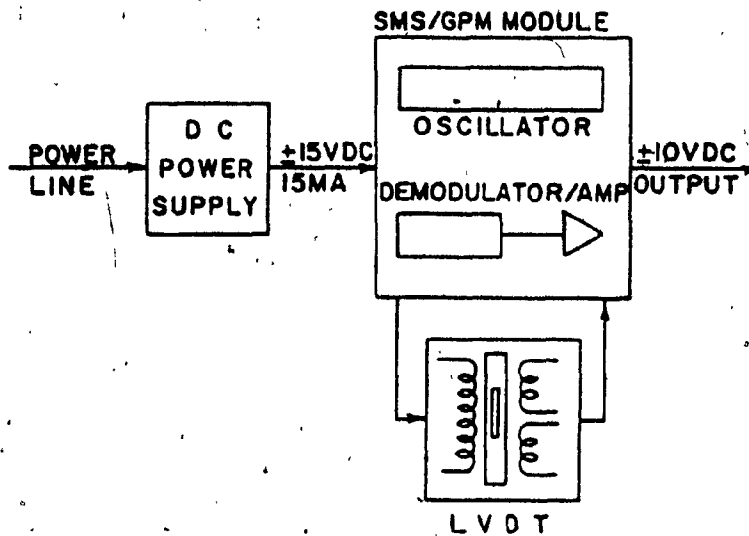


Fig. 2.18. LVDT and its Auxiliary Equipment- Schematic Diagram.



### 2.3.2. Performance Characteristics

The characteristics of a flow control servovalve are obtained for steady-state and dynamic conditions. The flow and pressure characteristic curves depict the overall operation of the valve under steady-state conditions; while the open-loop frequency response plot, with no load, gives the servovalve dynamic characteristics. The servovalve transient response was not considered in this study, however, transient response can be derived from the frequency response presented.

#### 2.3.2.1 Steady-State Characteristics

The servovalve flow curve shown in Fig. 2.19 was obtained as manufacturer's data. The curve was obtained by cycling the valve through its input current range. The curve shown is for zero pressure drop across the valve and a supply pressure equal to 1000 psi. From the curve, servovalve flow gain, hysteresis, linearity, deadband, rated current in either direction, null bias, and threshold can be obtained.

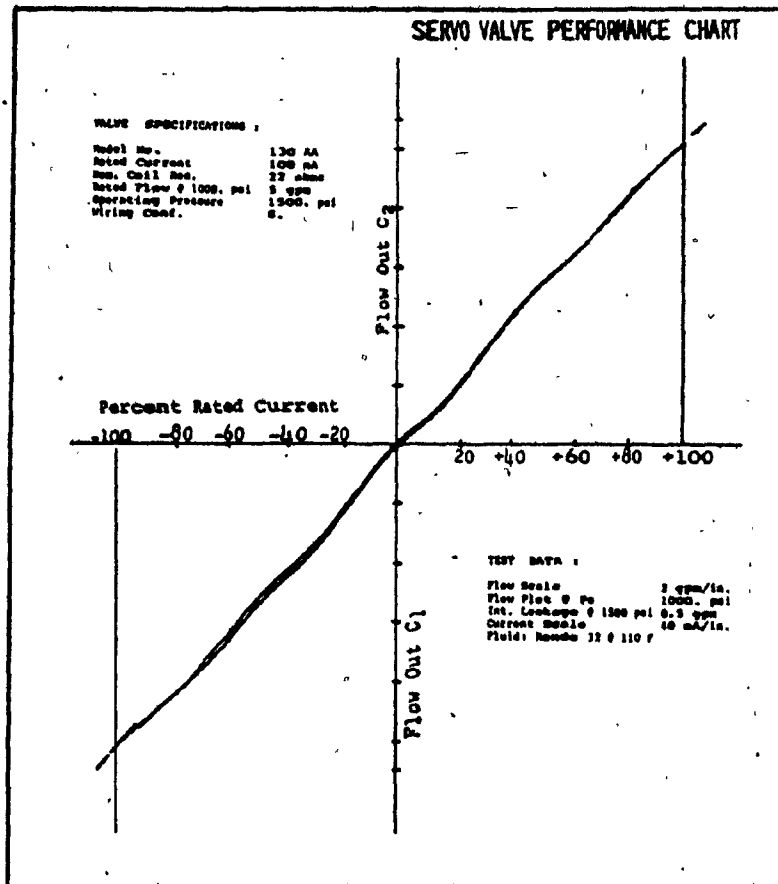


Fig. 2.19. Servo Valve Flow Curve

In Fig. 2.20 a sketch of the experimental set-up used to obtain the pressure gain curve is illustrated.

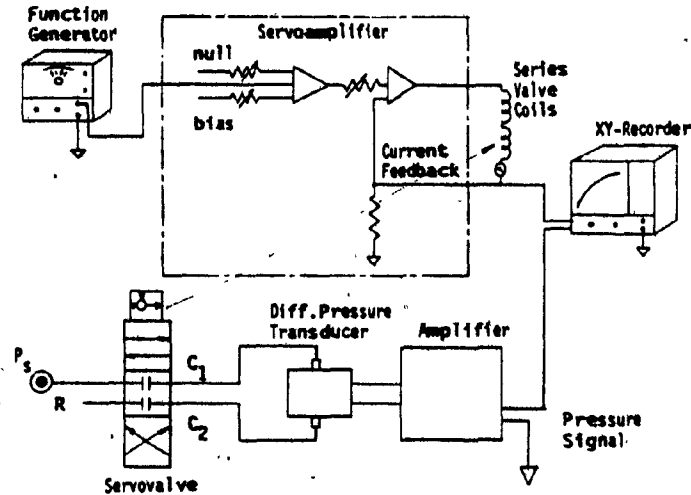


Fig. 2.20. Experimental Set-Up for the Pressure Gain Curve.

As can be noted, a differential pressure transducer is connected across the servovalve blocked control ports. The control pressure ports change as the valve spool moves from its centered position. The continuous pressure curve is shown in Fig. 2.21.

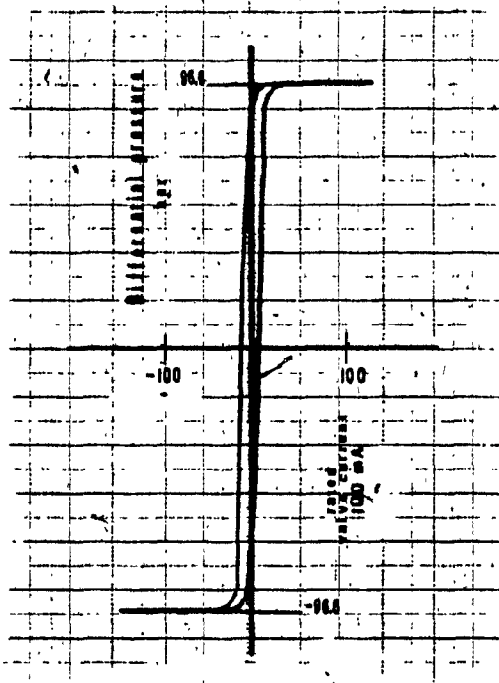


Fig. 2.22. Servovalve Control Ports Blocked Pressure Sensitivity Curve.

While the relationship between input current and output flow is essentially linear, the relationship between input current and output pressure is non-linear. Pressure gain is usually specified as the slope of the pressure curve between  $\pm 40\%$  of the maximum differential pressure across the valve. For the two curves shown, the servovalve flow gain is equal to  $3.1583 \times 10^{-6} \text{ m}^3/\text{s}/\text{mA}$  ( $0.1925 \text{ in}^3/\text{s}/\text{mA}$ ), while the pressure gain is equal to  $0.8136 \times 10^6 \text{ N}/\text{m}^2/\text{mA}$  ( $118 \text{ psi}/\text{mA}$ ).

#### 2.3.2.2 Dynamic Characteristics

The open loop frequency response plot of the servovalve was provided by the manufacturer, Fig. 2.22. That curve was obtained for a constant input current of small amplitude and zero load pressure drop. The frequency response curve is expressed as amplitude ratio, and phase lag. Amplitude ratio is the ratio of the servovalve control-flow amplitude to a sinusoidal input current amplitude at a particular frequency divided by the same ratio at the same input current amplitude but at a specified low frequency. Such a specified frequency is called "base frequency" whose value depends on the servovalve dynamics. The amplitude ratio is expressed in decibels where;  $\text{db} = 20 \log_{10} \text{AR}$ . The phase angle is the time separation between the two signals measured at a specified frequency and expressed

in degrees: thus,  $\text{deg} = \text{time separation, s} \times \text{frequency, Hz} \times 360$ .

The frequency response curve gives us an important tool to determine an approximate transfer function for an electrohydraulic servovalve. The difficulty in assuming an explicit transfer function for electrohydraulic servovalves is that many design factors and many operational and environmental variables produce significant differences in the actual dynamic response. Thus, it is often convenient in servoanalysis to represent an electrohydraulic servovalve by a simplified, equivalent transfer function. Such a representation is, at best, only an approximation of actual servovalve performance. However, the usefulness of linear transfer functions for approximating servovalve response in analytical work is well established [46].

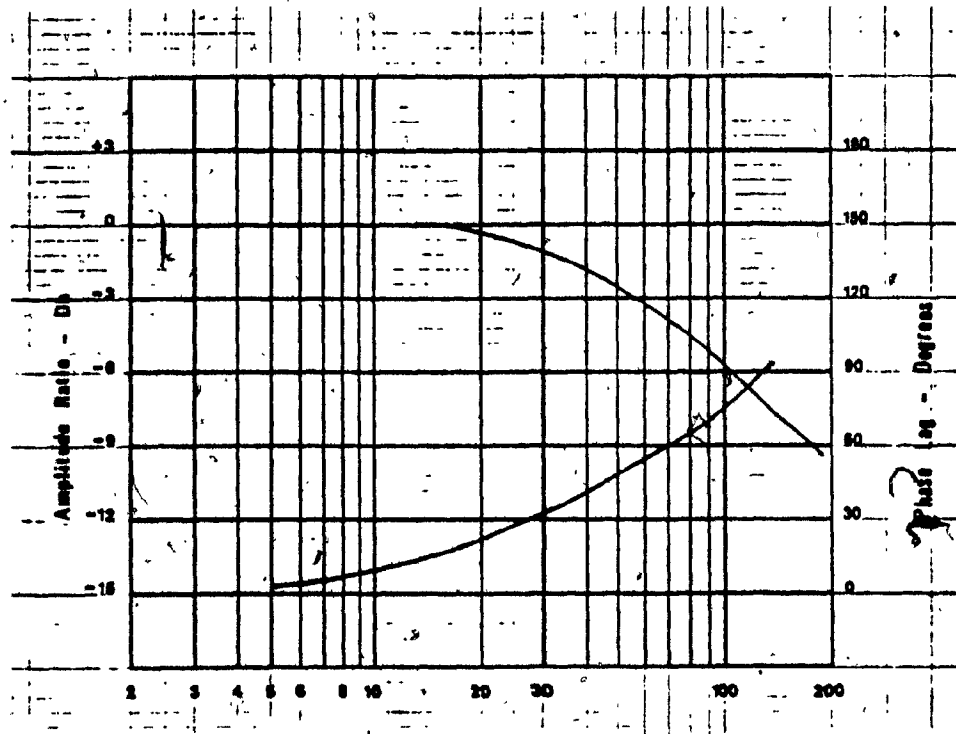


Fig. 2.22. Frequency Response for PEGASIS Servo Valve, Model 130AA- Experimental Values.

In our case, two models for the servovalve transfer function were assumed. In the open-loop dynamic characteristics of the servovalve controlled hydraulic motor, Chapter 6, a first-order transfer function was assumed, while in Chapter 7, a second-order transfer function has been assumed. The reasons for that are as follows:

In the open-loop tests of dynamic characteristics of the system, experimental tests to obtain the motor velocity transient and the open-loop frequency response were carried out. A theoretical analysis for that system was also performed. From that analysis, a transfer function between the motor velocity and servovalve stroke was obtained. Such a transfer function showed that the relationship between those variables ( $X_v$  and  $\omega_m$ ) can be represented as a second-order transfer function in which a hydraulic natural frequency was given by:

$$\omega_h = \sqrt{2 \beta_e D_m^2 / V_o J}$$

where  $\beta_e = 0.51708 \times 10^9 \text{ N/m}^2$   
 $D_m = 0.1226 \times 10^{-5} \text{ m}^3/\text{rad}$   
 $V_o = 0.14749 \times 10^{-3} \text{ m}^3$



For the moment of inertia, with values of 0.003, 0.03247, and 0.0428 N-m-s<sup>2</sup> which were the figures for the three discs employed in the tests, hydraulic natural frequencies of 9.43, 2.86, and 2.49 Hz resulted.

If these values are compared with those of the open-loop frequency response of the servovalve, Fig. 2.22, it can be noted that the servovalve contributes mainly to a phase lag for frequencies up to about 15 Hz. Thus, for the open loop dynamic characteristics of the servovalve controlled motor, it is clear that the physical system is the limiting dynamic element rather than the servovalve. So, in this case, it is only necessary to represent the valve response throughout a relatively low frequency spectrum. Therefore, a first-order transfer function can give a reasonable approximation for frequencies up to about 20 Hz. Fig. A-1, Appendix A, shows the servovalve frequency response with first-order transfer function fit.

For the Chapter 7, a second-order transfer function for the servovalve has been assumed. From the theoretical analysis carried out in that Chapter, the relationship between the servovalve stroke and motor torque was a first-order transfer function with an equivalent time constant determined by:

$$\tau_m = V_o / 2K_{ce} \beta_e$$

where  $V_o = 0.14749 \times 10^{-3} \text{ m}^3$

$$K_{ce} = 0.59384 \times 10^{-11} (\text{m}^3/\text{s}) / (\text{N}/\text{m}^2)$$

$$\beta_e = 0.51708 \times 10^9 \text{ N}/\text{m}^2$$

Substituting the values of  $V_o$ ,  $K_{ce}$  and  $\beta_e$  into the equation for  $\omega_m$ , a break frequency of 7 Hz for the open loop Bode plot between the servovalve stroke and the torque of hydraulic motor is obtained. For frequencies of operation greater than 20 Hz, a better approximation for the servovalve transfer function is obtained using a second-order transfer function, Fig. A.1.

Assuming a second-order transfer function for the servovalve current and servovalve stroke, a third-order system for the force servo system results; that assumption was confirmed in the experimental results obtained, see Section 7.4.2.

The second-order transfer function allows extending the range of useful approximation for the servovalve as can be observed in Fig. A.1. Thus, for a first-order transfer function, the range of useful approximation is up to 20 Hz, while for the second-order transfer function, a range of useful approximation up to 40 Hz can be obtained.

In summary, the following characteristics apply to the servovalve used, Table 2.3.

Table 2.3 Pegasus Servovalve Performance Characteristics

Rated Flow @ 1000 psi	5 GPM
Rated Current	100 mA
Freq. Response -3 db point	60 Hz
Phase Lag of 90 degrees	125 Hz
Int. Leakage @ 1000 psi	.3 GPM
Confined Oil	.1 cu. in.
Flow Tolerance	+ 10% - 0%
Linearity	5%
Threshold	1/2%
Hysteresis (total band)	3%
Pressure Gain (% $\Delta P$ / % $\Delta I$ )	13%

#### 2.4. FEEDBACK ELEMENTS

##### 2.4.1. Torque Sensor

A strain-gage torque sensor with built-in slip rings was used in this research as a torque measuring device. Torque is transmitted through a high tensile steel shaft to which is bonded a network of strain-gages, protected with a

tough resin film. Torsional shear strain causes a change in the resistance of the gages which are connected in a fully active four arm bridge which produces a linear output signal directly proportional to the transmitted torque.

Electrical connections between the rotor and stator of the transducer are made with silver slip rings and silver graphite brushes.

The torque transducer, Fig. 2.23, was manufactured by Experimental & Electronic Laboratories of British Hovercraft Corporation Limited, England. The model is a TT2/4/CA. The transducer specifications are shown in Table 2.4, and its calibration curve is illustrated in Fig. 2.24.

Table 2.4 Torque Sensor Specifications

Load Range	0 - 100 lb-ft
Maximum Load	200 lb-ft
Speed Range	0 - 6000 rpm
Sensitivity @ full load	2.260 mV/V
Bridge Resistance @ 20°C	601 ohms
Maximum Continuous Voltage	20 AC or DC
Maximum Total Error due to Linearity & Hysteresis	$< \pm 0.2\%$ F.S.
Moment of Inertia	$8.2 \times 10^{-5}$ in-lb-s <sup>2</sup>
Maximum Ambient Temperature	45°C

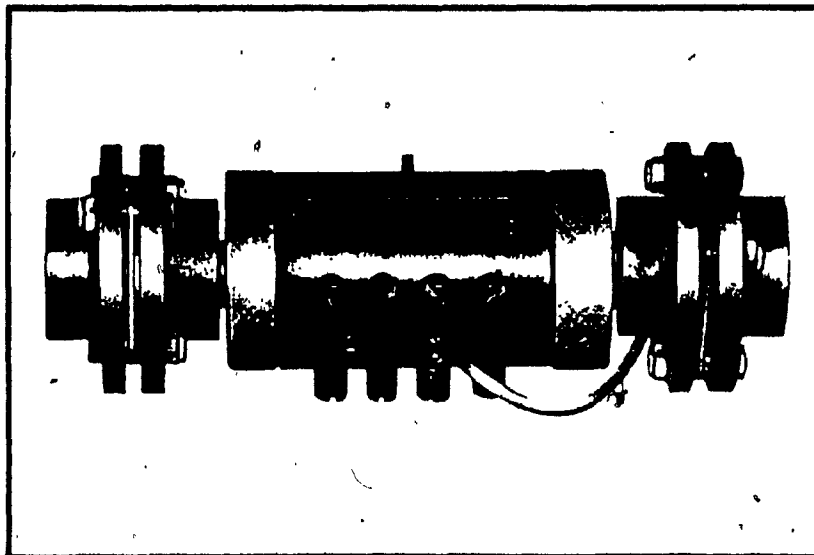


Fig. 2.23. Torque Transducer with Built-in Slip Rings.

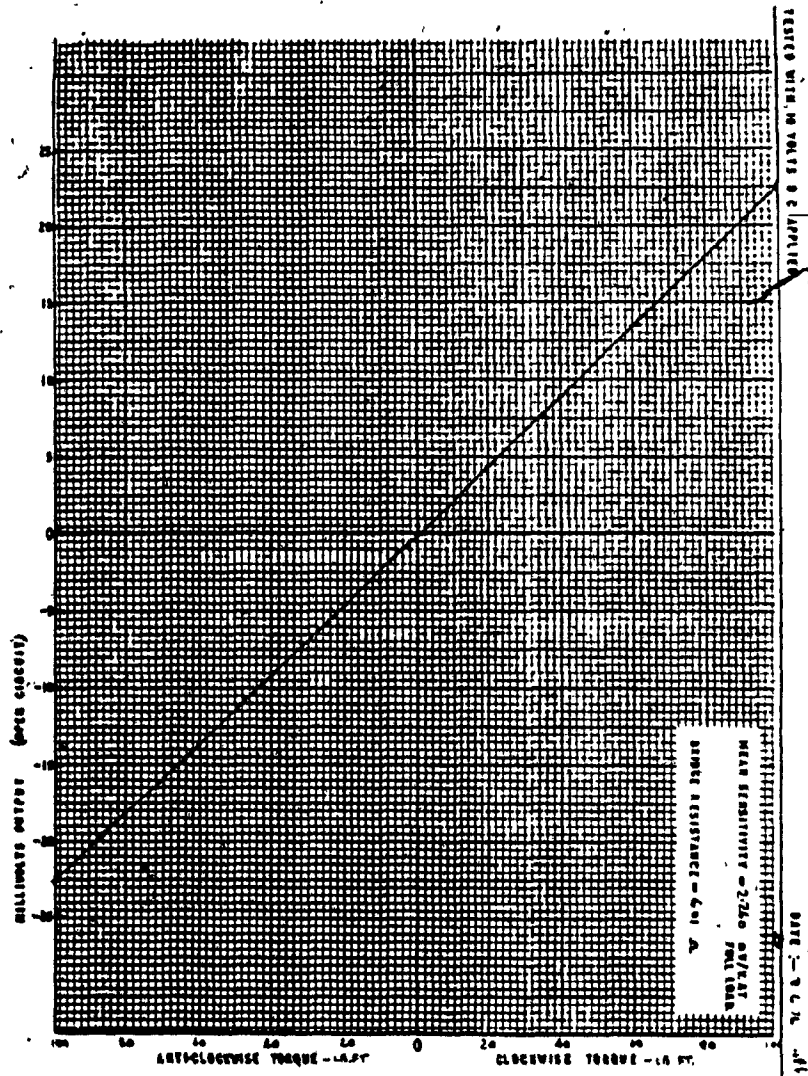


Fig. 2.24. Torque Sensor Calibration Curve.

### 2.4.2. Differential Amplifier

The output signal obtained from the torque transducer is in the order of few millivolts. The maximum output signal, in the event that full supply pressure is acting on the motor is only 2mV. Therefore, it was necessary to use a differential-input instrumentation amplifier, which besides increasing the torque sensor output signal, can adjust the gain of the torque feedback signal. Fig. 2.25 illustrates the electronic diagram of such an amplifier.

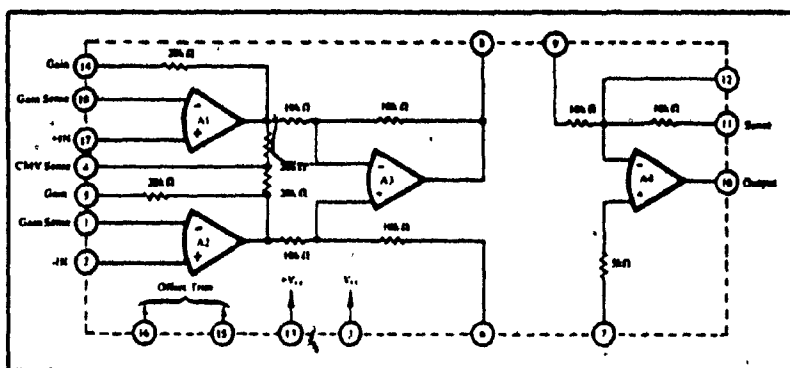


Fig. 2.25. Differential Amplifier-Simplified Schematic.

The differential amplifier provides connections to use an active low pass filter. Because of the inherent torque ripple of the hydraulic motor, a cut-off frequency of 30 Hz determined experimentally was selected.

Fig. 2.26 shows a schematic diagram of the external connections of the amplifier. The total gain is governed by the equation:

$$E_{out} = (E_1 - E_2) (1 + 40k/R_g) (10k + R_2) / (10K + R_1) \times A$$

$$A = 1 / \sqrt{1 + [2 \pi (10K + R_2) C \times f]^2}$$

where  $E_{out}$  = output voltage, mV

$E_1 - E_2$  = input differential voltage, mV

$R_g$  = external resistor of the first stage amplification, ohms

$R_1$  = external resistor of the second stage amplification, ohms

$R_2$  = external resistor of the second stage amplification, ohms

$C$  = external capacitor in Farads

$f$  = frequency, Hz

$k$  = factor equal to 1000.



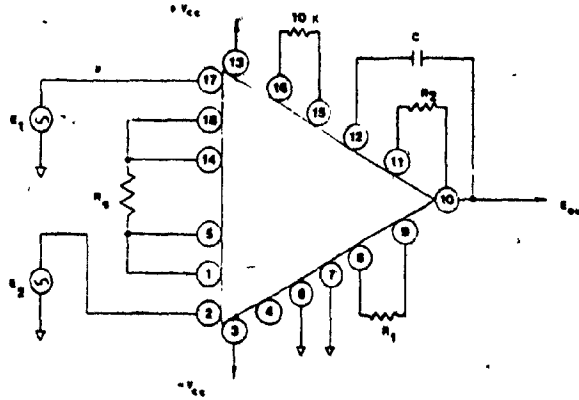


Fig. 2.26. Differential Amplifier External Connections.

The amplifier, model 3630, was manufactured by Burr-Brown Research Corporation. Its specifications are shown in Table 2.5.

Table 2.5 Differential Amplifier Specifications

Rated Output	$\pm 10V, \pm 5 \text{ mA}$
Rated Input	$\pm 10V$
Dynamic Response	2.5 kHz for gain = 1000
Power Supply	$\pm 15 \text{ VDC}$
Operating Temperature	- 25°C to + 85°C

### 2.4.3 LVDT Signal Conditioning Module

The LVDT signal conditioning module is used to provide an AC excitation signal @ 2.5 kHz, demodulation and signal amplification for the LVDT sensor. It converts the LVDT output into a filtered, high level DC signal which can drive voltmeters, high response recorders or other dynamic indicators. Fig. 2.27 shows a picture of the actual signal conditioning module, while the wiring diagram is shown in Fig. 2.28.

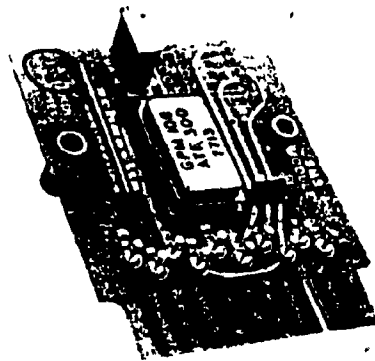


Fig. 2.27. LVDT Signal Conditioning Module-Actual Hardware.

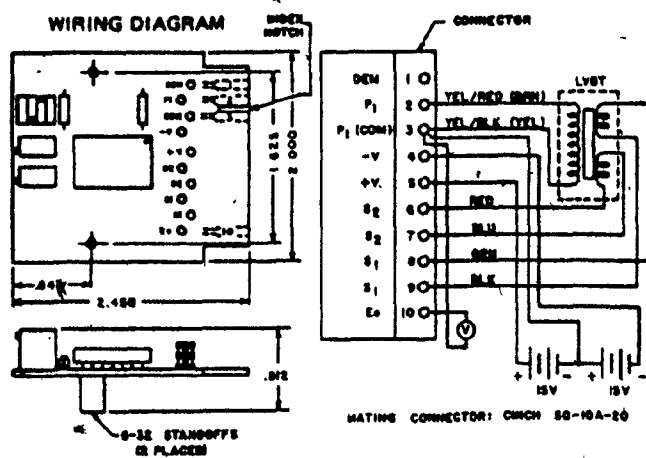


Fig. 2.28. LVDT Signal Conditioning Module Wiring Diagram.

This module provides important features such as zero and gain adjusts. Using the zero electrical adjust, the mechanical zero of the LVDT can be adjusted to coincide with the transducer electrical zero. The adjust of gain allows one to increase or decrease the LVDT output signal modifying thus the feedback signal of the servo-system as the LVDT is used as feedback element.

Fig. 2.29 shows a plot of LVDT signal versus servovalve current for a selected LVDT gain adjustment. A proportional relationship between the two signals is evident. The hysteresis (total band) is of 0.70 mA or 0.7% of the servovalve rated current.

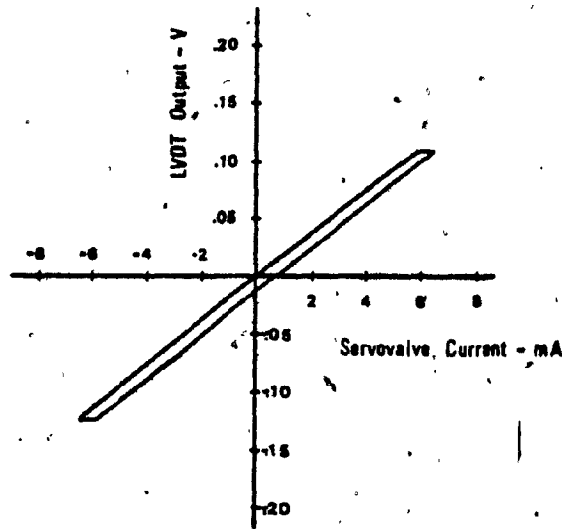


Fig. 2.29. LVDT Output versus Servovalve Current

## 2.5. The Controller

Fig. 2.30 shows the electronic diagram of the servo-controller used in this research. It was designed and built in the Fluid Power Research Lab at Concordia University.

The control mode is proportional. Thus, its output, the current into the servovalve coils, is directly proportional to the summation of voltage signals at the input of the amplifier.

Two major functions provided by the servo amplifier are: (1) control of the electrical current flowing into the torque motor coils of the servovalve as a function of the input voltages of the amplifier; and (2) limiting current drawn by the torque motor to a safe level.

The amplifier was designed taking into account the servovalve rated current. That is, the servo amplifier goes to saturation at the rated current of the valve, protecting the torque motor coils.

The controller consists of a preamplifier (operational amplifier A1 and A2), a feedback stage (operational amplifier A3), and a current amplifier which consists of the operational amplifier A4 and the power transistors Q1 and Q2. The torque motor coils are connected to the output terminals.

The selfcontained feedback circuit provides operational stability, linear response characteristics, and a means of adjusting gain.

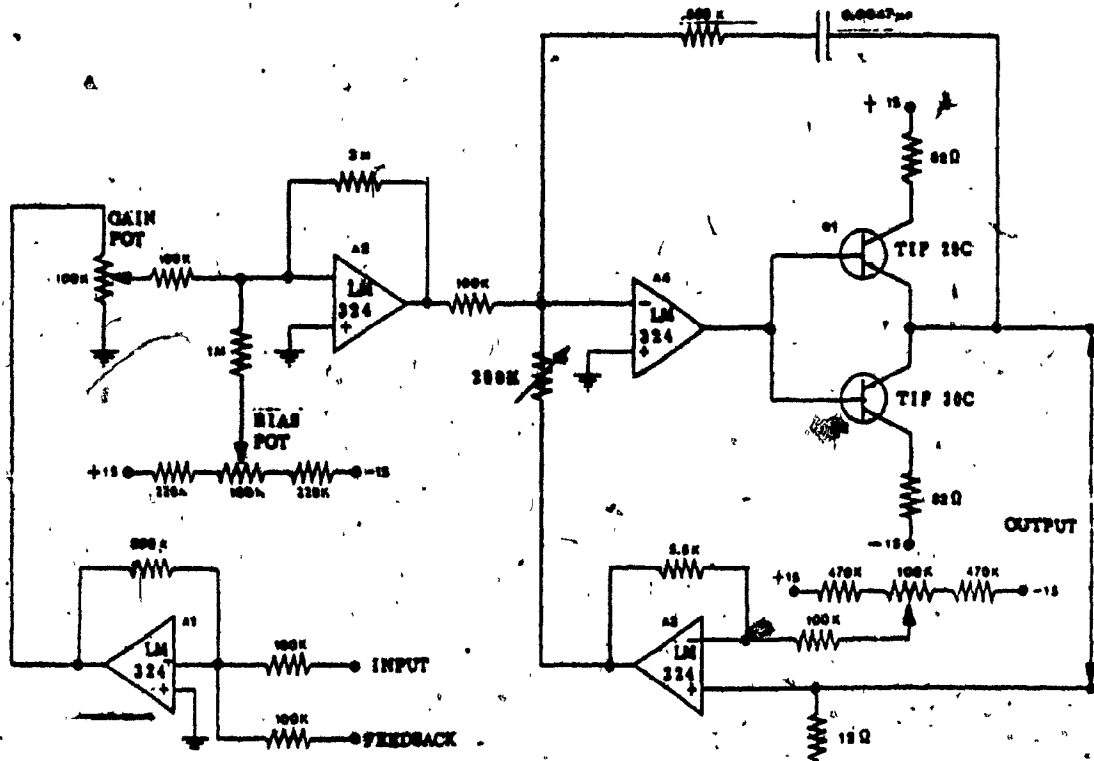


Fig. 2. 30. Servo Control Circuit-Electronic Diagram

Fig. 2.31 shows the input-output relationship of servocontroller for a particular gain of 17.5 mA/V. However, the gain to which the controller is adjusted depends on the particular characteristics of every servo system. A linear relationship between input and output of the servocontroller can be observed.

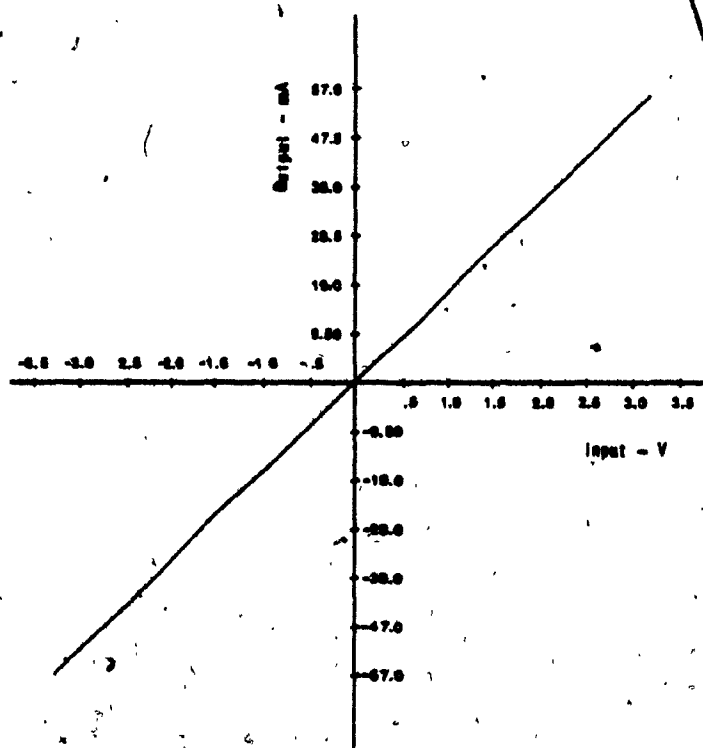


Fig. 2.31 Servocontroller Steady-State Characteristics.

It is important to know the dynamic characteristics of the servocontroller alone. In other words, to know its operational bandwidth. One way to find out that is by

obtaining the open-loop frequency response of such a servocontroller.

Frequency response characteristics in an open-loop configuration given in the form of Bode Plot are illustrated in Fig. 2.32. Amplitude ratio is presented as the ratio of the output current amplitude to a sinusoidal input voltage amplitude at a particular frequency divided by the same ratio at a specified low frequency (5 Hz).

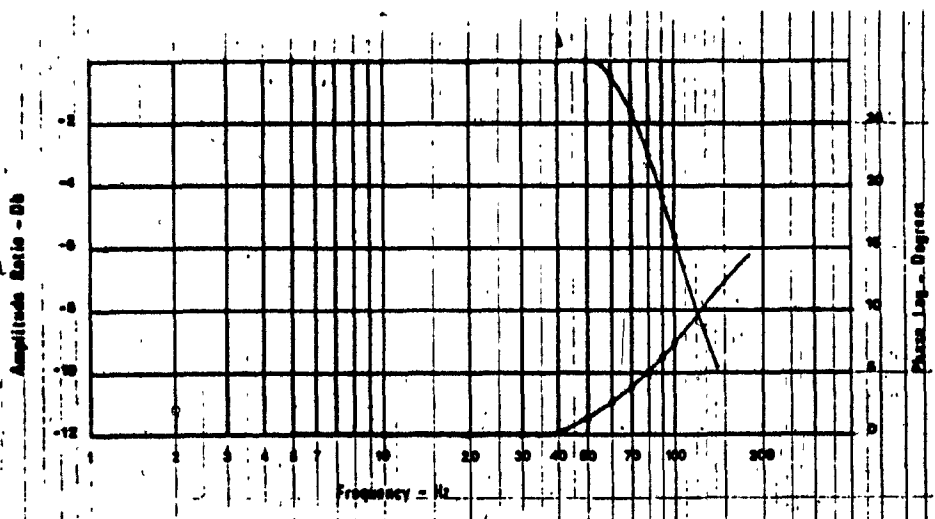


Fig. 2.32. Servocontroller Frequency Response-Open Loop



2.6. LOAD SYSTEM

2.6.1. Elements of the Load Torque

Two different load systems were devised. The first one consists of several steel discs of the same diameter but each one of different thickness. Each disc is composed of two halves to facilitate attachment to the shaft, Fig. 2.33. These discs were used as inertial loads to the motor to derive dynamic characteristics of the servovalve controlled motor.

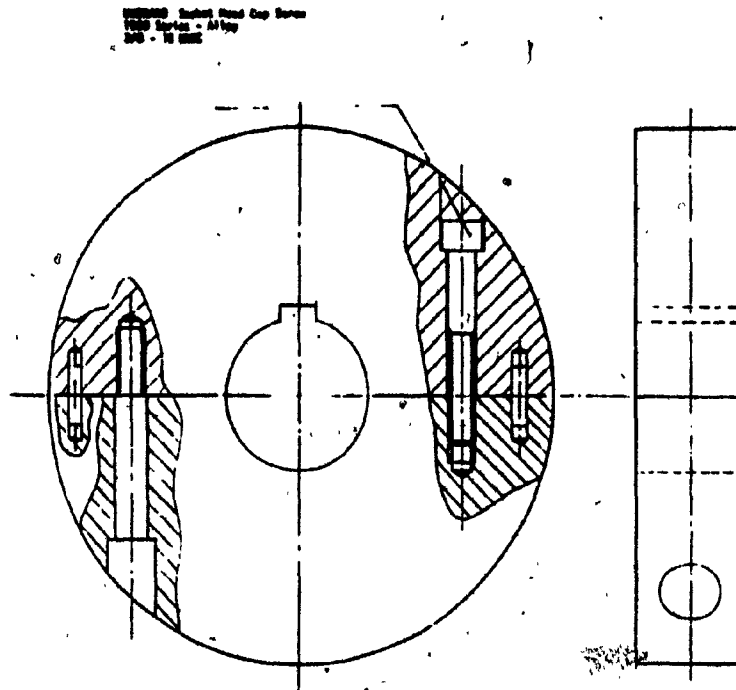


Fig. 2.33 Sectional View of the Steel Disc

Fig. 2.34 shows a schematic diagram of the second load system used. It consists of a hydraulic pump driven by the hydraulic motor, and an electrohydraulic servovalve used to create flow restrictions through the pump outlet port increasing the pumping pressure.

This system was used to derive the steady-state characteristics of the servovalve controlled motor.

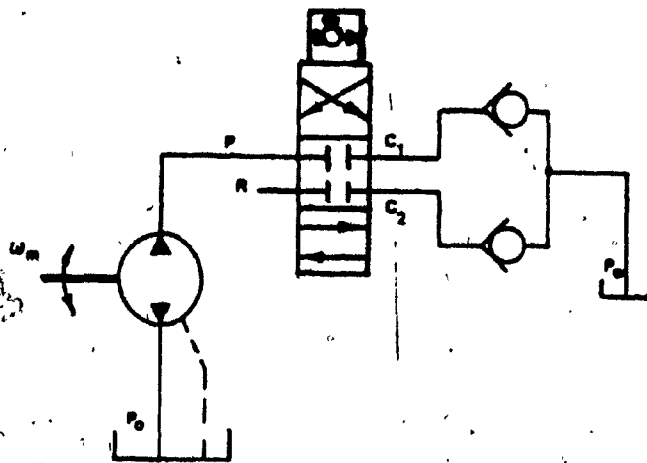


Fig. 2.34. Schematic of Loading System.

The pump was a bent-axis type, Fig. 2.35, whose specifications are shown in Table 2.6.

Table 2.6 Load Pump Specifications

Displacement	0.298 cu.in./rev
Flow @ 1000 rpm (Theoretical)	1.29 U.S. gpm.
Torque @ 1000 psi	47 lb-in
Moment of Inertia of Rotating parts	$1.2432 \times 10^{-3}$ lb-in-s <sup>2</sup>

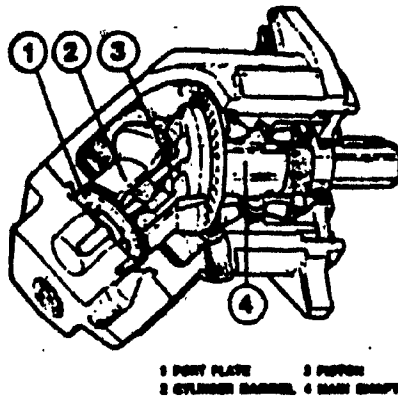


Fig. 2.35. Load Pump Sectional View

A two-stage, four-way, electrohydraulic servovalve, MOOG Model 62-105 was used as a restriction to the flow from the pump outlet port, Fig. 2.36.

The valve performance is illustrated by Fig. 2.37 showing the flow curve characteristics, and Fig. 2.38

showing a typical servovalve frequency response curve at no load.

The servovalve specifications are shown in Table 2.7.

Table 2.7 Load Servovalve Specifications

Supply Pressure	200 psi minimum
Rated Flow @ 1000 psi	2000 psi maximum
Valve Drop	5 gpm
Internal Leakage	< 0.4 gpm
Linearity	< 7%
Pressure Gain (% $\Delta P$ / % $\Delta I$ )	> 10%
Rated Current	$\pm$ 50 mA
Coil Connection	Series

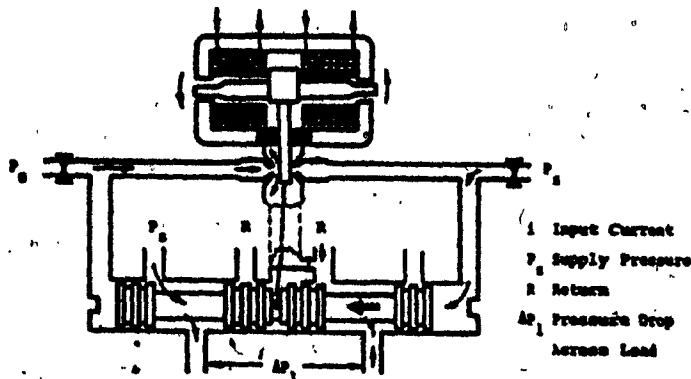


Fig. 2.36. Sectional View of MOOG Servovalve.

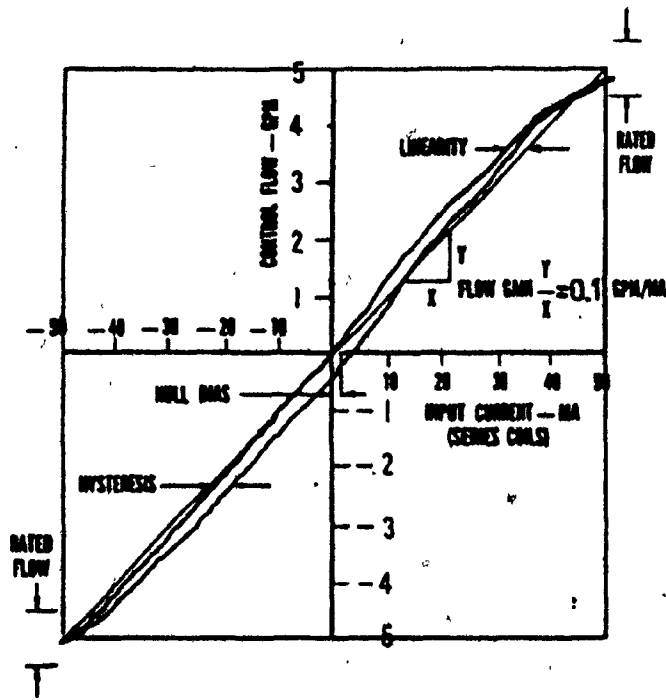


Fig. 2.37. Flow Curve Characteristics-MOOG Servo valve.

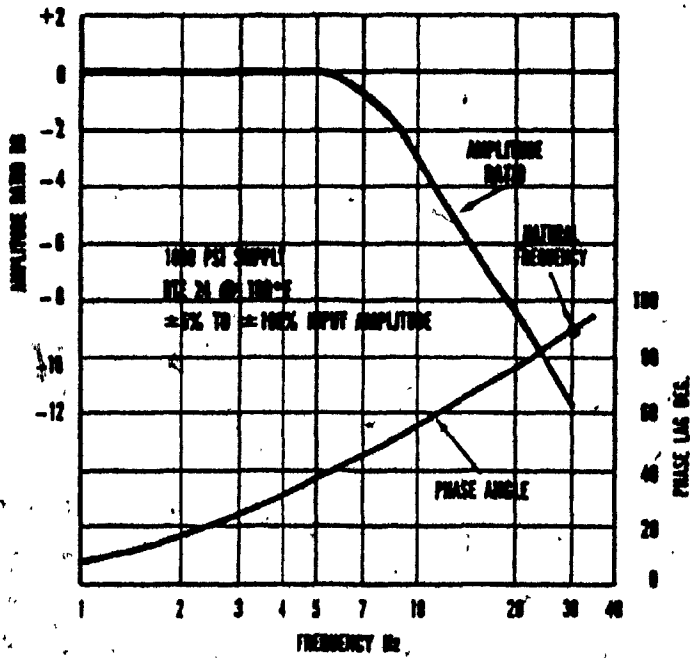


Fig. 2.38. Typical Frequency Response-MOOG Servo valve.

### 2.6.2. Analysis of the Loading System

In the following, a theoretical analysis of the load system is presented. The purpose is to determine how the variables which make up the load system (pump-servo valve) are related and how such variables affect the motor performance.

Let us consider the torques generated by the servomotor. The ideal motor torque is:

$$T_i = D_m (P_1 - P_2) \quad (2.1)$$

However, there are at least two major sources of torque losses which detract from the generated torque:

1. The viscous friction torque loss. This term is proportional to motor speed, and is given by:

$$T_d = B_m \omega_m \quad (2.2)$$

where  $B_m$  is viscous damping coefficient, N-m-s. The coefficient  $B_m$ , obtained experimentally in Chapter 5 was equal to 0.012 N-m-s. Thus, for a motor speed of 1000 rpm (104.7 rad/sec), a viscous friction torque loss of 1.25 N-m was obtained.

2. The Coulomb friction torque loss. The mechanism to translate ball motion into rotary shaft motion will cause a friction torque opposing motion of the motor shaft that is proportional to the pressure acting on the ball. The sign of this torque loss is dictated by the velocity of the motor. Other motor elements, such as bearings, are also loaded proportionally to the motor pressures and cause friction torque losses. Therefore the friction torque loss can be represented by:

$$T_f = \omega_m / |\omega_m| \cdot C_{TF} (P_1 - P_2) \quad (2.3)$$

where  $C_{TF}$  = internal friction coefficient,  $m^3$ . The coefficient,  $C_{TF}$ , obtained experimentally in Chapter 5 was equal to  $0.537 \times 10^{-6} m^3$ . For a pressure drop across the motor equal to  $6.894 \times 10^6 N/m^2$  (1000 psi), a friction torque of 3.70 N-m was obtained.

The coefficients  $B_m$  and  $C_{TF}$  were obtained experimentally and their values are given in Chapter 5.

In the analysis which follows, only the viscous friction torque,  $T_d$  is considered. The Coulomb friction torque,  $T_f$  is not taken into account, because the loaded steady-state characteristics of the motor were obtained for unidirectional motor velocities and in this case Coulomb

friction can be ignored.

The torque developed by the hydraulic motor is given by:

$$T_m = D_m \times (P_1 - P_2) - B_m \omega_m = J_L d \omega_m / dt + T_L \quad (2.4)$$

- where  $T_m$  = torque developed by motor, N - m -  
 $P_1, P_2$  = forward and return pressures, N/m<sup>2</sup>  
 $D_m$  = volumetric displacement of motor, m<sup>3</sup>/rad.  
 $J_L$  = total inertia of motor and load, N-m-s<sup>2</sup>  
 $B_m$  = total viscous damping coefficient (it includes motor, pump, bearing internal damping), N-m-s  
 $T_L$  = arbitrary load torque on motor, N-m  
 $t$  = time, s

A linear analysis was selected at least for a first approximation, for simplicity.

From Eq. (2.4) it can be noted that the torque developed by the hydraulic motor depends on the angular velocity,  $\omega_m$ , and the arbitrary load torque,  $T_L$ , i.e.,  $T_m = F(\omega_m, T_L)$ .



The necessary torque to turn the loading pump is given by:

$$T_p = D_p \times P_p + B_p \omega_m + \text{non-linear terms} \quad (2.5)$$

where  $T_p$  = torque took up by the pump, N-m

$D_p$  = pump displacement,  $m^3/\text{rad}$

$P_p$  = pressure difference across the pump,  $N/m^2$

$B_p$  = internal damping coefficient for pump, N-m-s

The term  $B_p \omega_m$  has been included in the  $B_m$  coefficient and as mentioned before, non-linear terms are ignored. Therefore, an equation which represents the load torque is:

$$T_L = T_p = D_p \times P_p \quad (2.6)$$

The flow through the pump is determined by:

$$Q_p = D_p \omega_m - C_{1p} \times P_p \quad (2.7)$$

where  $C_{1p}$  = internal or cross-port leakage coefficient of pump,  $(m^3/s)/(N/m^2)$

The linearized servovalve flow equation is determined by Eq. (2.8) (for a more detailed analysis, see Chapter 6).

$$Q_{v,1} = K_{q,1} \times X_{v1} - K_{c,1} \times P_p \quad (2.8)$$

where  $Q_{v,1}$  = flow of servovalve,  $m^3/s$   
 $K_{q,1}$  = valve flow gain,  $m^3/s/m$   
 $X_{v,1}$  = valve spool displacement from neutral,  $m$   
 $K_{c,1}$  = valve flow pressure coefficient,  
 $(m^3/s)/(N/m^2)$

Application of the continuity equation to a control volume formed by the pump-servovalve yields:

$$Q_p - Q_{v,1} = V/\beta_e \cdot dP_p/dt \quad (2.9)$$

where  $V$  = volume of forward chamber (includes servovalve, connecting line or manifold, pump passages, and volume swept by pistons),  $m^3$

$\beta_e$  = effective bulk modulus of system (includes oil, entrapped air, hoses, etc.),  $N/m^2$

Substituting Eqns. (2.7), and (2.8) into Eqn. (2.9) and taking the Laplace transform gives:

$$D_p \omega_m - C_{1p} P_p - (K_{q,1} X_{v,1} - K_{c,1} P_p) = V/\beta_e \cdot s P_p \quad (2.10)$$

Rearranging the equation above and replacing the term  $P_p$  by  $T_L/D_p$ :

$$D_p \omega_m - K_{q,1} X_{v,1} = (C_{1p} - K_{c,1} + V/\beta_e s) T_L/D_p \quad (2.11)$$

If,  $C_{1,p} = K_{c,1}$  is replaced by  $K_{1,1}$ , Eqn. (2.11) becomes:

$$D_p \omega_m - K_{q,1} x_{v,1} = K_{1,1} (1 + V/\beta_e K_{1,1} \cdot s) \cdot T_L / D_p \quad (2.12)$$

From Eqn. (2.12), it can be concluded that the load torque depends on the motor velocity,  $\omega_m$ , and spool valve displacement,  $x_{v,1}$ .

A block diagram for Eqn. (2.12) is shown in Fig. 2.39.

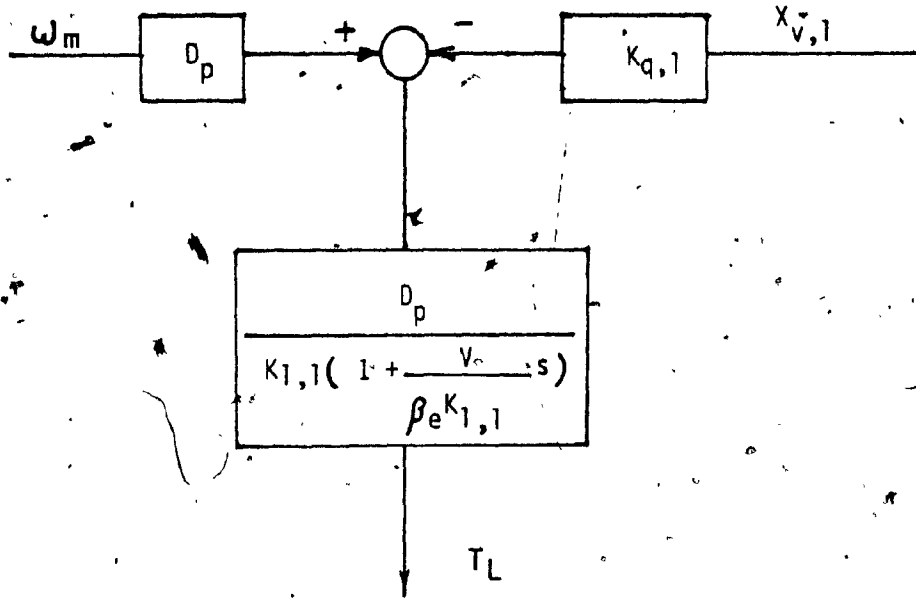


Fig. 2.39. Block Diagram for the Load System.

A brief examination of the block diagram leads to the conclusion that an increase of the motor velocity results in an increase of the load torque. On the other hand, an increase of the spool valve displacement will result in a decrease of the load torque.

The load system imposes some limitations in determining the steady-state characteristics of the valve controlled motor. If the motor is stopped, there is no flow through the pump, therefore no load torque present on the motor shaft. Thus, that system does not allow the motor to reach a stall position.

## CHAPTER 3

### DEVELOPMENT OF EXPERIMENTAL TEST STAND

#### 3.1. Introduction

Experimental tests have been performed in order to derive the characteristics of the servovalve controlled hydraulic motor. A complete test stand was designed and built for that purpose.

The design of the test stand is based on a torque feedback system which has the capability of controlling torque developed by the motor. Figs. 3.1 and 3.2 show pictorial views of the complete experimental set-up.

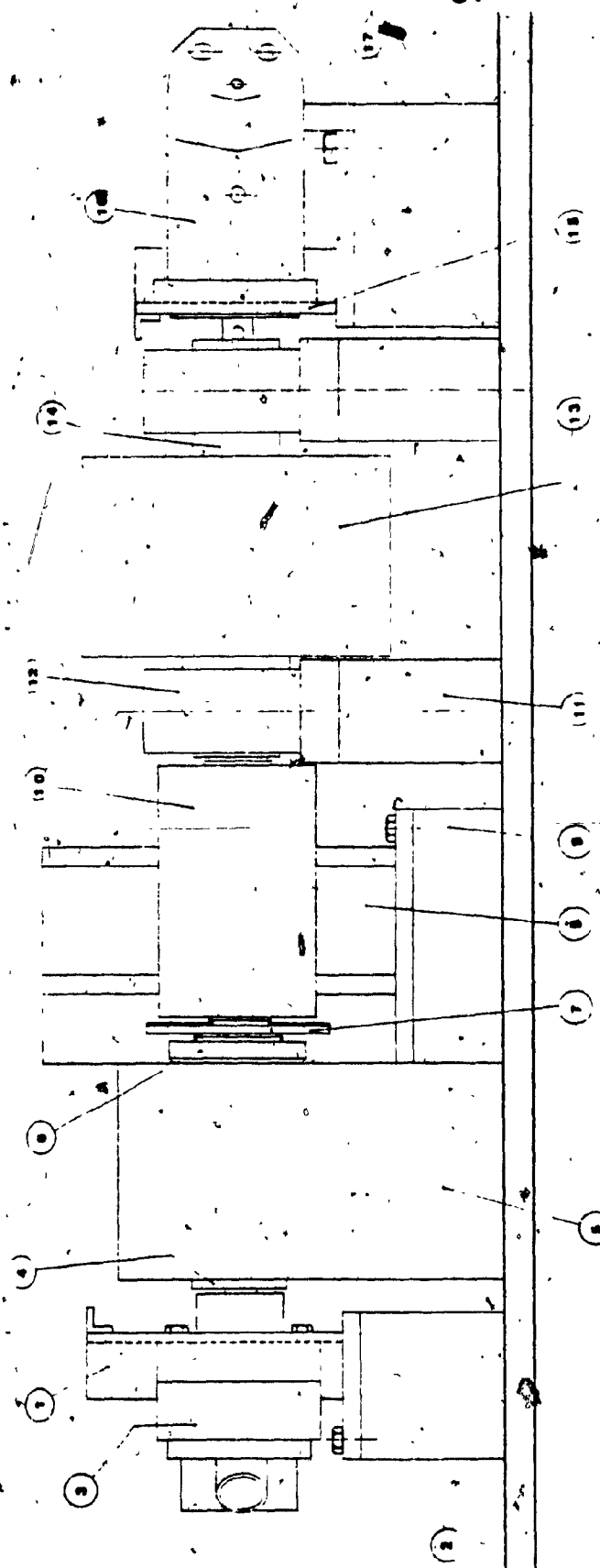
The test stand for this research was designed both to test the motor used in this project, and also as a general purpose test stand suitable for testing other hydraulic motors. Several features were considered during the test stand design:

1. To provide the user with easily mountable (or dismountable) platform for the motor to be tested.

2. To provide all necessary hydraulic connectors to carry out the required tests.

3. To provide transducers and measuring instruments to enable the user to obtain the necessary data with minimum consumption of time.

4. The loading of the motor should be such that it can be tested within a reasonable range of operation.



- 1. Hydraulic Motor Bracket
- 2. Hydraulic Motor
- 3. Transmission Shaft
- 4. Bearing or Mounting
- 6. Locknut
- 7. Gear
- 8. Gear Box
- 9. Gear Box Support
- 10. Foreve Transducer
- 11. Pillow Block Base
- 12. Pillow Block and Bearings
- 13. Plywood
- 14. Transmission Shaft
- 15. Hydraulic Pump Bracket
- 16. Hydraulic Pump Bracket Support
- 17. Hydraulic Pump Bracket Support

Fig. 3.1. Side View of Experimental Test Stand (Complete)

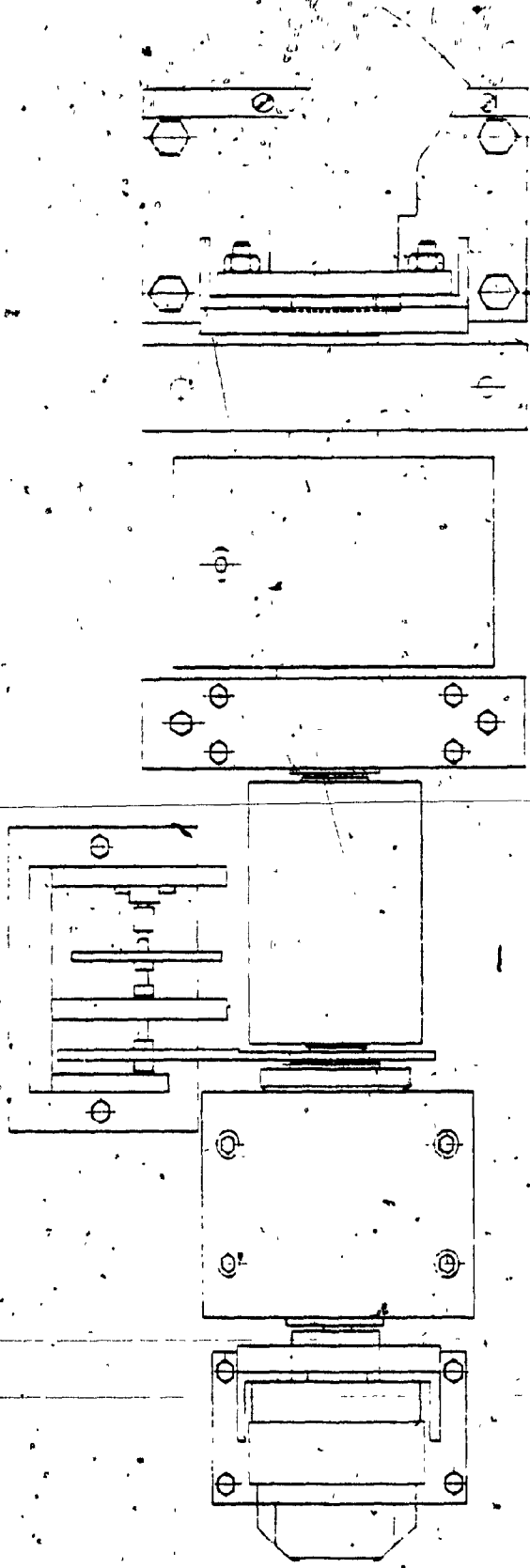


Fig. 3.2. Top View of Experimental Test Stand (Complete).



Fig. 3.2 shows a block diagram of the experimental test stand. It is evident that a closed-loop servo controls the torque imposed on the motor shaft. As was explained earlier in section 2.6.2, the load torque depends on two variables: the motor speed and the valve stroke of the loading valve. When a fixed position for the spool loading valve is selected, then the torque created on the motor shaft should depend only on the motor speed. Thus, in order to impose a constant torque on the motor shaft regardless of the motor velocity, it is necessary to use a closed-loop system to control the valve stroke.

The motor has a displacement of  $0.47 \text{ in}^3/\text{rev}$  and the servovalve which controls the motor has a rated flow of 5 gpm, resulting in a maximum motor speed of 2460 rpm (where  $N=Q/D_m$ ) without taking into account the motor and valve leakages. The pump has a displacement of  $0.298 \text{ in}^3/\text{rev}$  and the loading servovalve has a rated flow of 5 gpm. Thus, the loading pump can be driven up to a speed of 3880 rpm. The motor has a minimum speed of 5 rpm, while that of the pump is 200 rpm.

The motor has a specified torque of 7 lb-in/100 psi, while the theoretical value of the loading pump is 4.7 lb-in/100 psi. For a pressure drop of 1000 psi across the motor, the torque generated by the motor is 70 lb-in.

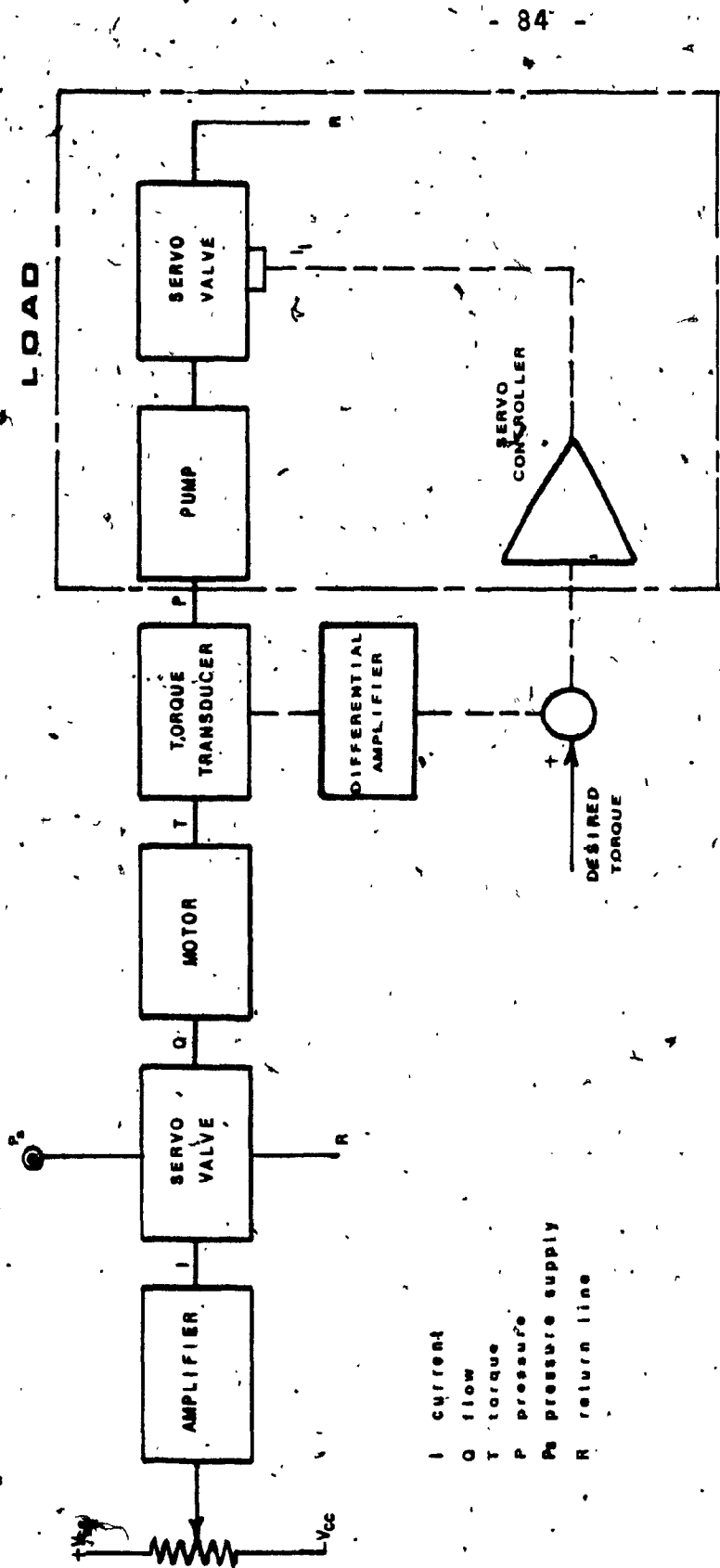


Fig. 3.3. Block Diagram of the Experimental Test Stand.

In order to impose 70 lb-in on the motor shaft, the pump outlet pressure should be equal to 1500 psi. However, the maximum pressure delivered by the pump in the experiments was 1200 psi, resulting in a torque on the motor shaft equal to 56.4 lb-in.

In summary, the following specifications apply to the loading pump-servo valve.

Minimum Velocity	:	200 rpm
Maximum Velocity	:	3880 rpm
Maximum Torque	:	56.4 lb-in (6.37 N-m)

Safety is one of the important considerations in test stand design. Thus, to control the peak pressure value in the hydraulic driving system a pressure relief valve was inserted on the supply line. The digital simulation of the system which was performed before the experimental test stand was built helped predict conditions whereby cavitation could occur in the motor chamber during the transient response tests.

Another important point concerning safety was in the design of the steel discs used as inertial masses. A very careful analysis of the size of bolts and number of them required in each disc was carried out. Bolt size and number was based on the maximum motor shaft angular velocity

used in the tests.

The hydraulic power supply unit, Fig. 3.4, used in all tests contains a variable displacement piston pump which is manufactured by Sperry Vickers, and the specifications are shown in Table 3.1.

Table 3.1 Hydraulic Power Unit Specifications

Theoretical Max. Displ.	23.71 cu. in./rev
GPM Delivery (Rated)	120
Drive Speed	1200 rpm
Pressure: Rated	3000 psi
Maximum	5000 psi

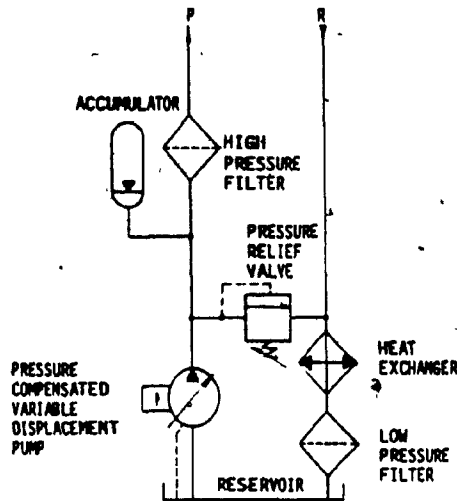


Fig. 3.4. Hydraulic System Schematic Diagram.

### 3.2. Test Stand Design Stage

The design of an appropriate test stand was based on the rotary actuator characteristics to be determined and on the types of tests required to establish or obtain such characteristics. Since the test stand is also intended for future general use, the main features considered in the design were the following:

1. Ease of modification was required so that a sequence of tests could be performed without major changes. For example, when the system was to be tested with no load, the hydraulic pump was removed. In the other tests to determine the dynamic characteristics, several steel discs were attached to the transmission shaft without removing it from the structure.

2. No flexible couplings were used. Better dynamic test results were obtained and backlash effects were eliminated. The use of rigid couplings, however, resulted in an increase in cost because a fine alignment of the rigid coupling was required.

3. High speed, low friction bearings were selected. As stated before, high motor speeds were expected. Low friction bearings were required in order to avoid an

additional increase of the viscous friction torque of the system.

4. Types of load to be used. As mentioned before, two load systems were used. The first consisted of a steel disc attached to one of the transmission shafts. The second was a hydraulic pump controlled by a servovalve to restrict the flow through the pump outlet port.

Each inertial disc was made up of two segments. That allowed tests of the hydraulic rotary actuator using various inertial masses without disassembling any part of the test stand. The two-half discs were joined using bolts. Such design prompted the following considerations:

For the bolts:

- (a) type of bolt to be selected
- (b) bolt-preload
- (c) number of bolts to be used for disc
- (d) length and engagement of the screw threads

For the whole disc:

- (a) maximum angular velocity to be used
- (b) relationship between the internal force and the external force applied
- (c) resultant load on each bolt
- (d) resultant compression of the connected members.

5. Location of Servovalve and Hydraulic Motor. The performance of a closed-loop servo system depends mainly on the resonant frequency of the system, which is determined by the amount of fluid under compression and the inertia mass of the actuator assembly. Because natural frequency is inversely proportional to the square root of the amount of fluid under compression, the amount of such a fluid should be kept to a minimum. Thus, the servovalve was located as near as possible to the hydraulic motor to keep the length of the piping connections to a minimum.

6. Hydraulic Supply System. The hydraulic motor used in this research was a reversible one as was the hydraulic pump used as a load device. Because the motor had to be tested in both directions of rotation, it was necessary to design a hydraulic supply system in such a way that the lines of the pump worked according to the direction of rotation of the motor. For instance, for the clockwise rotation of the motor the return line of the pump turned into the pressure line as the motor switched the direction of rotation. That hydraulic system consisted of a high cylindrical tank to produce at its bottom a pressure head bottom equal to 3 psi, and of four check valves which allowed the change of direction of the hydraulic fluid fed to the pump. Two of the check valves had setting pressure

of 2.5 psi, the other two check valves had setting pressure of 20 psi. A schematic diagram of the hydraulic supply system is shown in Fig. 3.7.

### 3.3 Test Stand Assembly and Tune-Up

1. Assembly. At this stage provisions for additional hydraulic connections were taken. Those connections allowed the use of a pressure transducer connected across the hydraulic motor ports as well as to the main pressure line. A needle valve was also located across the actuator lines to provide a controlled leakage.

A very careful alignment was carried out by checking different parts of the transmission shafts. Thus, disalignment greater than  $\pm 0.004$  inches was not tolerated. Such a fine alignment was dictated by the torque transducer and the rotary actuator specifications.

2. Tune-Up. Some adjustment and balance problems came up during this stage. Thus, the final adjustment for the gears was made after several runs.

Balancing is the technique of correcting or eliminating unwanted vibration forces. Such forces cause vibrations which subject bearings to repeat loads that cause



parts to fail prematurely by fatigue. Vibrations also cause an increase in the ripple of angular velocity and torque signals which are not desirable. In order to balance parts, an arrangement as shown in Fig. 3.5 was built.

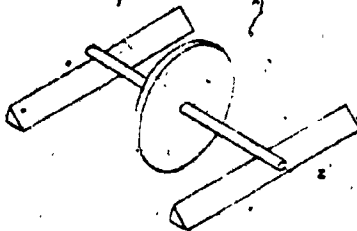
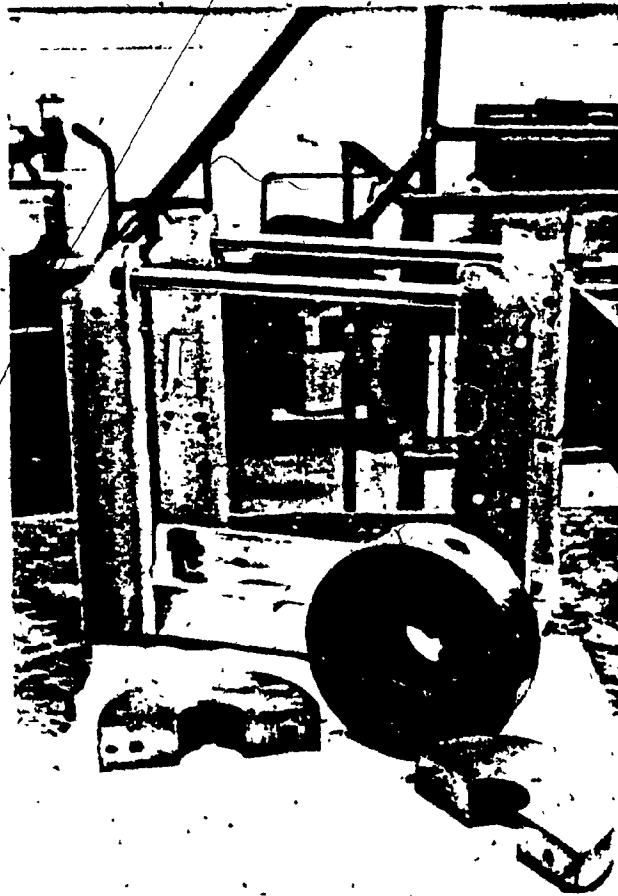


Fig. 3.5. Equipment for Balancing Inertial Masses and Transmission Shaft..

### 3.4. Test Stand for Steady-State and Dynamic Characteristics.

Fig. 3.6 shows a schematic of the experimental test stand for testing the characteristics of the servovalve controlled hydraulic motor in steady-state without load. To determine the steady-state characteristics for the loaded motor a test stand configuration as shown in Fig. 3.7 was used.

Fig. 3.8 shows a schematic of the experimental test stand for testing the dynamic characteristics of the valve controlled hydraulic motor. In this case, a pure inertial mass was used as a load system.

Details of all tests carried out are described in Chapters 5 and 6.

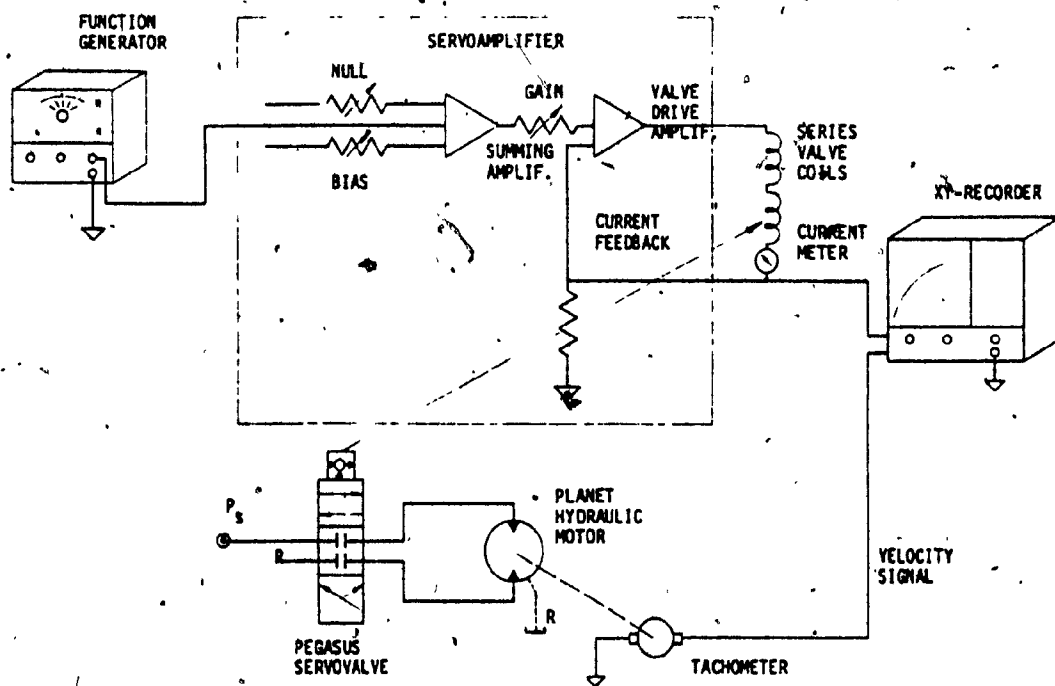


Fig. 3.6. Experimental Test Stand Schematic.  
Steady-State Characteristics-No Load.

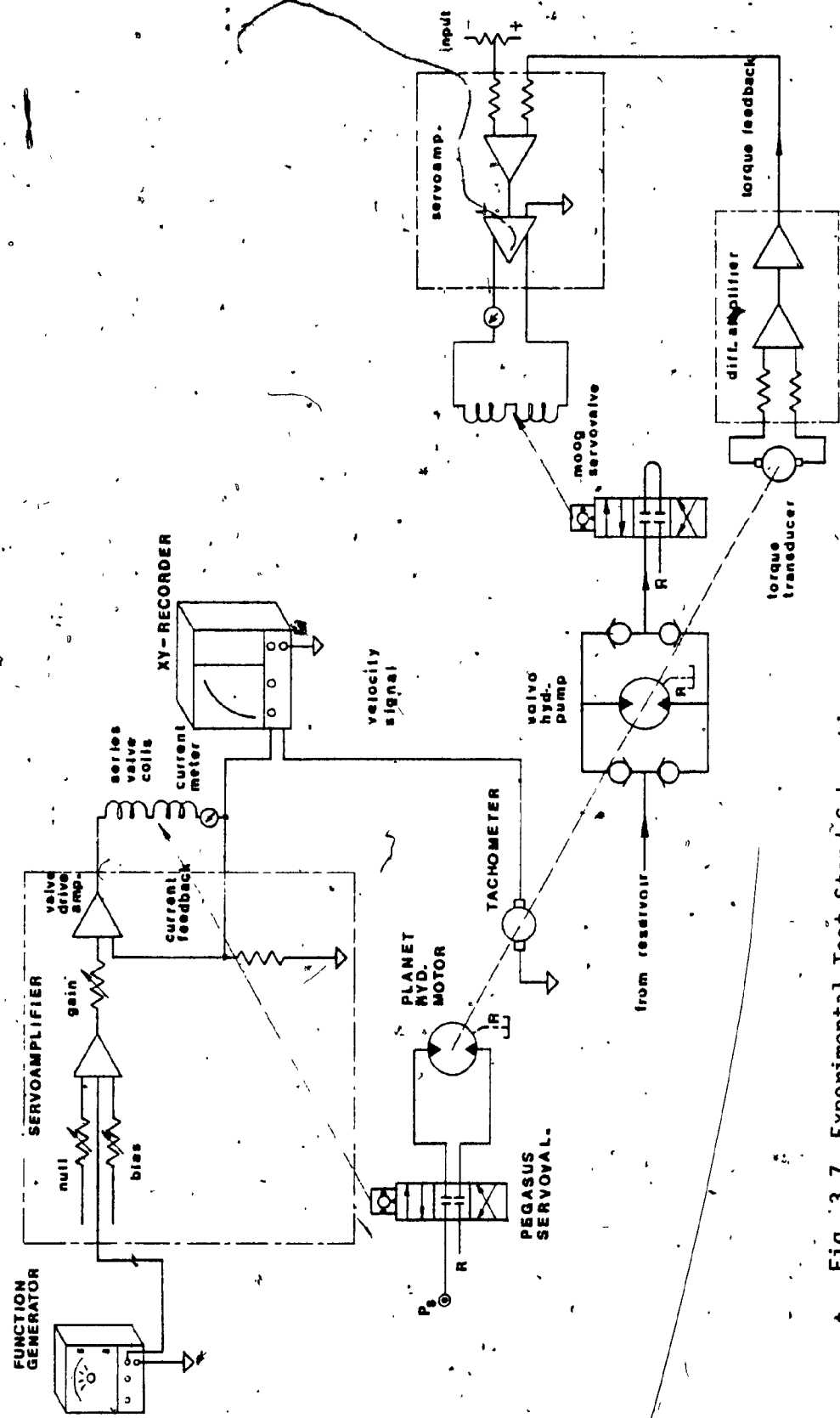


Fig. 3.7. Experimental Test Stand Schematic. Steady State Characteristics-Load Applied.

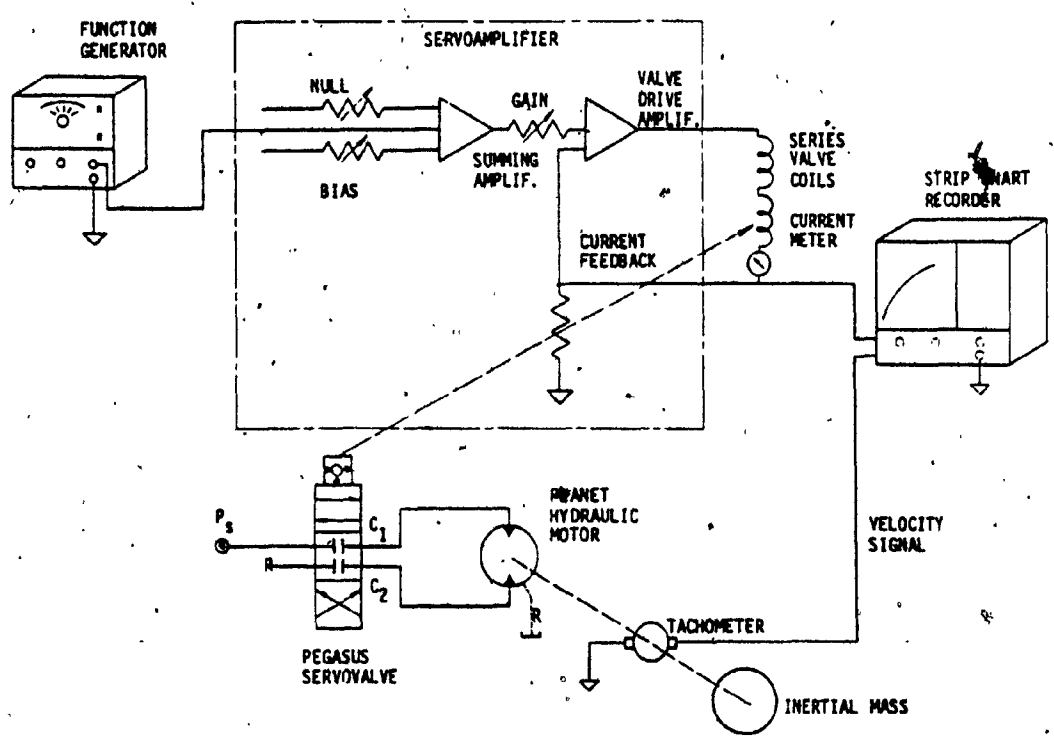


Fig. 3.8. Experimental Test Stand Schematic.  
Dynamic Characteristics-Inertial Load.

## CHAPTER 4

### MODELLING OF A VALVE CONTROLLED MOTOR SIMULATION OF THE OPEN LOOP VELOCITY TRANSIENT RESPONSE

#### 4.1 General

The purpose of modelling the valve controlled motor was to develop a computer simulation model to aid in the planning of the system test parameters such as the selection of servovalve current step size for the open-loop velocity transient response tests.

The selection of the servovalve current step size plays an important role. When the size of the step current fed to the servovalve coils is too large while inertia load is present, excessive pressure transient peaks are produced in the motor lines. In addition, cavitation in the return line may occur.

Another important aspect at this stage of the research was an improved understanding of the system behaviour. Thus, the effects of parameters such as the servovalve and motor leakage, motor friction, inertia of load, on overall system performance were comprehended more fully.

A system can be represented schematically by a block diagram, each block being associated with it a transfer

function describing the relevant input-output relationship. Also, a complex block diagram incorporating many elements with relatively simple transfer functions can be reduced to a single block with a higher order transfer function relating the system output to the system input. In studying the system behaviour it is desirable to determine the system reaction to various input or disturbance functions.

If the form of both the input function and the transfer function is simple, the dynamic response can be determined analytically by solving the governing differential equation. If the response is required for a number of different input functions, or for a number of different system parameters, the analytical approach may be ineffective.

It is useful to be able to obtain time response traces quickly, particularly for complex systems, or where it is necessary to investigate the effect of parameter changes. This can be satisfactorily achieved by computer solution of the governing equations. Computer solutions can be achieved by means of analogue computers or digital computers.



In this work, the evaluation of system performance is carried out by constructing analytical models using MIMIC, a digital computer simulation language.

The constants and parameters used in the digital simulation were obtained as follows:

1. Manufacturers' Data.

Motor Displacement,  $D_m$  ( $m^3/\text{rad}$ )

Oil Density,  $\rho$  ( $\text{kg}/m^3$ )

Motor Leakage Coefficient,  $C_l$  ( $m^3/s$ ) ( $N/m^2$ )

Servo valve constant,  $K_v = \pi D_s$  (m)

where  $\pi = 3.1416$

$D_s =$  spool diameter

Servo valve rated flow,  $Q_{\max}$  ( $m^3/s$ )

Servo valve rated current,  $I_{\max}$  (mA)

Servo valve underlapped region,  $X_{vo}$  (m)

2. Experimental Data. As part of the project, tests to determine the motor internal coefficient,  $C_{TF}$ , as well as the total viscous damping coefficient of the system,  $B_m$ , were performed.

Motor internal coefficient,  $C_{TF}$  ( $m^3$ )

Total viscous damping coefficient (it includes motor, bearings internal damping),  $B_m$  (N-m-s)

3. Measured Data.

Volume of oil under compression,  $V_1, V_2$  ( $m^3$ )

4. Calculated Data

Equivalent time constant of the servovalve,  
 $T_v$  (s).

Servovalve spool displacement gain,  $K_x$  (m/mA)

Inertia of load,  $J_L$  ( $N-m-s^2$ )

5. Estimated Data

Effective bulk modulus,  $\beta_e$  ( $N/m^2$ ) [27]

Discharge coefficient,  $C_d$  [27]

The numerical values for all the coefficients are given in Appendix B.

In the first part of this chapter the development of a mathematical model of all essential system components is presented. In the second part, the digital simulation model using the MIMIC language is presented. Finally, some experimental and theoretical results are given.

#### 4.2. Development of the Model

The system model was segmented into modules comprising models of individual components, to accommodate the changes and corrections required during system development. A schematic diagram of the system is illustrated in Fig. 4.1. The diagram shows all important system parameters and constants. The following paragraphs describing the development of individual component models, should be read with reference to this diagram.

For the dynamic modelling, the time domain approach was chosen, since it is suitable for MIMIC simulation.

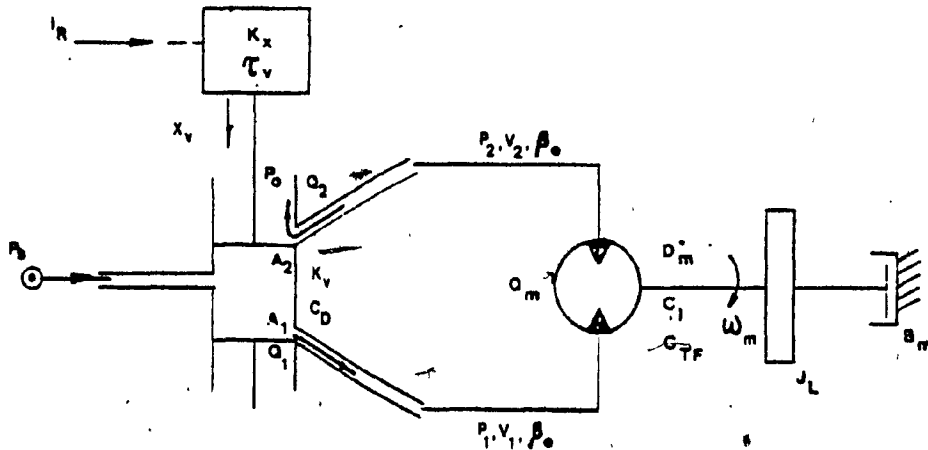


Fig. 4.1. Simplified System Diagram for Modelling Purposes

#### 4.2.1. Input Reference Signal

Since dealing with an open-loop servo system, it is not necessary to include in the model the part corresponding to the servocontroller. Thus, the input signal to the servovalve coils can be modelled as a step function whose amplitude can be varied.

$$I_R = \begin{cases} 0, & t < 0 \\ I_R, & t \geq 0 \end{cases} \quad (4.1)$$

#### 4.2.2. Electrohydraulic Servovalve

a) Servovalve transfer function. A first-order relationship is assumed between spool position and input current:

$$X_V = K_X / \tau_V \int_0^t (I_R - I_F) dt + X_{V0} \quad (4.2)$$

where the spool position feedback signal is given by:

$$I_F = X_V / K_X \quad (4.3)$$

b) Flow Equations. The output stage of the servovalve is the four-way spool valve. With respect to the lap, the spool valve is modelled as slightly underlapped, according to the technical specifications given by the servovalve manufacturer. A schematic of the underlapped spool valve is shown in Fig. 4.2.

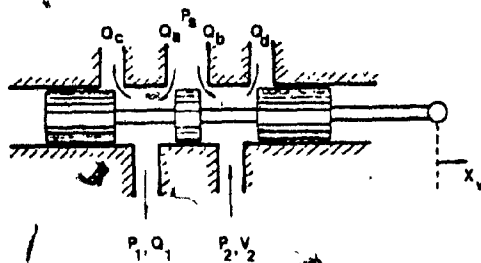


Fig. 4.2. Underlapped Spool Valve

The flow equations are given as follows [44]:

$$\text{If } X_{v0} + X_v > 0 : Q_a = C_d K_v (X_{v0} + X_v) \sqrt{\frac{2}{\rho} (P_s - P_1)} \quad (4.4)$$

$$Q_d = C_d K_v (X_{v0} + X_v) \sqrt{\frac{2}{\rho} P_2} \quad (4.5)$$

$$\text{If } X_{v0} - X_v > 0 : Q_b = C_d K_v (X_{v0} - X_v) \sqrt{\frac{2}{\rho} (P_s - P_2)} \quad (4.6)$$

$$Q_c = C_d K_v (X_{v0} - X_v) \sqrt{\frac{2}{\rho} P_1}$$

$$\text{If } X_{vo} + X_v \leq 0 : Q_a = Q_d = 0 \quad (4.7)$$

$$\text{If } X_{vo} - X_v \leq 0 : Q_b = Q_c = 0 \quad (4.8)$$

The flow  $Q_1$  is given by:

$$Q_1 = Q_a - Q_c \quad (4.9)$$

The flow  $Q_2$  is given by:

$$Q_2 = Q_d - Q_b \quad (4.10)$$

All the servovalve coefficients used in this part are detailed in Appendix A.

#### 4.2.3. Conduits

The pressure losses in the conduits are neglected. The model expresses the pressure build-up due to the difference between the flow-in and flow-out of the volume of control applied to each motor chamber. The effects of the oil under compression has been included in the model, and the oil temperature and density have been considered to be constant.

Application of the continuity equation to each motor chamber yields:

$$Q_1 - Q_m = V_1 / \beta_e \cdot dP_1 / dt \quad (4.11)$$

Solving the above equation for  $P_1$ :

$$P_1 = (\beta_e / V_1) \int_0^t (Q_1 - Q_m) dt + P_{10} \quad (4.12)$$

and,  $-Q_2 + Q_m = V_2 / \beta_e \cdot dP_2 / dt \quad (4.13)$

Solving the above equation for  $P_2$ :

$$P_2 = (\beta_e / V_2) \int_0^t (-Q_2 + Q_m) dt + P_{20} \quad (4.14)$$

#### 4.2.4. Hydraulic Motor

The hydraulic motor shall be described by a flowrate and torque equations.

a) Flowrate equation. It can be assumed that the leakage flow is proportional to the pressure difference across the motor:

$$Q_m = D_m \omega_m + C_l P_L \quad (4.15)$$

where  $C_L$  is the leakage coefficient and can be obtained from  $Q_m$  vs  $P_L$  plot at a motor constant velocity.

b) Torque equation. The form of torque equation can be assumed as:

$$T_m = D_m \omega_m - C_{TF} P_L \quad (4.16)$$

where  $C_{TF}$  is the Coulomb friction coefficient and can be obtained from  $T_m$  vs  $P_L$  plot for the motor shaft locked. The term which corresponds to the viscous friction coefficient of the motor has been included in the equation of the load, Eq. 4.17. Such a term,  $B_m$ , was not only obtained for the hydraulic motor, but also for the rest of system rotating parts (bearings which support the shafts of transmission).

#### 4.2.5. Load

The load equation is based on the acceleration of the inertia mass by the motor torque. The model includes the inertia torque,  $J_L d\omega_m/dt$ , and friction torque:  $C_{TF} P_L$ , and  $B_m \omega_m$ . Thus, for the velocity of the load:

$$\omega_m = (1/J_L) \int_0^t (T_m - B_m \omega_m) dt + \omega_{m0} \quad (4.17)$$



#### 4.3. Mimic Model

A digital simulation for the system evaluation was developed using MIMIC, a digital simulation language. The MIMIC listing is given in Appendix B. The MIMIC model includes all components and calculation loops described in Section 4.2.

#### 4.4. Simulation vs. Experimental Results

Fig. 4.3 shows the experimental and theoretical results of the velocity transient response for step inputs of 18 mA and 24 mA. In Fig. 4.4 are illustrated the results of the velocity transient response for a step input of 24 mA, with a larger inertia load used. Finally, in Fig. 4.5, the pressure transients in the motor pressure line for the same inertia load and two different step functions of current are presented.

As can be noted, a good agreement between the experimental and theoretical results has been achieved.

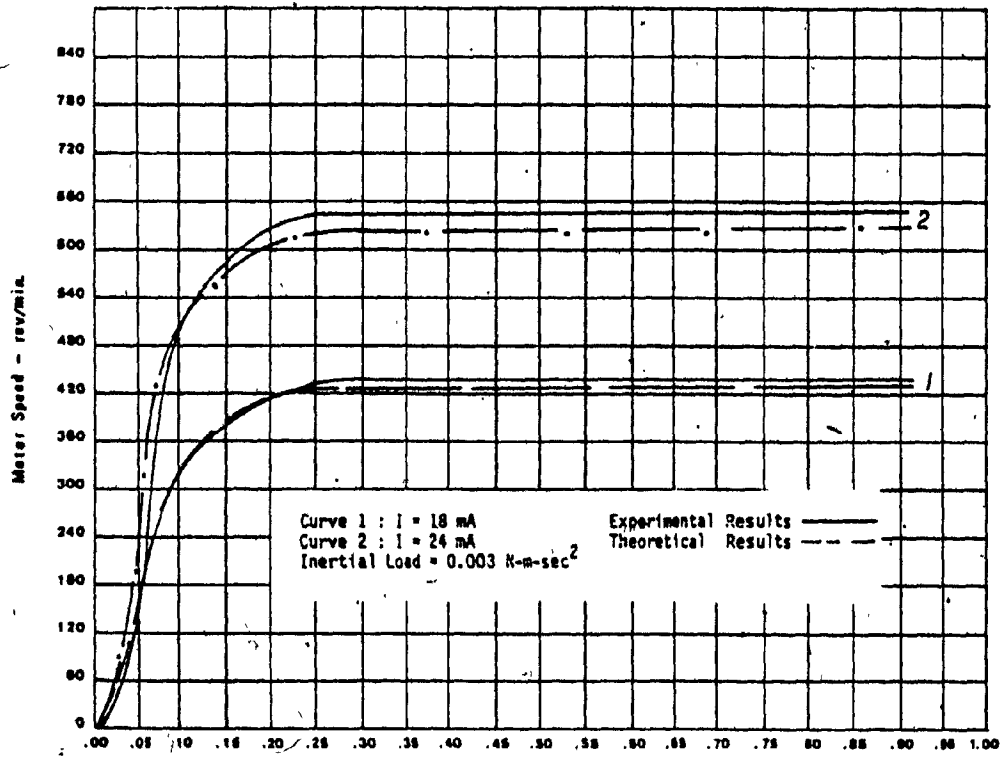


Fig. 4.3. Velocity Transient Response for Step Functions of 18 mA and 24 mA. Experimental and Theoretical Results

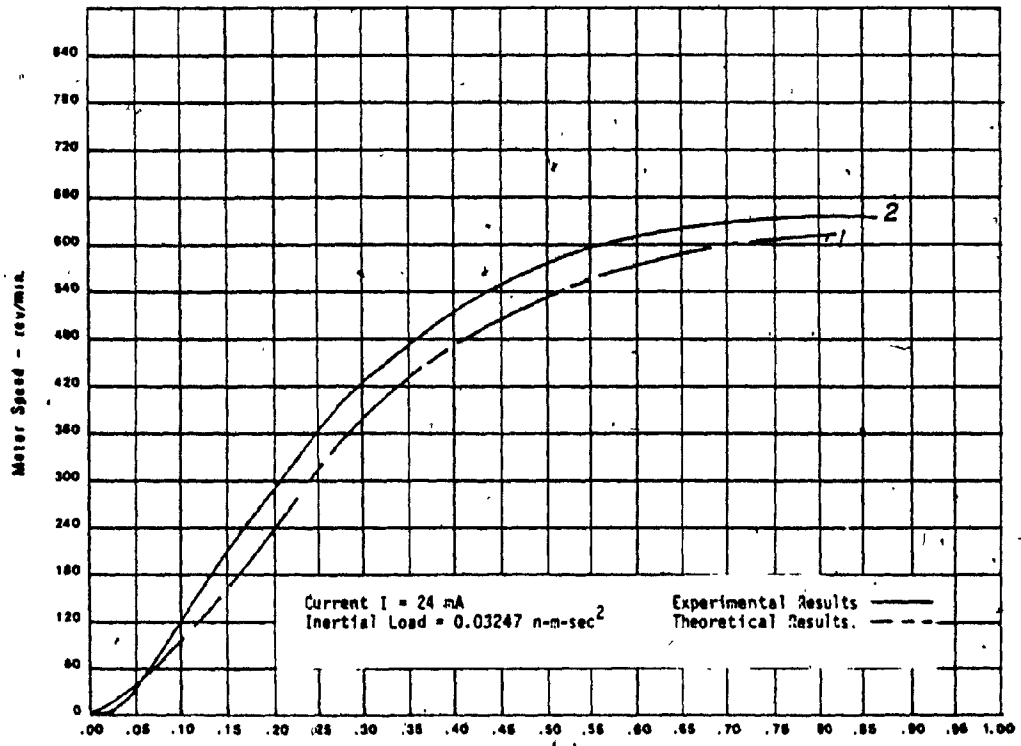


Fig. 4.4. Velocity Transient Response for Step Function of 24 mA. Experimental and Theoretical Results.

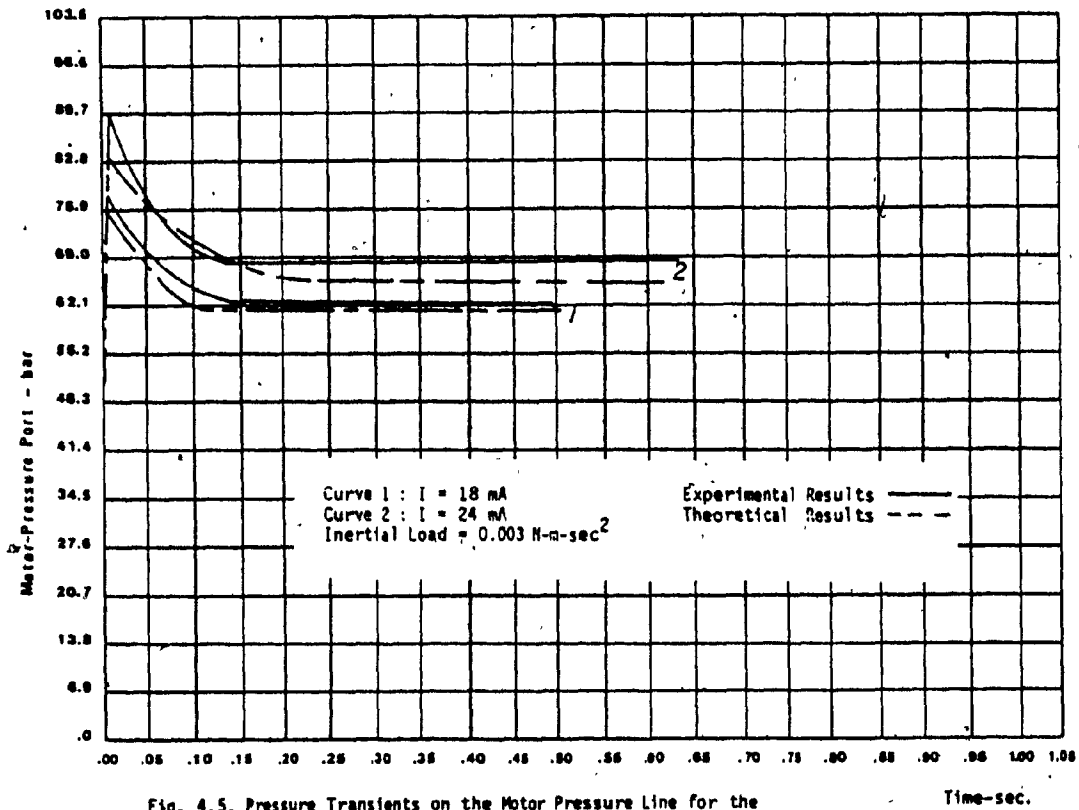


Fig. 4.5. Pressure Transients on the Motor Pressure Line for the same Inertial Load. Experimental and Theoretical Results.

## CHAPTER 5

### SERVOVALVE-MOTOR PERFORMANCE: STEADY-STATE CHARACTERISTICS

#### 5.1 General

This chapter deals with the servovalve-motor characteristics obtained for steady-state conditions.

The experimental set-up shown in Fig. 5.1 was used to obtain the unloaded and loaded characteristics for the valve-motor combination. A closed-loop torque servo system on the loading section was used to select the loading torque.

The following analysis ignores dynamic conditions as well as non-linear terms due to torque developed by the hydraulic motor.

The flow rate through the electrohydraulic servovalve can be approximated as a linear function of input current and load pressure in the region of an operating point:

$$Q_v = K_Q I - K_C P_L \quad (5.1)$$

where  $I$  = servovalve current, mA

$K_Q$  = Flow gain coefficient,  $m^3/s/mA$

$K_C$  = Pressure gain coefficient,  $m^3/s/(N/m^2)$

$P_L$  = Pressure drop across the load,  $N/m^2$

In the case of a servovalve controlled fluid motor, Fig. 5.1, the total flow rate through the valve must be equal to the flow through the motor including the leakage flow. The flow due to the compressibility of oil is neglected. Thus:

$$K_{QI} - K_{cPL} = Q_m + Q_l \quad (5.2)$$

Flow rate through the motor is given by  $Q_m = D_m \omega_m$   
where  $D_m$  = Motor displacement,  $m^3/\text{rad}$   
 $\omega_m$  = Motor angular velocity,  $\text{rad/s}$

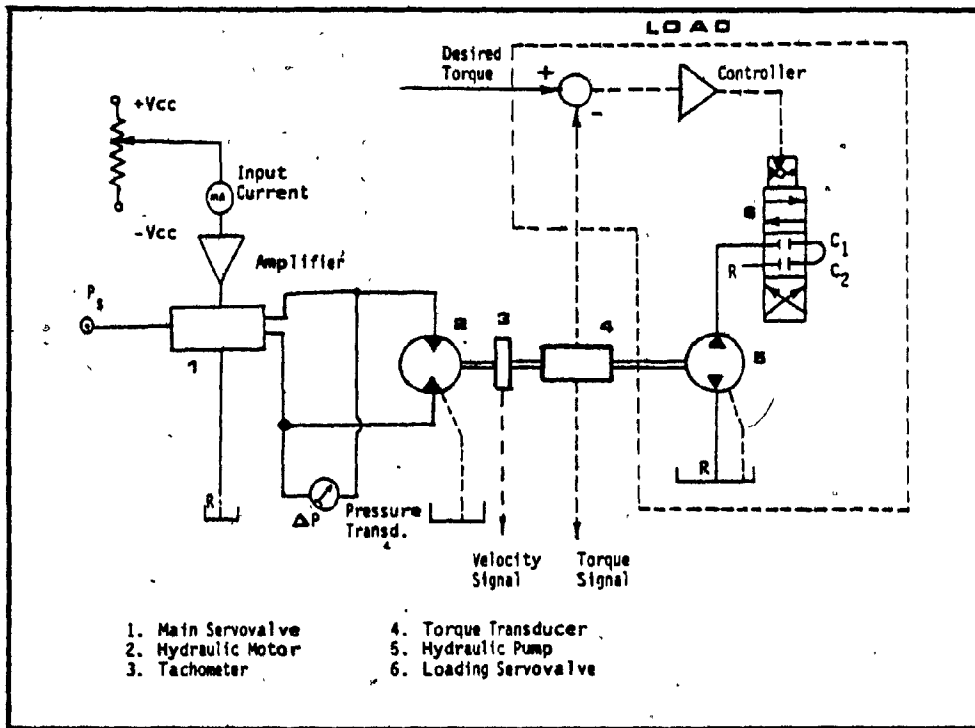


Fig. 5.1. Simplified Experimental Set-Up for Determining Steady-State Characteristics.

7

Motor leakage in hydraulic motors can be classified as internal or cross-port leakage between the motor chambers, and external leakage from each motor chamber past the pistons to case drain. Because all mating clearances in a motor are intentionally made small to reduce losses, these leakage flows are laminar and, therefore, proportional to the pressure [27]. Total leakage flow in a motor can be calculated by using the equation  $Q_l = C_l P_l$ .  $C_l$  is the leakage coefficient and can be obtained from  $Q_m$  versus  $P_l$  plot at a constant motor velocity.

Substituting the terms for  $Q_l$  and  $Q_m$  into Eq. (5.2), one has:

$$K_Q I - K_C P_L = D_m \omega_m + C_l P_l \quad (5.3)$$

Positive displacement motors are those in which energy is periodically added by application of force, to one or more movable boundaries of any desired number of enclosed fluid-containing volumes. In the positive displacement machines fluid passes through the inlet into a chamber which expands in volume and fills with fluid. The volume expansion causes shaft rotation in a motor in contrast to a pump where the reverse is true, that is, the volume expansion is caused by shaft rotation.



In positive displacement motors the torque developed by hydraulic motors is given by:

$$T_m = D_m P_L - B_m \omega_m = T_L \quad (5.4)$$

where,  $B_m$  = Viscous damping coefficient, N-m-s.

$T_L$  = Torque delivered to the load, N-m

Combining Eqns. (5.3) and (5.4), Eq. (5.5) results in:

$$D_m \omega_m + (K_C + C_1) B_m / D_m \times \omega_m = K_Q I - (K_C + C_1) T_L / D_m \quad (5.5)$$

Rearranging the above equation:

$$\omega_m = \frac{K_Q}{D_m + (K_C + C_1) B_m / D_m} I - \frac{(K_C + C_1) / D_m}{D_m + (K_C + C_1) B_m / D_m} T_L \quad (5.6)$$

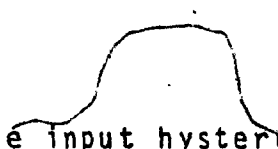
The above equation shows how the motor speed,  $\omega_m$ , the main servovalve current,  $I$ , and the loading torque,  $T_L$ , are related. Thus, motor speed depends not only on the servovalve current but also on the load torque applied to the hydraulic motor.

## 5.2. Unloaded Valve-Motor Characteristics

Two important tests were performed to determine the unloaded valve-motor characteristics. In this part of the work the hydraulic pump (5), and servovalve (6) were not used.

### 5.2.1. Motor Shaft Angular Velocity versus Servovalve Current Characteristics

Fig. 5.2 shows how the motor speed varies as the servovalve current is cycled from negative to positive rated current. The unloaded motor speed/valve current characteristic allows to see the servovalve hysteresis and the motor friction effects.



In order to illustrate the input hysteresis value better, Fig. 5.3 is shown indicating a hysteresis width of 3mA. The hysteresis width is composed of servovalve hysteresis equal to 1.5 mA (servovalve manufacturer's data) and the motor friction torque effects at starting, which in this case are equal to 1.5 mA. Thus, for a greater friction torque at starting of the motor, a greater hysteresis width should be expected.

The velocity gain of the valve-motor combination is also determined from this test. The velocity gain is the basic steady-state gain used in the servo-system design. It is the slope of the motor speed/servo valve current plot. The value equal to 28.70 rev/min per mA was obtained.

As Eq. (5.6) shows, the velocity gain is affected by the leakage coefficients of the servo valve and motor,  $K_c$  and  $C_1$  respectively, as well as by the viscous damping coefficient,  $B_m$ .

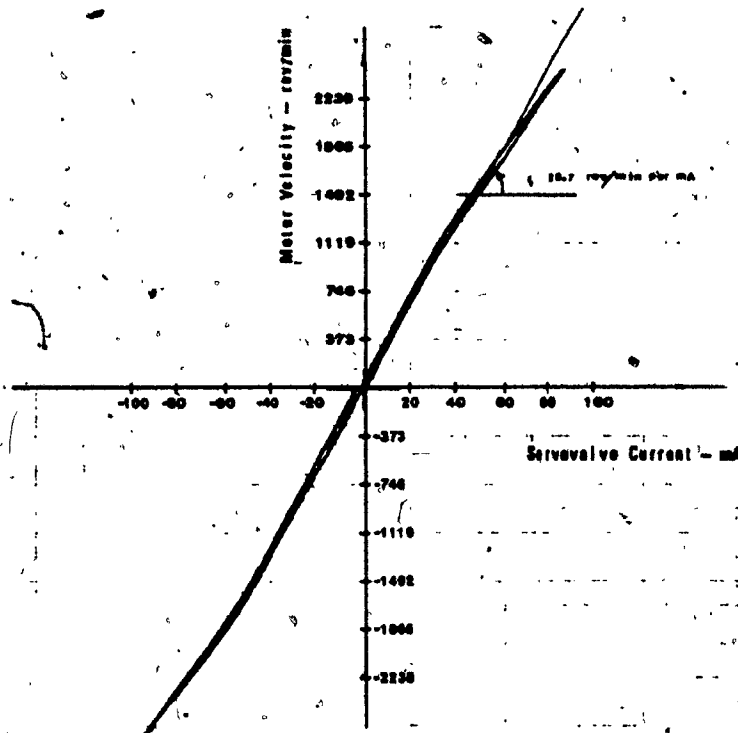


Fig. 5.2. Unloaded Motor Speed/Servo Valve Current Characteristics.

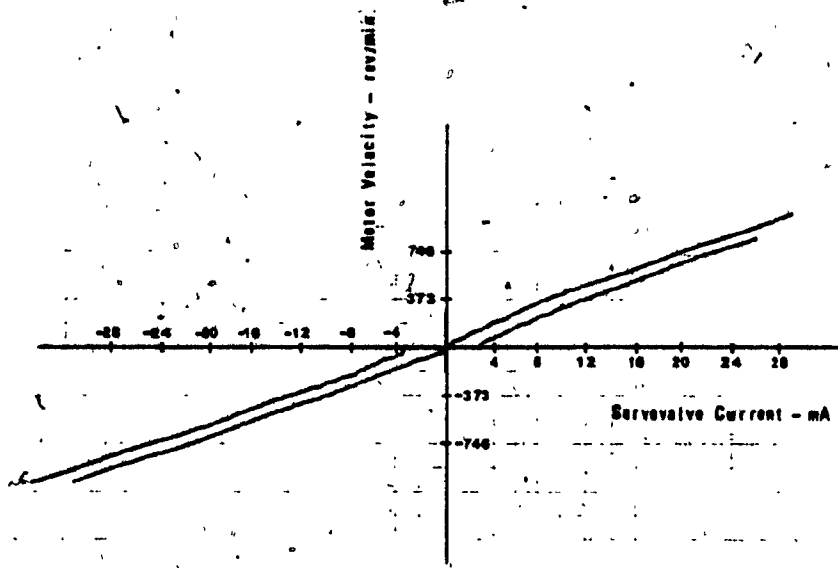


Fig. 5.3. Unloaded Motor Speed/Servo Valve Current Characteristics-Hysteresis Region Amplified.

### 5.2.2 Viscous Damping Coefficient

Fig. 5.4 shows the unloaded pressure difference across the hydraulic motor versus the motor speed characteristic. Important results can be observed: (a) breakout pressure peaks of the motor which have an adverse effect on the stiffness, stability, and low speed behaviour of the closed-loop system [1], and (b) the viscous damping coefficient of the motor-torque transducer-bearings combination. The pressure difference loss gradient is 9.22 bar (133 psi) per 1000 rev/min.

The viscous damping coefficient is calculated as follows. The torque developed by the hydraulic motor is given by:

$$T_m = D_m P_L - B_m \omega_m - C_{TFPL} = J_L \cdot d \omega_m / dt + T_L \quad (5.7)$$

For steady-state conditions, the term corresponding to the inertial mass is zero, and because no external load was applied to the hydraulic motor to determine the coefficient  $B_m$ ,  $T_L$  is also equal to zero. Hence, Eq. (5.7) can be written as:

$$D_m P_L = B_m \omega_m + C_{TFPL} \quad (5.8)$$

where  $C_{TF}$  = motor internal friction coefficient. That coefficient was obtained experimentally (see Section 5.3) and the value is equal to  $0.5375 \times 10^{-6} \text{ m}^3$ . From Fig. 5.4, for a motor speed of 1120 rev/min, a motor pressure difference of 24.08 bar (349 psi) is obtained. Replacing the values for  $C_{TF}$ ,  $\omega_m$ , and  $P_L$  into Eq. (5.8) a value equal to 0.012 N-m-s for  $B_m$  is obtained.

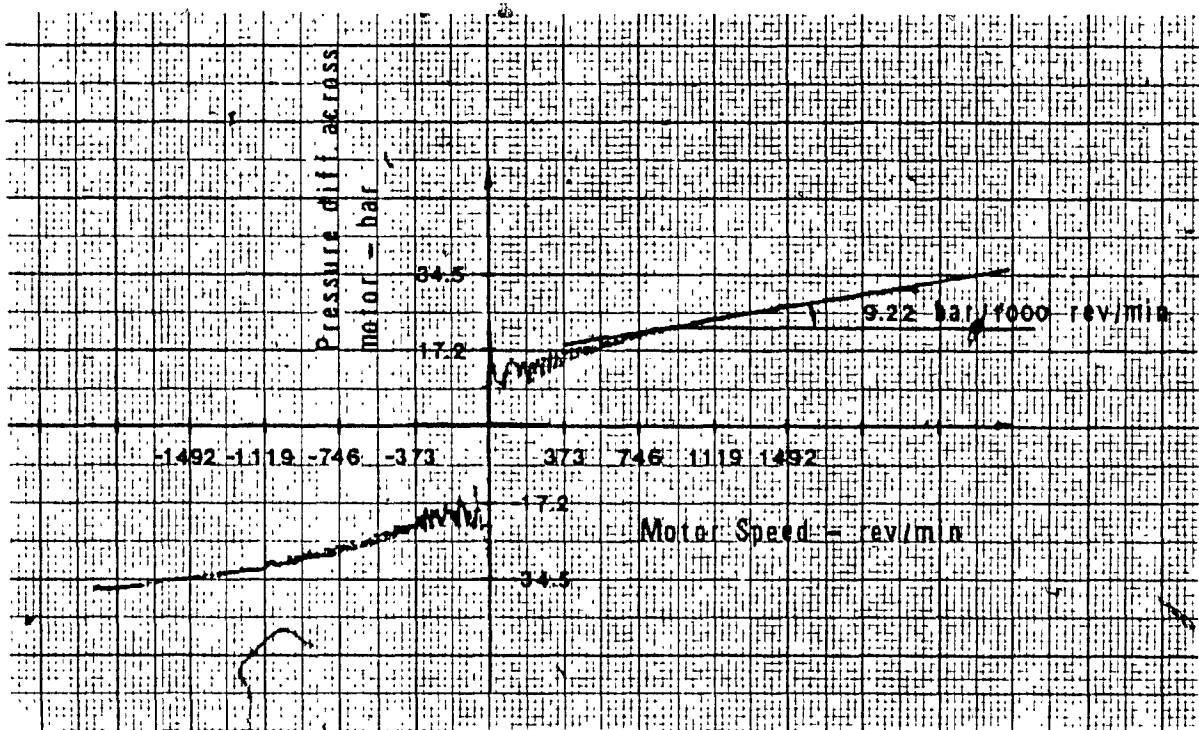


Fig. 5.4. Unloaded Pressure Diff. across the Motor versus Motor Speed Characteristics.

### 5.3. Hydraulic Motor Friction Torque

Fig. 5.5 shows a plot of the torque developed by the motor against its pressure drop as the motor shaft is locked. This test was done to define the non-linear frictional term,  $C_{TF}$ .

Fig. 5.5 also shows the linear equation of the torque developed by the motor without friction effects. The deviation between the experimental and theoretical curves defines the internal friction effects of the motor. From Fig. 5.5, a motor friction coefficient,  $C_{TF}$ , of  $0.5375 \times 10^{-6} \text{ m}^3$  is obtained. The motor friction is affected by the pressure drop across the motor but is independent of motor speed.

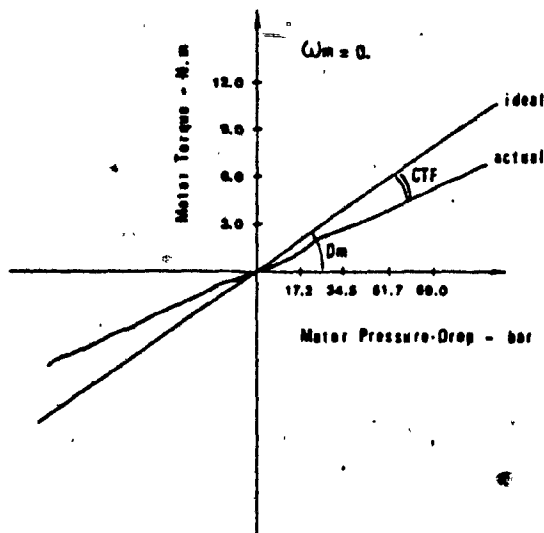


Fig. 5.5. Motor Torque versus Motor Pressure Drop-Shaft Locked.



#### 5.4. Loaded Valve-Motor Characteristics

In this section the complete test system as illustrated in Fig. 5.1 has been used. As stated in Chapter 2, the loading torque to the motor depends on two variables: the servovalve spool position,  $X_v$ , and the motor speed,  $m$ . In order to generate a constant loading torque applied to the motor, a closed-loop servo torque was implemented.

Results presented on the following two sections were obtained using a hydraulic motor with the same technical specifications as the one used in the previous sections. This motor suffered a motor shaft damage and had to be replaced.

The motor tested differed significantly in small signal characteristics. Thus, in Fig. 5.6 a dead-band of 10 mA is observed, while the dead-band of the second motor was only 3 mA (Fig. 5.2).

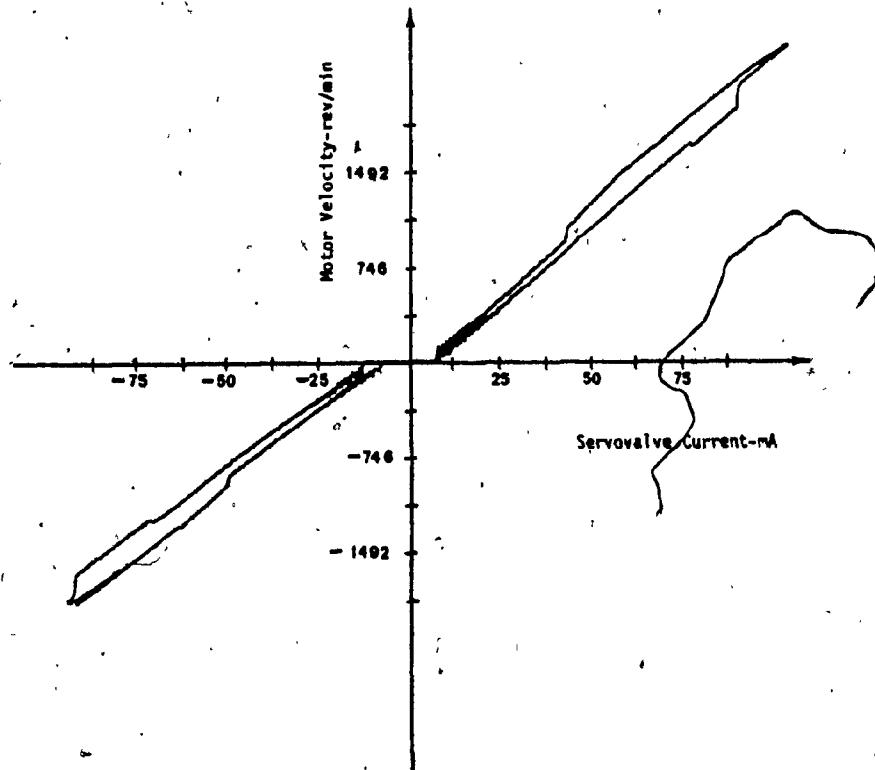


Fig. 5.6. Unloaded Motor Speed/Servovalve Current Characteristics. Motor Employed to Determine the Loaded Valve-Motor Characteristics.

#### 5.4.1 Angular Velocity of the Motor Shaft versus Motor Torque Characteristics

Fig. 5.7 depicts the motor speed versus motor torque characteristics as several values of servovalve currents are applied.

The curves were obtained as follows:

1. A value for the current of the main servovalve was chosen (25 mA).
2. No load was applied to the motor shaft so that rated current was fed to the motor coils of the loading servovalve, and the hydraulic motor reached a maximum speed for the current of 25 mA.
3. Electrical signals from the torque transducer and tachometer were connected to the XY-plotter.
4. The desired torque of the closed-loop was varied in such a way to apply to the hydraulic motor shaft different loading torque levels.
5. A different current for the main servovalve was selected and the above steps were repeated.

As a result of the above procedure, the set of curves shown in Fig. 5.7 was obtained. The results can be interpreted with the help of Eq. (5.6). With no load applied to the motor, maximum motor speed is reached. For a greater value of current fed to the servovalve, a greater motor speed results. The curves obtained are a set of straight lines with a slope given by the coefficient of the variable,  $T_L$ . The slope has a negative value. For  $T_L = 0$  the motor runs at maximum speed. With increasing load torque, the motor speed decreases until it stalls.

5.4.2. Angular Velocity of Motor Shaft versus Servovalve  
Current Characteristics

Fig. 5.8 shows the set of curves obtained as a fixed load torque is applied to the motor and the system servovalve is cycled from zero to positive rated current and from zero to negative rated current. Five different torque levels applied to the motor were selected.

From Fig. 5.8 a dead-band of about 10 mA is observed. The dead-band is composed of a servovalve dead-band equal to 1.5 mA (servovalve manufacturer's data) and the motor friction torque at starting, which in this case is equal to 8.5 mA.

Results obtained in this section can be explained again by using Eq. (5.6). The higher loading torque is selected, the lower values for the motor speed are obtained.

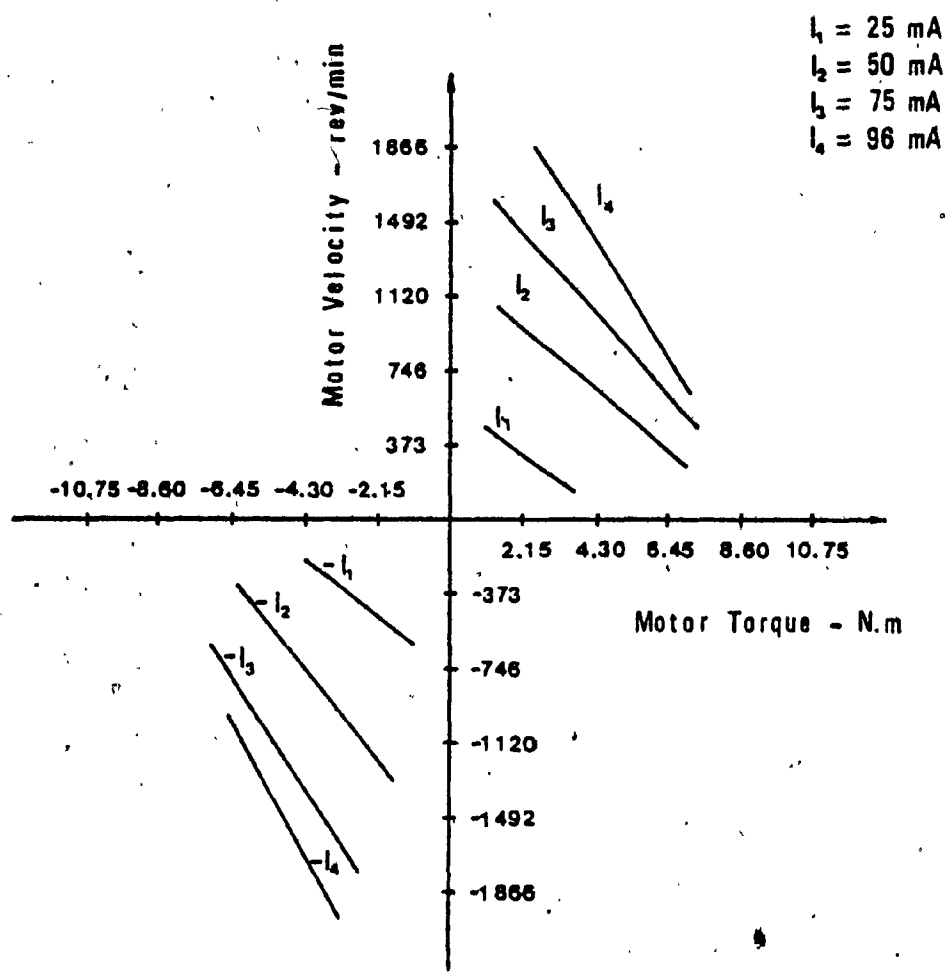


Fig. 5.7. Motor Speed/Motor Torque Characteristics for Several Values of Servovalve Current .

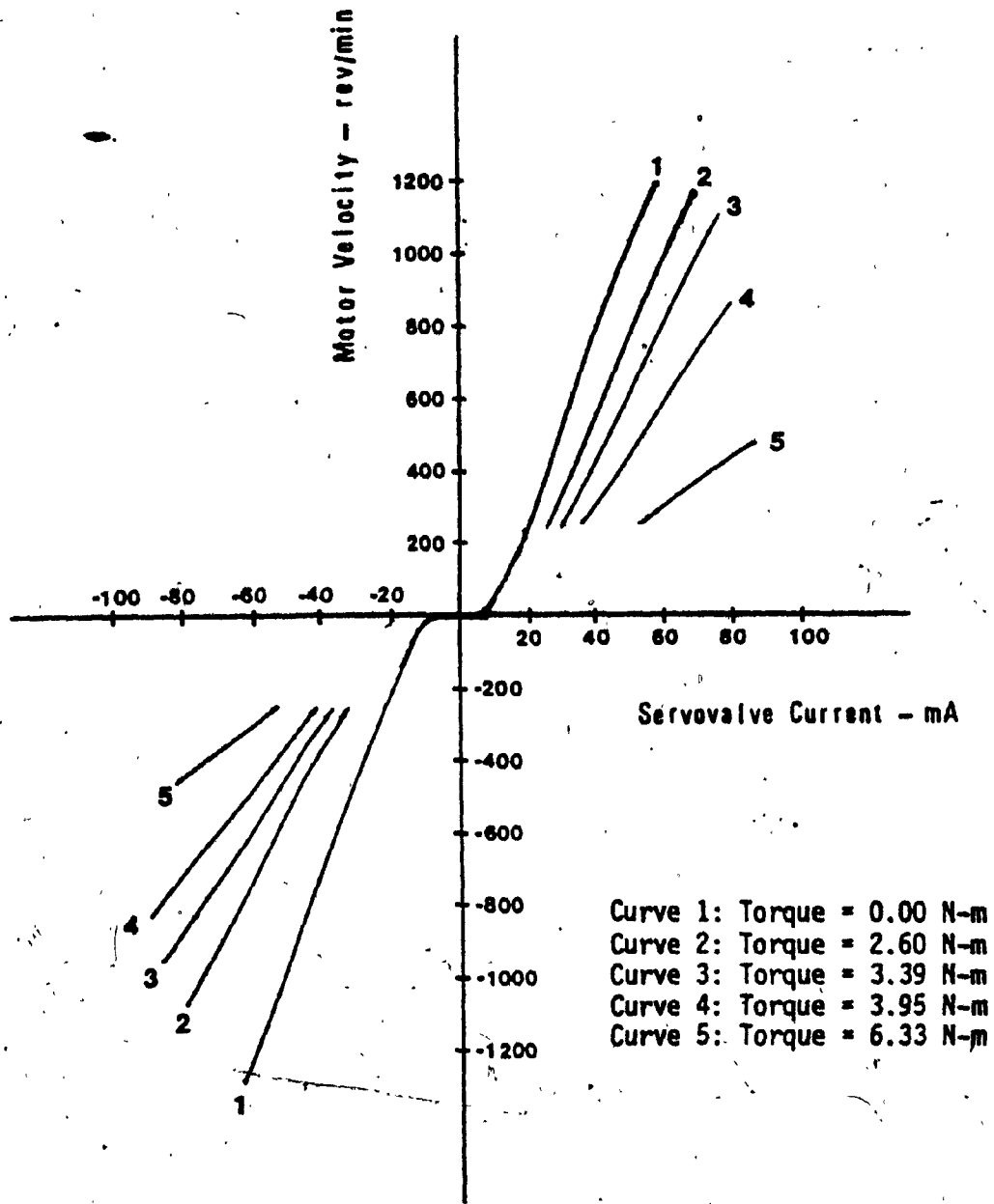


Fig. 5.8. Loaded Motor Speed/Servovalve Current Characteristics.

### 5.5. Summary and Discussion of Results

Based on the evaluation of the experimental results obtained, it can be stated that the experimental test stand used in this research is suitable for general use in evaluating the steady-state characteristics of virtually any hydraulic motor within the size range of the stand.

Results illustrated in Fig. 5.2 show that the second motor presented symmetrical characteristics with respect to flow. Furthermore, because of the low value shown for the dead-band of the motor servovalve combination, it is apparent that the motor had a low value of internal friction at starting.

On the other hand, the original motor employed to determine the loaded servovalve-motor characteristics presented some irregularities. Thus, the results illustrated in Fig. 5.6 were not symmetric with respect to flow, and discontinuities in the flow through the motor were also observed. Furthermore, a greater dead-band was observed, which was due to a higher internal friction of the original motor at starting.

Loaded valve-motor characteristics can be considered acceptable, however, some irregularities were also observed.

Thus, the results presented in Fig. 5.7 show a set of straight lines which should be parallel according to Eq. (5.6). The difference in slope is mainly due to the non-linear effects of the motor friction torque.

Differences in motor velocity presented in Fig. 5.8 are due to the asymmetric characteristics with respect to flow through the motor as stated before.



## CHAPTER 6

### SERVOVALVE-MOTOR PERFORMANCE: DYNAMIC CHARACTERISTICS

#### 6.1 General

In this chapter, the open-loop dynamic characteristics of the valve controlled motor are presented. Tests to determine the motor velocity transient response and frequency response were performed.

Fig. 6.1 shows a block diagram of the set-up used. A signal generator was employed to provide the excitation signal to the amplifier. The motor velocity was obtained using a tachometer attached to the motor shaft. A pressure transducer connected to the motor pressure line was utilized to record pressure transients. Finally, a strip chart recorder was used to obtain the values of the motor velocity and the motor line pressure.

A theoretical analysis of the valve controlled motor based on linear theory is also included.

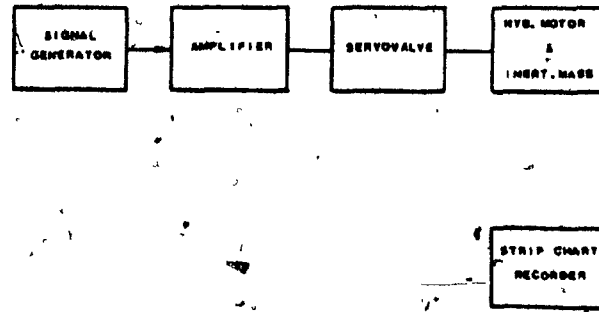


Fig. 6.1. Block Diagram of Set-Up to Obtain Dynamic Characteristics of the Valve Controlled Motor.

## 6.2. Theoretical Analysis of Valve Controlled Motor

Fig. 6.2 shows a schematic for the valve-motor combination.

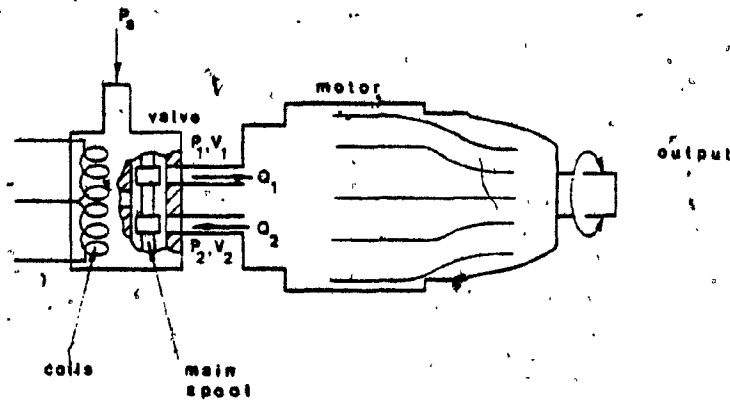


Fig. 6.2. Valve-Motor Combination.

Flow through sharp-edged orifices is predicted by applying the "square root" law [44]. Treating the annular orifices formed within the valve in this way gives:

$$Q_1 = C_d \pi D_s X_v (P_s - P_1)^{1/2} (2/\rho)^{1/2} \quad (6.1)$$

and

$$Q_2 = C_d \pi D_s X_v (P_2 - P_0)^{1/2} (2/\rho)^{1/2} \quad (6.2)$$

where  $Q_1, Q_2$  = forward and return flows,  $m^3/s$   
 $P_1, P_2$  = forward and return pressures,  $N/m^2$   
 $D_s$  = spool diameter, m  
 $P_s$  = supply pressure,  $N/m^2$   
 $P_0$  = return line pressure,  $N/m^2$   
 $\pi$  = 3.1416  
 $\rho$  = oil density,  $kg/m^3$   
 $X_v$  = spool displacement, m  
 $C_d$  = discharge coefficient. A discharge coefficient of  $C_d = 0.61$  is often assumed for all sharp-edged orifices [27].

Equations (6.1) and (6.2) may be simplified by making certain assumptions or approximations to the actual situation with real values. One assumption is that the

valving orifices are matched. Matched orifices require that  $Q_1 = Q_2$ , implying that  $P_s - P_1 = P_2 - P_0$ , [27]. The other assumptions are that the return pressure,  $P_0$  is neglected because it is usually much smaller than the other pressures involved. By introducing the term  $P_L = P_1 - P_2$  we have  $P_s - P_L = 2P_2$  and  $P_s + P_L = 2P_1$ .

The linearized servovalve flow equations are:

$$Q_1 = K_q X_v - 2 K_c P_1 \quad (6.3)$$

$$Q_2 = K_q X_v + 2 K_c P_2 \quad (6.4)$$

where  $K_q$  = valve flow gain coefficient,  $m^3/s/m$

$K_c$  = valve flow pressure coefficient,  $(m^3/s)/(N/m^2)$

The flow gain coefficient,  $K_q$ , is given by:

$$K_q = C_d \pi D_s \sqrt{(1/\rho) (P_s - P_L)} \quad (6.5)$$

while the flow-pressure coefficient,  $K_c$  is given by:

$$K_c = \frac{C_d \pi D_s X_v \sqrt{(1/\rho) (P_s - P_L)}}{2 (P_s - P_L)} \quad (6.6)$$

As can be noted in Eqs. (6.3) and (6.4), the flow pressure coefficient for each port is twice that for the valve as a whole because  $K_c$  had been defined with respect to  $P_L$ . Adding the servovalve flow equations gives

$$q_L = K_q X_v - K_c P_L \quad (6.7)$$

where  $q_L = (Q_1 + Q_2)/2 =$  load flow,  $m^3/s$

$P_L = P_1 - P_2 =$  load pressure difference,  $N/m^2$

This is the usual form of the linearized flow equation of the servovalve. The load flow represents the average of the flows in the lines and cannot be interpreted as being equal to the flow in each line unless external leakage is zero.

In examining the motor chambers and assuming that the pressure in each chamber is the same everywhere and does not cavitate; fluid velocities in the chambers are small so that minor losses are negligible; and temperature and density are constant. Application of the continuity equation to each motor chamber yields:

$$Q_1 - Q_m = V_1 / \beta_e \cdot dP_1/dt \quad (6.8)$$

$$Q_m - Q_2 = V_2 / \beta_e \cdot dP_2/dt \quad (6.9)$$

where the motor flow has been defined as

$$Q_m = D_m \omega_m + C_l P_L$$

and  $C_l$  = internal or cross-port leakage (i.e., leakage from one motor line to the other) coefficient of motor,  $(m^3/s)(N/m^2)$

$\beta_e$  = effective bulk modulus of system (includes oil, entrapped air, and mechanical compliance of chambers),  $N/m^2$

$V_1$  = average contained volume of forward chamber (includes servovalve, connecting line or manifold, and motor passages),  $m^3$

$V_2$  = average contained volume of return chamber (includes servovalve connecting line or manifold, and motor passages),  $m^3$

$D_m$  = volumetric displacement of motor,  $m^3/\text{rad}$

$\omega_m$  = angular velocity of motor shaft,  $\text{rad/s}$

$t$  = time,  $s$

It is desirable and possible to express the continuity equation in a more useful form; thus, substituting Eqs. (6.3), (6.4), and the motor flow equation into Eqs. (6.8), and (6.9) and then adding them yields:

$$q_L = (Q_1 + Q_2)/2 = D_m \omega_m + C_l P_L + (V_0/2\beta_e) \cdot dP_L/dt \quad (6.10)$$

where  $V_0 = V_1 = V_2$

Equation (6.10) can now be written using the Laplace transformation:

$$q_L = D_m \omega_m + C_1 P_L + (V_o/2 \beta_e) s P_L \quad (6.11)$$

Eq. (6.11) is the basic form of the continuity equation for all hydraulic actuators. The flow term which is proportional to the pressure derivative is known as the flow compressibility. Thus, the load flow  $q_L$  is consumed by leakage, flow to displace the actuator, and flow stored due to compressibility. Substituting Eq. (6.7) into Eq. (6.11), the basic form of the continuity equation is:

$$K_q X_v - (C_1 + K_c + V_o/2 \beta_e \cdot s) P_L = D_m \omega_m \quad (6.12)$$

the equation above can be simplified by defining  $K_{ce} = C_1 + K_c$ , where  $K_{ce}$  is the total flow-pressure coefficient,  $(m^3/s)/(N/m^2)$

hence:

$$K_q X_v - K_{ce} (1 + V_o/2 \beta_e K_{ce} \cdot s) P_L = D_m \omega_m \quad (6.13)$$

A block diagram which represents the variables  $X_v$ ,  $P_L$ , and  $\omega_m$  is shown in Fig. 6.3.

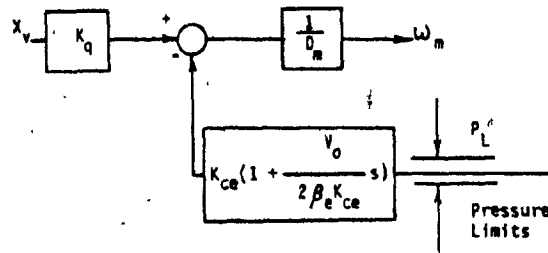


Fig. 6.3. Block Diagram for  $X_v$ ,  $\omega_m$ , and  $P_L$ .

The torque balance equation as the non-linear terms are neglected is given by:

$$D_m (P_1 - P_2) = J_L \frac{d\omega_m}{dt} + B_m \omega_m + T_L \quad (6.14)$$

Taking Laplace transforms, Eq. (6.14) becomes:

$$D_m P_L = J_L s \omega_m + B_m \omega_m + T_L \quad (6.15)$$

where  $P_L = P_1 - P_2$

If Eq. (6.15) is combined with the results obtained in the block diagram of Fig. 6.3, a complete block diagram for the



valve controlled motor is obtained, Fig. 6.4. In order to simplify the analysis, a predominant inertia load acting on the motor has been supposed, and  $T_L$  has been taken equal to zero.

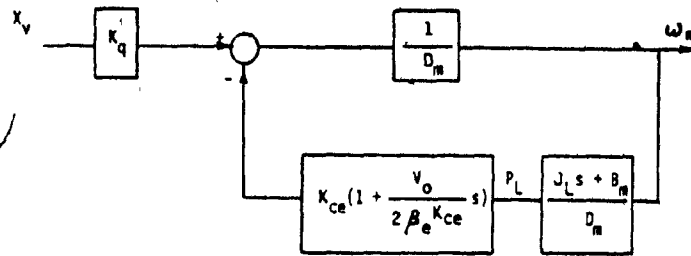


Fig. 6.4. Valve Controlled Motor Block Diagram.

A transfer function that relates the motor speed,  $\omega_m$ , and the valve stroke,  $X_v$ , is given below:

$$\omega_m / K_q X_v = \frac{1/D_m}{\frac{V_o J_L}{2\beta_e D_m^2} s^2 + \left( \frac{K_{ce} J_L}{D_m^2} + \frac{V_o B_m}{2\beta_e D_m^2} \right) s + \left( 1 + \frac{K_{ce} B_m}{D_m^2} \right)} \quad (6.16)$$

The term  $K_{ce} B_m / D_m^2$  can be neglected compared with the unity, as long as the accuracy of results obtained can be

kept within an acceptable margin. In this case, Eq. (6.16) reduces to:

$$\frac{\omega_m}{X_v} = \frac{K_q/D_m}{\frac{V_o J_L}{2 \beta_e D_m^2} s^2 + \frac{(K_{ce} J_L + V_o B_m)}{D_m^2} s + 1} \quad (6.17)$$

Eq. (6.17) shows that the relationship between the motor velocity,  $\omega_m$ , and the valve stroke,  $X_v$  is related by a second-order system. In steady-state conditions, the motor velocity is affected by the servovalve flow gain coefficient,  $K_q$ , and the motor volumetric displacement,  $D_m$ , as was demonstrated before. Expressions for the hydraulic natural frequency, and the hydraulic damping ratio are as follows:

$$\omega_h = (2 \beta_e D_m^2 / V_o J_L)^{1/2} \quad (6.18)$$

$$\delta_h = \frac{K_{ce}}{D_m} (J_L \beta_e / 2V_o)^{1/2} + \frac{B_m}{4D_m} (2V_o / \beta_e J_L)^{1/2} \quad (6.19)$$

$\omega_h$  = hydraulic undamped natural frequency, rad/s

$\delta_h$  = hydraulic damping ratio, dimensionless.

When the contribution of the second term of Eq. (6.19) to the hydraulic damping ratio is very small, then  $\delta_h$  can be approximated to:

$$\delta_h = (K_{ce}/D_m) (J_L \beta_e / 2V_0)^{1/2} \quad (6.20)$$

### 6.3. Transient Response Tests

Transient response tests were carried out using a step function as an input. The amplitude of the step was selected with reference to the results obtained from the digital simulation described in Chapter 4. By using the simulation, problems such as high pressure peaks and the possibility of cavitation in the motor chambers were predicted.

In all the tests carried out, a hydraulic power supply of 1500 psi has been used (recall Section 3.1).

Servo valve current and motor speed are directly related in steady-state conditions, and result in increases in servo valve and motor leakage respectively. Hence a valve controlled motor system exhibits increased damping, due to flow dissipation of energy. Fig. 6.5 depicts the velocity response for several current levels. It can be observed

that a higher damping coefficient is obtained as the step of servovalve current is increased.

Increasing the motor inertia load results in correspondingly higher acceleration forces and therefore an increase in pressure transient effects. Fig. 6.6 shows the pressure transients on the motor pressure line while Fig. 6.7 shows the velocity response. Results from Fig. 6.7 are predicted by the theoretical analysis made previously, i.e. the greater the motor inertia load, the slower speed response is obtained.

A step function from zero to a selected amplitude was used as the excitation signal for driving the servovalve coils. When the servovalve current returned to the zero level, the servovalve ports closed, and the oil flow was trapped. That situation along with other external conditions such as servovalve current level, and the motor inertia load produced cavitation in the motor chambers. Results of the above tests are presented in Fig. 6.8 for a motor inertia load of  $0.04283 \text{ N-m-s}^2$ . Curve 1 shows the pressure transient effects for a 24 mA where no cavitation was observed. In curve 2 the pressure transient effects for a 32 mA current are presented. There, the pressure motor line reached a value of at least zero psig. Pressures below

atmospheric pressure were not recorded since the pressure transducer used registered only pressures above the atmospheric pressure.

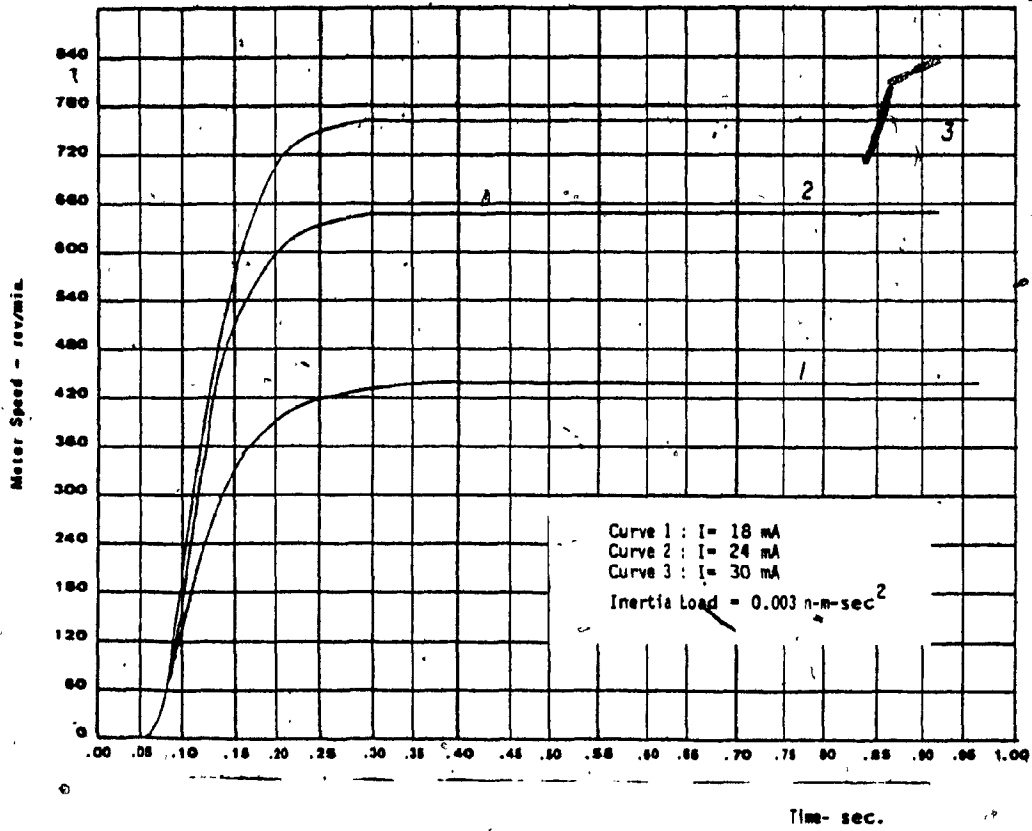


Fig. 6.5. Experimental Transient Motor Velocity Response of the System for Several Current Levels.

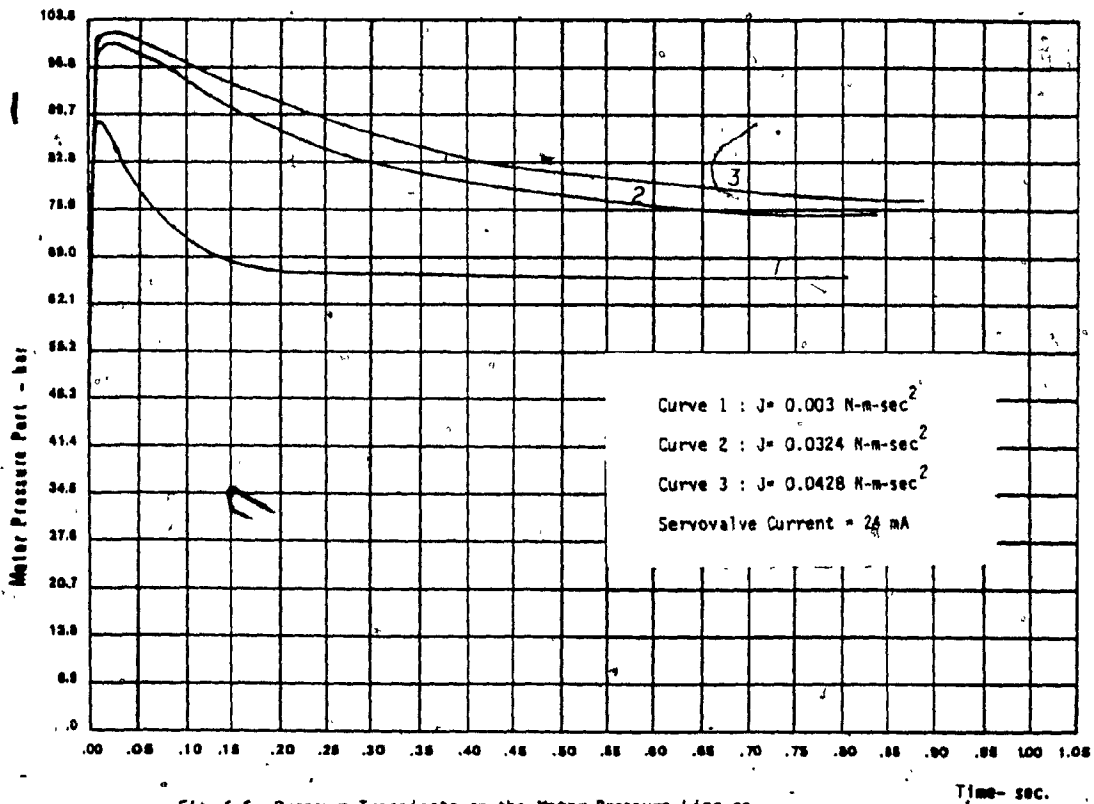


Fig. 6.6. Pressure Transients on the Motor Pressure Line as Several Motor Inertia Loads are Used.

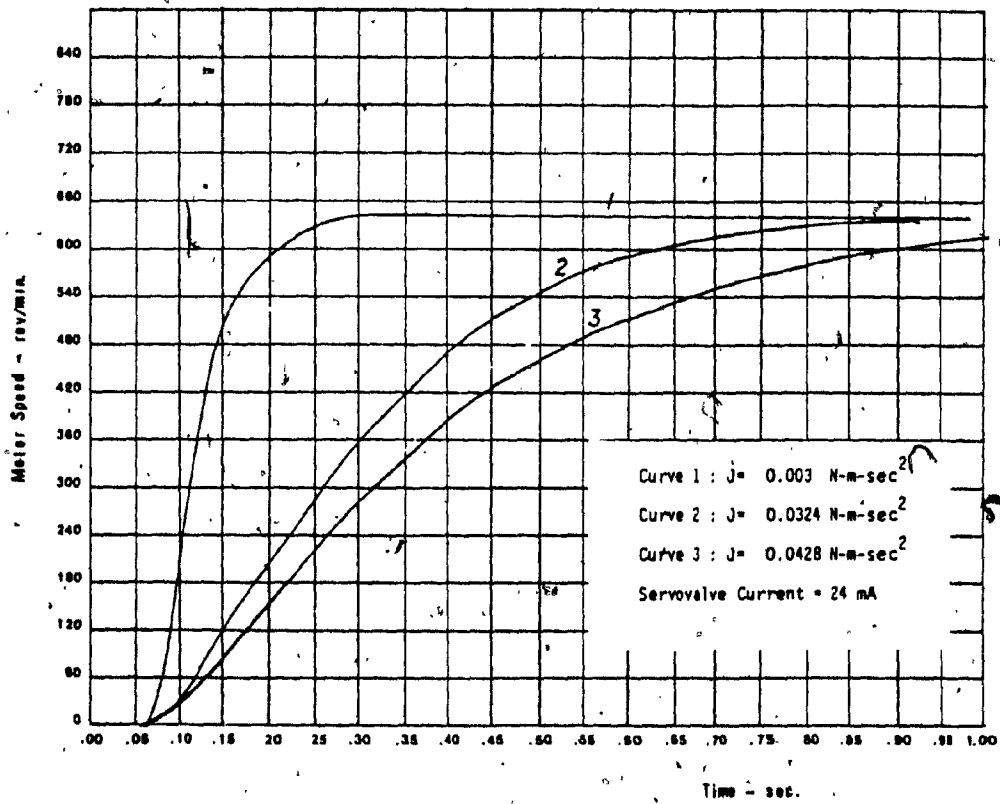


Fig. 6.7. Experimental Transient Velocity Response of the System for Various Motor Inertia Loads.



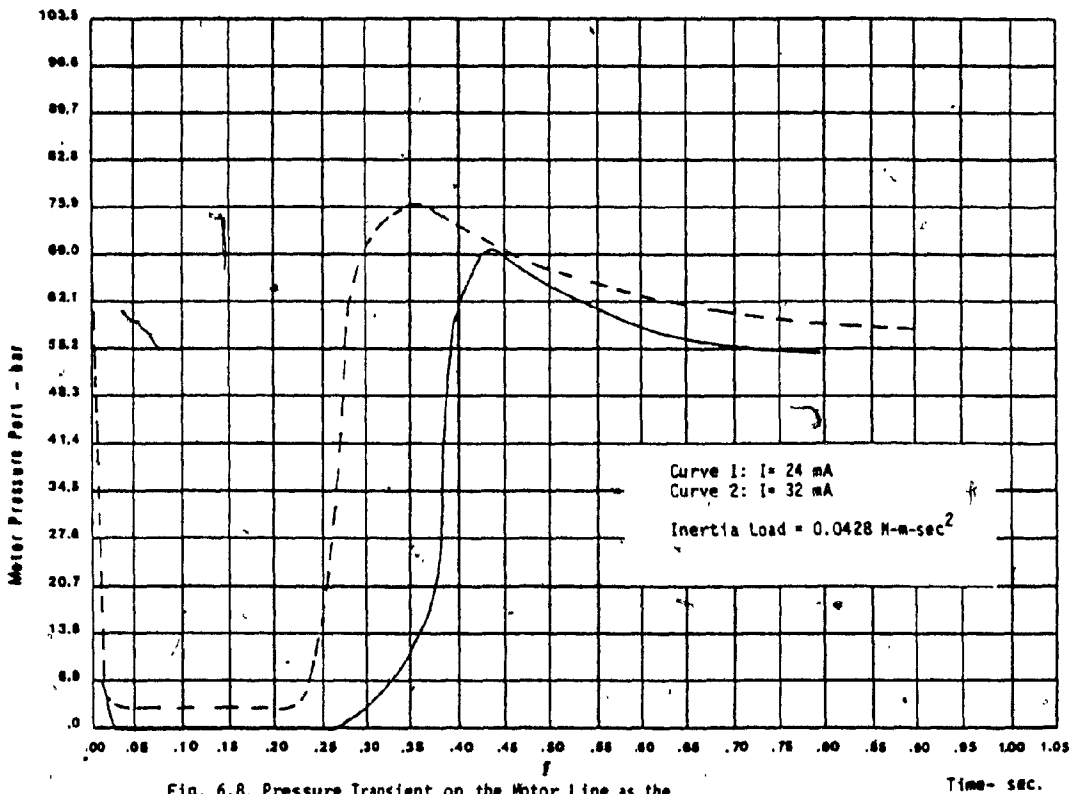


Fig. 6.8. Pressure Transient on the Motor Line as the Hydraulic Motor is suddenly Stopped.

Time- sec.

#### 6.4. Frequency Response Tests

Open-loop frequency response data are widely used to represent the dynamics of control systems. From this data, closed-loop stability and performance can be predicted and electronic compensation networks designed.

The test waveform was selected so that the valve oscillated about neutral position at different amplitudes. A base frequency of 0.1 Hz was chosen.

Most of the tests were carried out using flexible hoses between the servovalve and motor ports. A test using rigid piping is included in order to show the effects of flexible housing on the system performance.

The results are presented in Bode diagram form. Families of curves are used to demonstrate the effect of various control parameters.

Fig. 6.9 depicts the results obtained for a constant motor inertia load and current step inputs of 24 mA, 48 mA, and 60 mA. Increases in input amplitude result in increases in the valve stroke as well as in the motor speed. Consequently the valve and motor leakages increase. Thus,

it is found that damping increases and apparent natural frequency decreases as input amplitude increases. Similar results were obtained by Merritt [27], and Bell and Cowan [1].

Results obtained for a constant current amplitude and motor inertia loads of 0.003, 0.03247, and 0.04283 N-m-s<sup>2</sup> are presented in Fig. 6.10. The effects of increasing the motor inertia load are as predicted by theory.

Fig. 6.11 shows the results obtained for flexible hoses and for rigid piping used between the servovalve and motor ports. By using rigid piping a higher value for the bulk modulus is obtained. Thus, as predicted by theory the apparent natural frequency increases.

Fig. 6.12 shows a comparison between the results obtained for rigid piping, servovalve current of 24 mA and inertia load of 0.003 N-m-s<sup>2</sup> and the theoretical results as predicted by theory. The numerical values used in this part are shown in Appendix B.

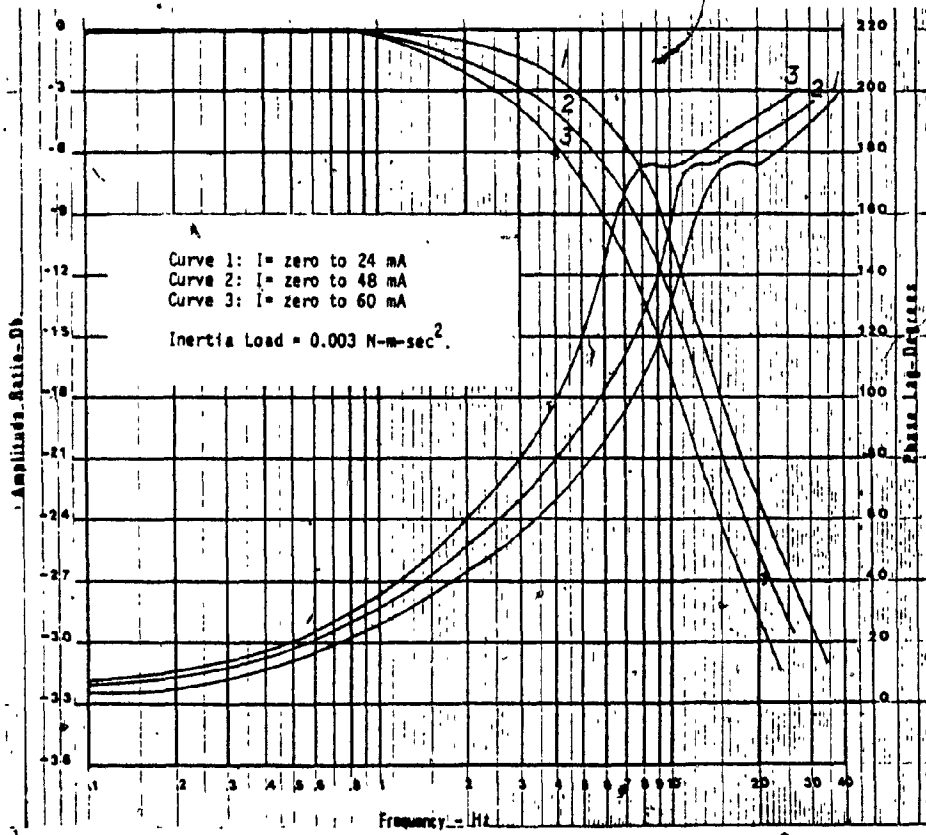


Fig. 6.9. Frequency Response Tests-Servovalve Current Amplitude about Null Variable.

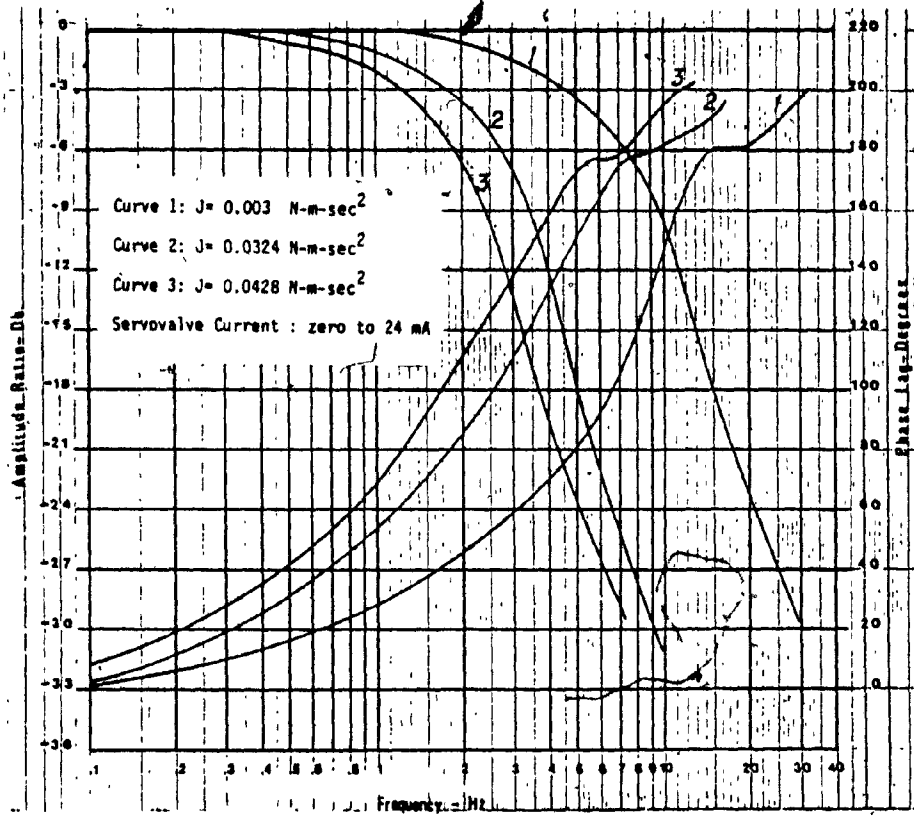


Fig. 6.10. Frequency Response Tests - Inertia Load Variable.

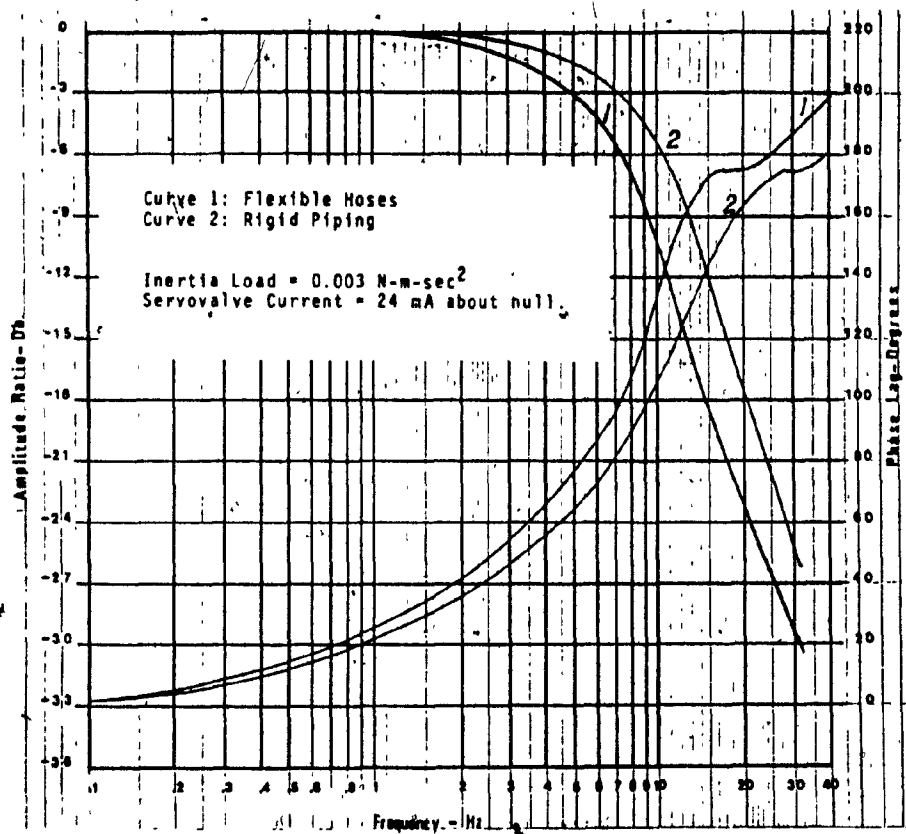


Fig. 6.11. Frequency Response Tests-Flexible Hoses and Rigid Piping Used.

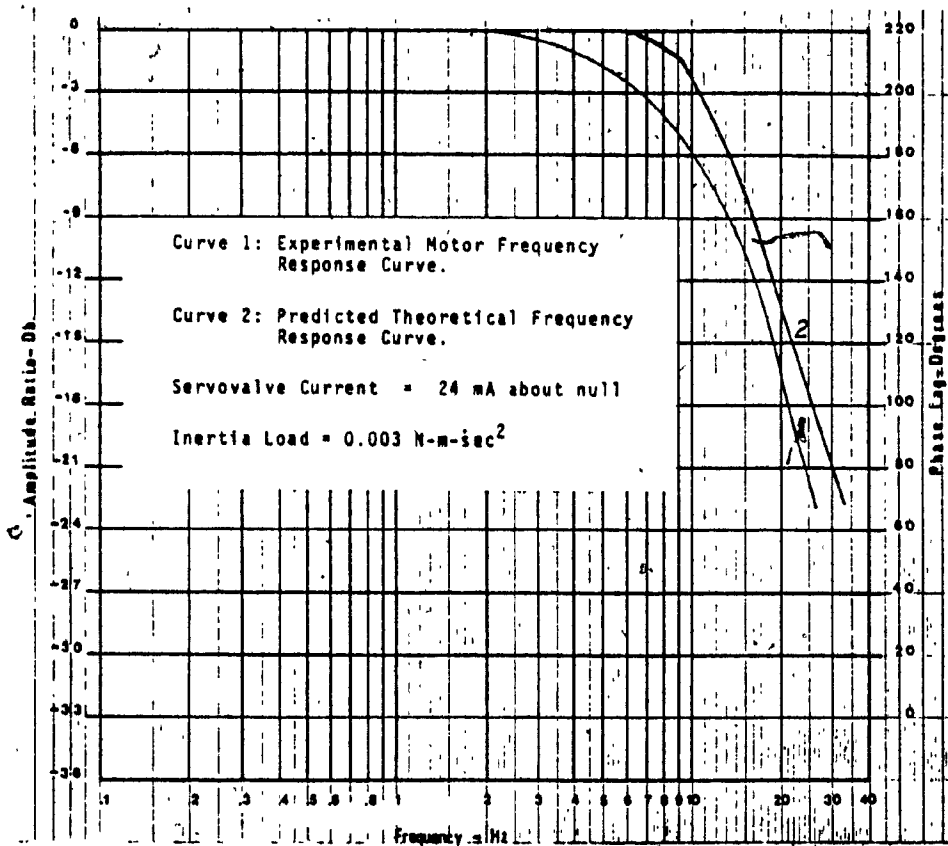


Fig. 6.12. Frequency Response Tests-Amplitude Ratio of Theoretical and Experimental Results.

## 6.5. Summary and Discussion of Results

Transient and frequency response results have been presented for a valve controlled hydraulic motor.

The results of the open-loop frequency response show that system behaves mainly as a second-order system with a slope for the amplitude ratio of -12 db/Octave. Thus, the contribution of the amplifier and valve dynamics to the complete system are almost negligible. The frequency response plot of the amplifier, Fig. 2.32, shows a bandwidth of 70 Hz. The servovalve frequency response, Fig. 2.22, shows mainly a lag contribution to the system around 20 Hz. That explains why the open-loop velocity frequency response presents a phase lag of  $210^\circ$  for frequencies near 25 Hz.

The pressure peaks recorded indicate that the use of cross-port pressure relief valve is desirable. Even though a digital simulation was used to predict the step current amplitudes for driving the hydraulic motor and thus to avoid the possibility of having cavitation in the motor chambers; cavitation took place when the hydraulic motor was suddenly stopped. In other words, in the digital simulation implemented, the case when the motor was driven from a determined speed to zero was not considered. Thus, for certain external factors such as the level of current



applied to the servovalve and the external inertial mass driven by the motor, cavitation took place as shown in Fig. 6.8.

Merritt [27], and Bell and Cowan [1] suggest inserting a relief valve across the lines to avoid cavitation in the motor chambers (a similar relief valve is required to protect the other chamber). This safety relief valve helps prevent cavitation by dumping fluid to the forward chamber.

Fig. 6.12 shows the theoretical and experimental results obtained for a current amplitude of 24 mA and inertial mass of 0.003 N-m-s<sup>2</sup>. For the calculation, a bulk modulus of 0.517 x 10<sup>9</sup> N/m<sup>2</sup> (77550 psi) was used. Such a value for bulk modulus of a system is considered low. In previous works carried out by Merritt [27] and Stringer [44], the value of the bulk modulus around 0.6888 x 10<sup>9</sup> N/m<sup>2</sup> (100,000 psi) was suggested. The low bulk modulus value observed by the author can be explained by the leakage of the hydraulic motor. Fig. 6.13 shows a schematic diagram of a linear actuator filled with fluid under compression. Bulk modulus can be calculated as follows:

$$\beta = - \frac{\Delta P}{\Delta V/V} \quad (6.21)$$

where  $\Delta P$  = pressure increase exerted on the fluid and container

$\Delta V$  = decrease in the initial volume

$V$  = initial volume of liquid

$\Delta V$  is composed of change of volume due to compressibility and change of volume due to leakage. Thus, an increase in the leakage causes an apparent decrease in the bulk modulus value.

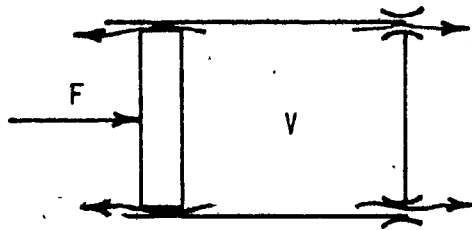


Fig. 6.13. A Linear Actuator Filled with Liquid under Compression.

## CHAPTER 7

### DESIGN OF CLOSED-LOOP FORCE SERVO SYSTEM

#### 7.1 Introduction

This chapter deals with the design and test of a closed-loop force servo-system based on the components discussed previously.

The key element in this servo system is a servovalve with an LVDT attached to the servovalve spool, a ball-piston hydraulic motor, and a tension-compression load cell which is used as the main feedback. Motor shaft rotation was prevented by a clamp in all tests.

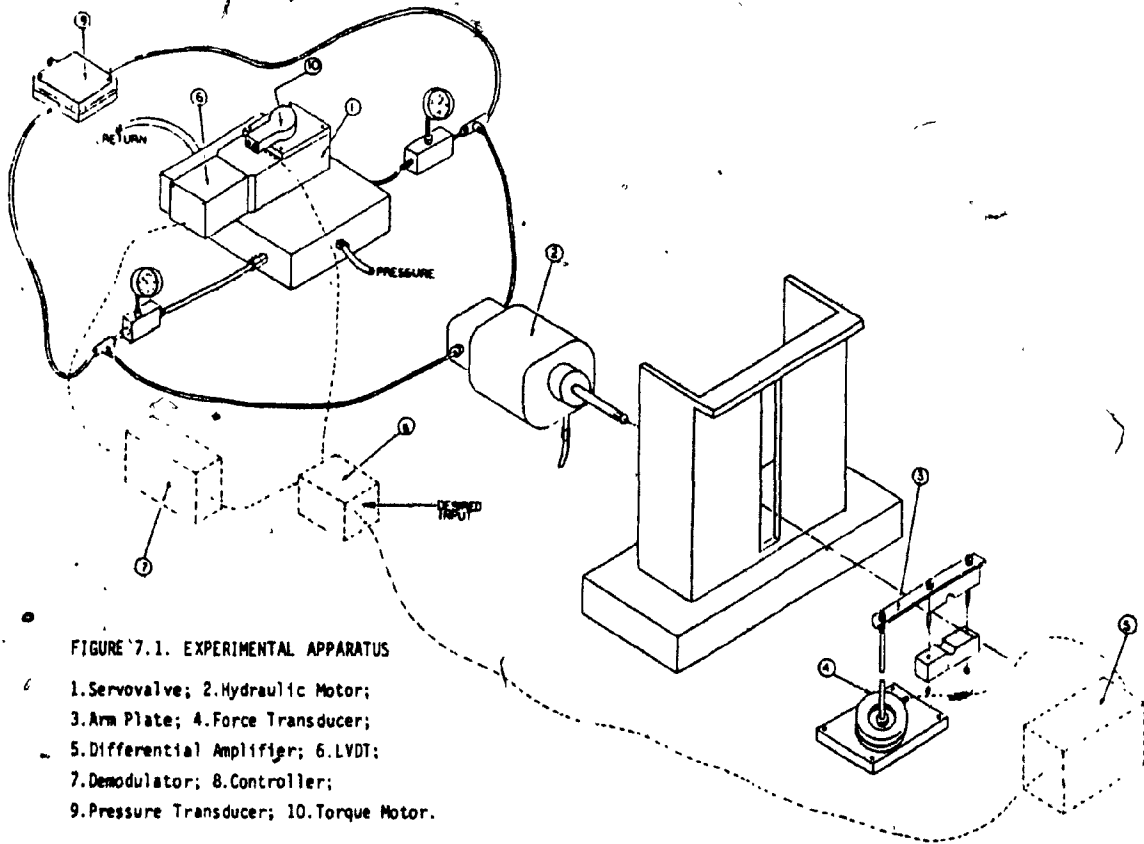
A theoretical analysis has been included in order to study the effects of the various components on overall system performance.

Several steady-state and dynamic test results are included.

#### 7.2. Experimental Set-Up

Fig. 7.1 shows the experimental apparatus used. The servovalve (1) controls the hydraulic motor (2) which converts the hydraulic energy into mechanical energy. The mechanical arm (3) transforms the torque developed by the

hydraulic motor into force applied to the tension-compression load cell (4) generating the main feedback signal (5). In addition, a second feedback is generated by the servovalve LVDT (6), and the LVDT signal conditioning module (7). A proportional controller is used in this loop (8). A pressure transducer (9) serves to investigate the relationship between the differential pressure across the motor and the torque developed by the motor.



The load cell used as the principal feedback element was preferable to the torque transducer described in Section 2.4.1 since it was difficult to eliminate the effects of backlash in the mechanical coupling between the torque transducer and the motor shaft. The load cell was rated at  $\pm 100$  lbf.

As before, a supply pressure of 1500 psi was used through all the tests.

### 7.3. Theoretical Analysis and Block Diagram of the System.

The following tests were carried out with the motor shaft clamped to prevent rotation. Thus, the theoretical analysis is simplified because the motor shaft velocity is zero and only leakage due to the servovalve and motor and the effects of the compressibility of the hydraulic oil are significant in the flow equations.

Recalling Eqs. (6.7) and (6.11) developed in Chapter 6:

$$q_L = K_q X_v - K_c P_L \quad (7.1)$$

$$q_L = C_1 P_L + (V_o/2 \beta_e) s P_L \quad (7.2)$$

where  $q_L$  = load flow,  $m^3/s$

$K_q$  = valve flow gain coefficient,  $(m^3/s)/m$

$K_c$  = valve flow-pressure coefficient,  $(m^3/s)/(N/m^2)$

$x_v$  = valve stroke, m

$P_L$  = pressure drop across the hydraulic motor,  $N/m^2$

$C_L$  = internal leakage coefficient of motor,  $(m^3/s)/(N/m^2)$

$V_o$  = volume of oil under compression,  $m^3$

$\beta_e$  = effective bulk modulus of the system,  $N/m^2$

$s$  = Laplace operator

Substituting Eq. 7.1 into Eq. 7.2:

$$K_q x_v - K_c P_L = C_L P_L + V_o / 2 \beta_e s P_L \quad (7.3)$$

The torque developed by the hydraulic motor is given by:

$$T_m = D_m P_L \quad (7.4)$$

where  $D_m$  = motor displacement,  $m^3/rad$

Replacing the variable  $P_L$  given by Eq. 7.4 into Eq. 7.3 and rearranging terms it follows that:

$$K_q V_v = (K_c + C_1 + \frac{V_o}{2\beta_e} s) \frac{1}{D_m} T_m \quad (7.5)$$

Eq. (7.5) determines the relationship between the motor torque and valve stroke. Thus, the transfer function for  $T_m$  and  $X_v$  is obtained:

$$\frac{T_m}{X_v} = \frac{K_q D_m / K_{ce}}{1 + (V_o / 2K_{ce} \beta_e) s} \quad (7.6)$$

where  $K_{ce} = K_c + C_1$

The torque developed by the hydraulic motor is:

$$T_m = F \times b \quad (7.7)$$

where  $F$  = Force exerted on the load cell, N

$b$  = distance between the center of motor shaft and load cell, m

A differential amplifier with a gain equal to 150 was used to increase the load cell output (for details of the differential amplifier see Section 2.4.2). The relationship between the force applied to the load cell and its electrical output is given by:

$$E_0 = K_f \cdot F \cdot K_{DA} \quad (7.8)$$

where  $E_0$  = differential amplifier output, mv  
 $K_f$  = slope of the force cell calibration curve, mV/N  
 $K_{DA}$  = differential amplifier gain, dimensionless

\* For the electrohydraulic servovalve used, a second order transfer function is used, matched to the manufacturer's data. The transfer function showed a good approximation for the servovalve amplitude ratio as well as to the phase-lag for frequencies up to 40 Hz:

$$X_v/I = K_x \omega_n^2 / (s^2 + 2\xi \omega_n s + \omega_n^2) \quad (7.9)$$

where  $I$  = torque motor current, mA  
 $\xi$  = damping ratio of servovalve, dimensionless  
 $\omega_n$  = natural frequency of servovalve, rad/s  
 $K_x$  = servovalve spool displacement gain, m/mA

A block diagram of the closed-loop force servo system is shown in Fig. 7.2.

4



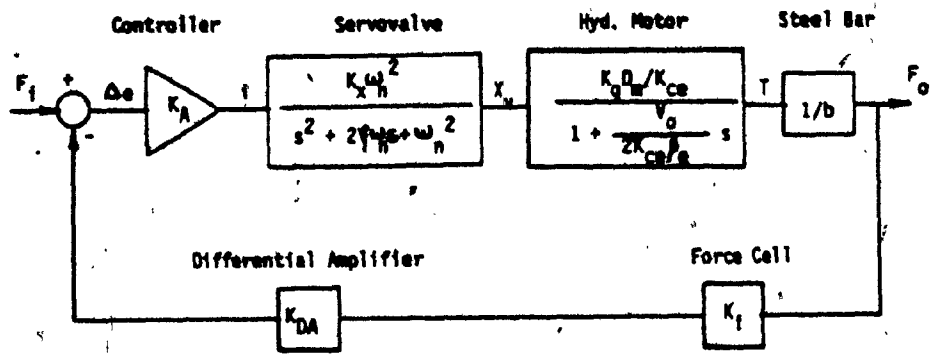


Fig. 7.2. Block Diagram of the Force Servo System.

From the block diagram a transfer function for  $F_o$  and  $F_i$  is obtained:

$$\frac{F_o}{F_i} = \frac{\frac{K_A K_x}{(s\omega_n)^2 + (2\xi\omega_n)s + 1} \cdot \frac{K_q D_m / K_{ce}}{1 + (V_o / 2K_{ce} \beta_e) s} \cdot 1/b}{1 + \frac{K_A K_x}{(s\omega_n)^2 + (2\xi\omega_n)s + 1} \cdot \frac{K_q D_m / K_{ce}}{1 + (V_o / 2K_{ce} \beta_e) s} \cdot 1/b \cdot K_{DA} K_f} \quad (7.10)$$

The above equation is simplified by defining:

$$\tau_m = V_0 / 2K_{ce} \beta e$$

$$K_2 = K_A K_x (K_q D_m / K_{ce}) \cdot 1/b$$

$$K_3 = K_2 \cdot K_{DA} K_f$$

hence,

$$\frac{F_0}{F_1} = \frac{K_2}{1 + \frac{K_3}{(s/\omega_n)^2 + (2\xi/\omega_n)s + 1} (1 + \tau_m s)} \quad (7.11)$$

Further simplifications in Eq. (7.11) result in the following equation:

$$\frac{F_0}{F_1} = \frac{K_2}{[(s/\omega_n)^2 + (2\xi/\omega_n)s + 1] (1 + \tau_m s) + K_3} \quad (7.12)$$

If a step function of amplitude  $F_1 = AmV$  is applied to the system, the steady-state value for  $F_0$  will be:

$$F_0 = \lim_{s \rightarrow 0} s \cdot F_0(s)/F_1(s) \cdot A/s = \frac{A \cdot K_2}{1 + K_3} \quad (7.13)$$

The characteristic equation of the closed-loop transfer function, Eq. (7.12), indicates that the force servo system is a third-order system.

#### 7.4. Performance Characteristics of the System

In this section the results of several tests carried out in order to investigate the performance of the force servo system are presented. A steady-state test was carried out to obtain the relationship between the torque developed by the motor and the pressure drop across it. Several dynamic tests were performed to obtain the response of the closed-loop force system to a step change of input and to determine the system bandwidth.

##### 7.4.1. Motor Torque versus Motor Pressure Drop Characteristics

The torque developed by the hydraulic motor for a given motor pressure drop can be compared to the theoretical motor torque, which is given by the equation  $T_m = D_m P_L$ . The deviation between the experimental and theoretical values reveals the Coulomb friction of the motor mechanism.

Fig. 7.3 shows a set of curves of the motor torque plotted against the motor pressure drop. The curves were obtained for various positions of the motor shaft. The characteristics depend on the motor shaft position. Each graph of Fig. 7.3 shows a different shape. The differences in the results can be attributed to the pintle-rotor assembly of the motor. As described in Section 2.2.2, the pintle - rotor assembly forms the valve which controls the fluid to the motor chambers. However, the effect of the valving is not observed at frequencies higher than 1.5 Hz.

The hysteresis observed in each graph of Fig. 7.3 are due to the motor hysteresis and motor friction. The backlash effects are due to the pintle-rotor assembly of the hydraulic motor.

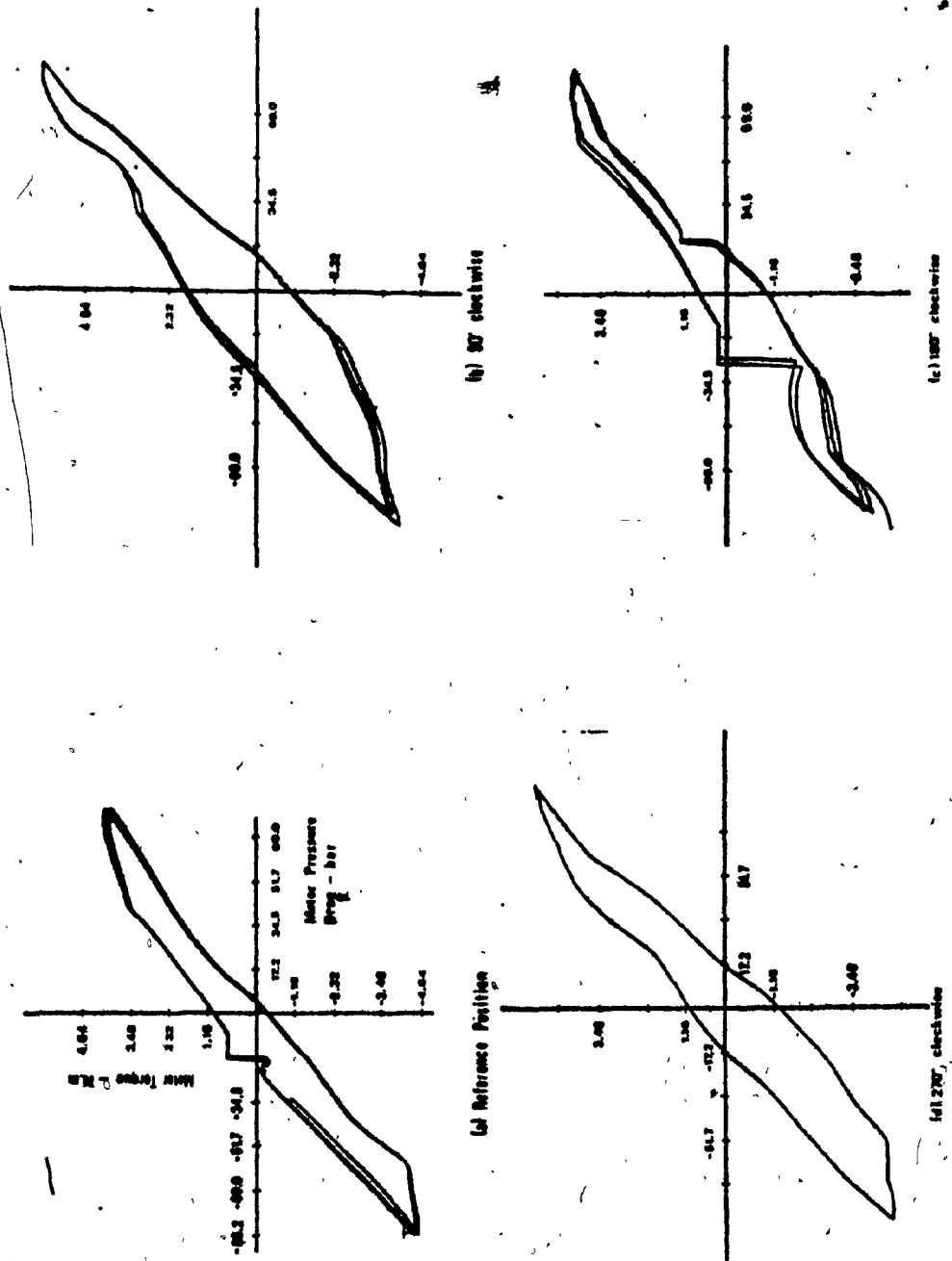


Fig. 7.3. Motor Torque Versus Motor Pressure Drop - Motor Shaft Locked. Four Different Motor Shaft Positions.

#### 7.4.2. Transient Response of the System.

Transient response tests were carried out using a step input as the excitation signal.

Fig. 7.4 shows the result obtained as a step function equivalent to 13.3 lbf is fed to the system. Because of the high gain of the servocontroller which was of 0.15 mA/mV, the steady-state error obtained was less than 3.0%.

Fig. 7.5 shows the system step input response for a very high servocontroller gain. It can be seen that the system became oscillatory. The result is typical of third-order systems. The system non-linearities coupled with the very high system gain cause the limit cycle oscillations.

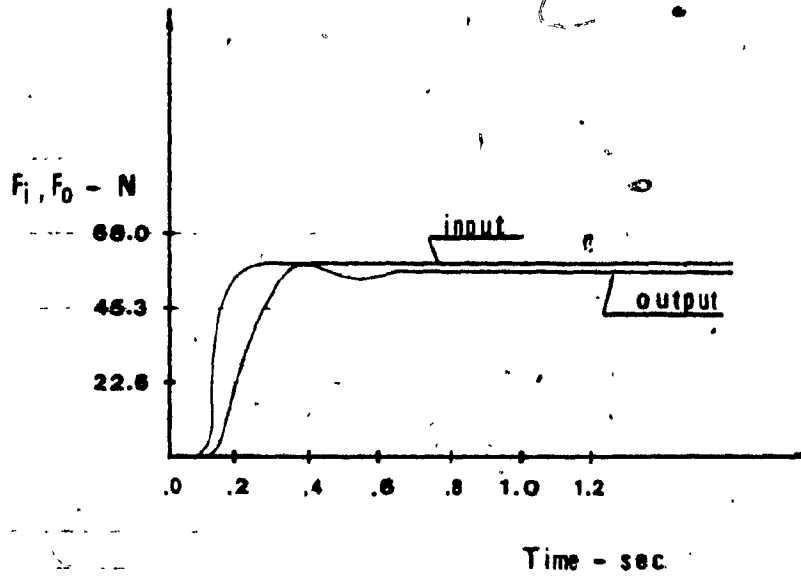


Fig. 7.4. Closed-Loop Force Servo System  
Transient Response-System: Stable.

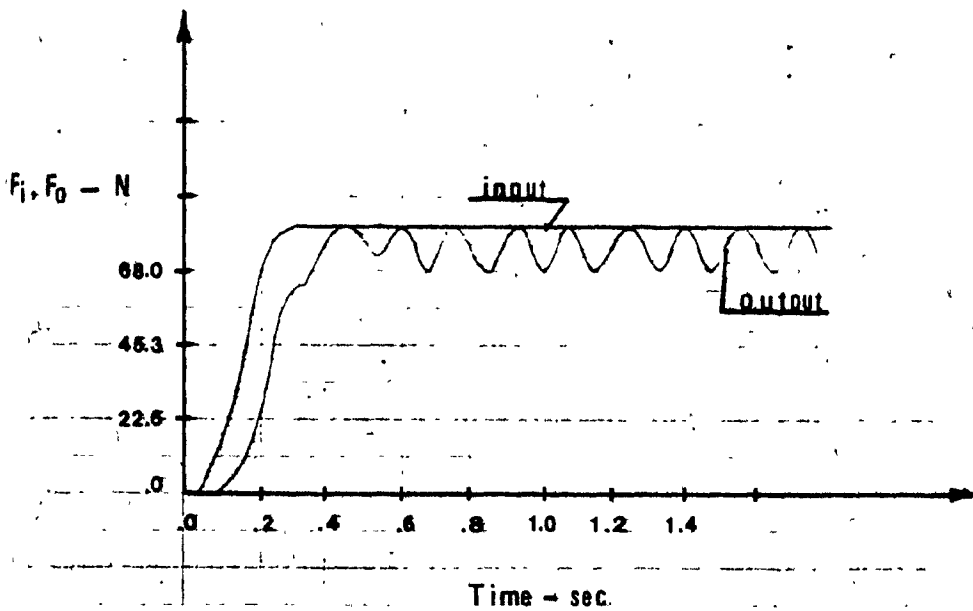


Fig. 7.5. Closed-Loop Force Servo System  
Transient Response-System: Oscillatory

#### 7.4.3. Closed-Loop Frequency Response of the System

The closed-loop frequency response plot provides a further measure of the performance of the system under investigation. Several definitions of bandwidth can be used [2], but the most common definition of bandwidth is the frequency at which the amplitude ratio is attenuated to 0.707 (-3 db) from its low frequency value.

In Fig. 7.6 the closed-loop frequency response plots for two values of the reference signal are shown. Curve (1) was obtained for a reference signal equivalent to  $\pm 3.3$  lbf, while curve (2) was obtained for a reference signal equivalent to  $\pm 7.7$  lbf. These results were obtained, when only the signal from the force cell was used as a feedback.



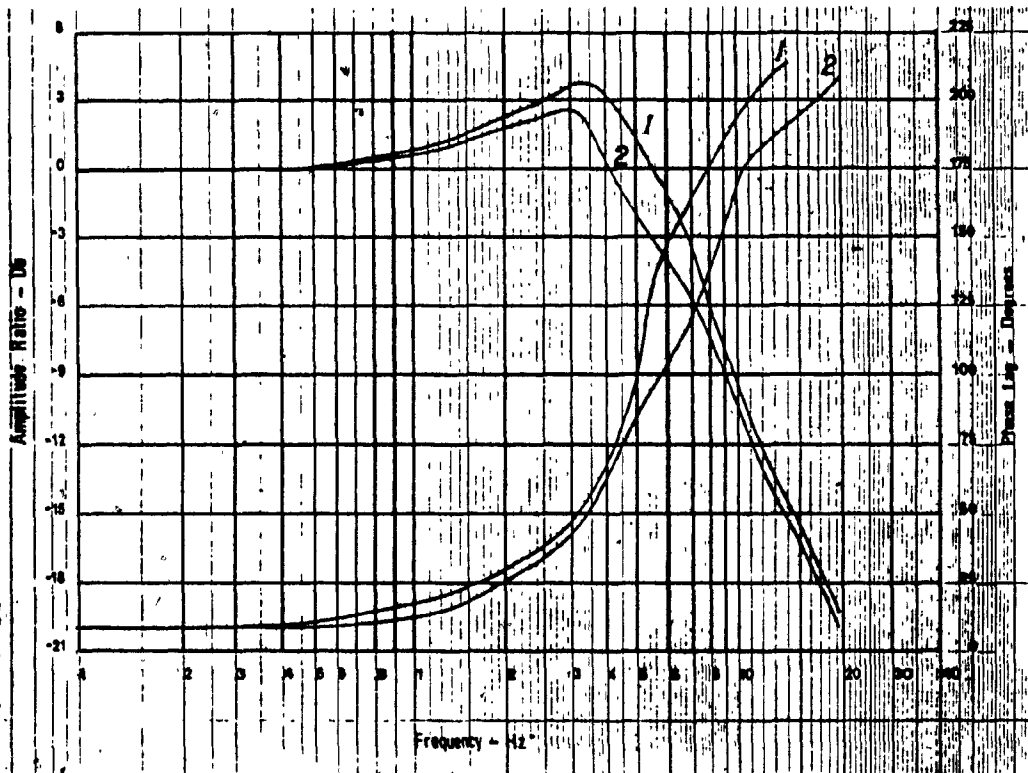


Fig. 7.6. Force Servo System Closed-Loop Frequency Response Plot.

#### 7.4.4. Effects of Servovalve Dither on Amplitude Response

Results illustrated in Fig. 7.3, Section 7.4.1., show that the hydraulic servo system has non-linearities which affect system performance. As a consequence, the output waveform is not in exact proportion to the input signals.

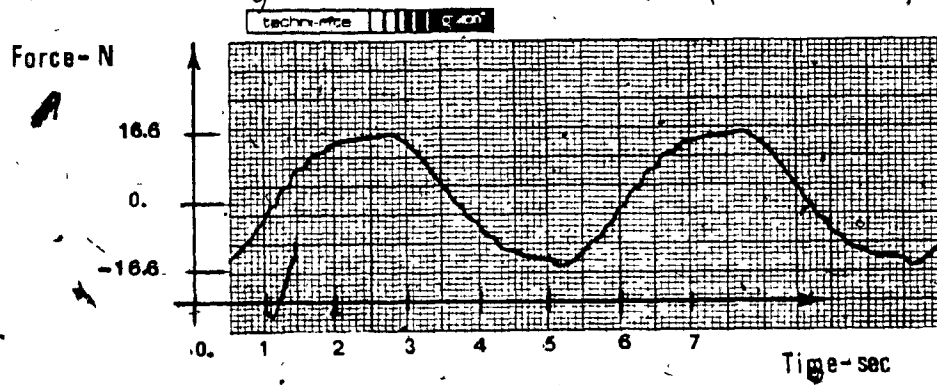
One of the methods used to reduce the effect of non-linearities on the system performance is the application of a dither signal. Dither is a high frequency sinusoidal signal of small amplitude which is added to the control signal at the input. The minute valve spool motion induced by the dither signal reduces the effects of the static friction. Furthermore the motion of the valve spool is also effective in preventing silting. The small contamination particles in the fluid at the metering orifices are kept in agitation and are swept through as the orifice opens during the dither cycle.

The dither amplitude should not be too large, otherwise it is transmitted to the load which could result in an excessive wear of the drive system.

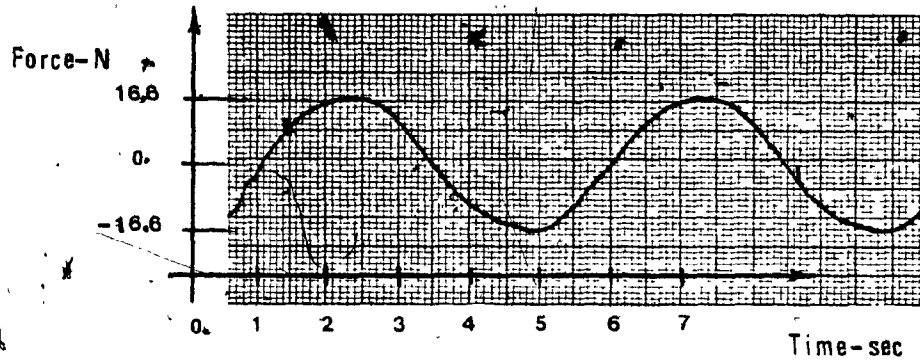
The dither frequency should be considerably in excess of the expected signal frequencies and should not coincide with resonances in the servovalve or in the actuator or load;

otherwise fatigue failures could occur. To determine the dither frequency, it is necessary to have the information concerning the open-loop response of the servovalve as well as the operating frequencies of the entire system.

Servovalve dither was used in the closed-loop force servo system for operating frequencies of 0.1 Hz and 4.0 Hz. The amplitude of the dither signal was approximately  $\pm 5\%$  of the servovalve rated current while the dither frequency was selected equal to 70 Hz. The results of the tests with 0.1 Hz input are shown in Fig. 7.7. As can be seen, the use of dither improved the fidelity of the system response significantly.

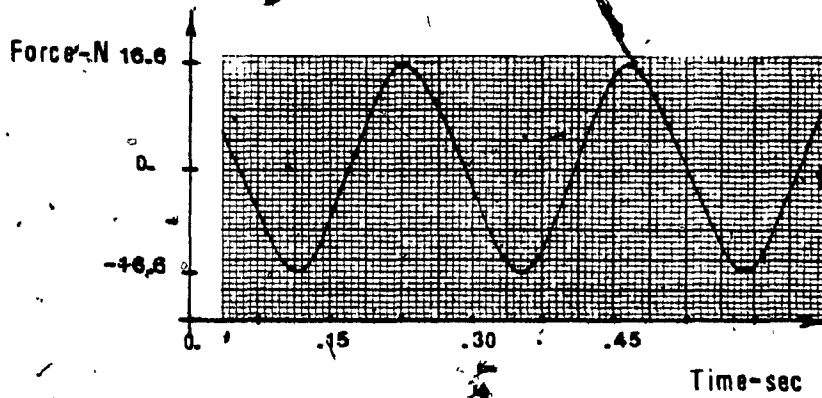


(a) Output Waveform-No Dither Used.

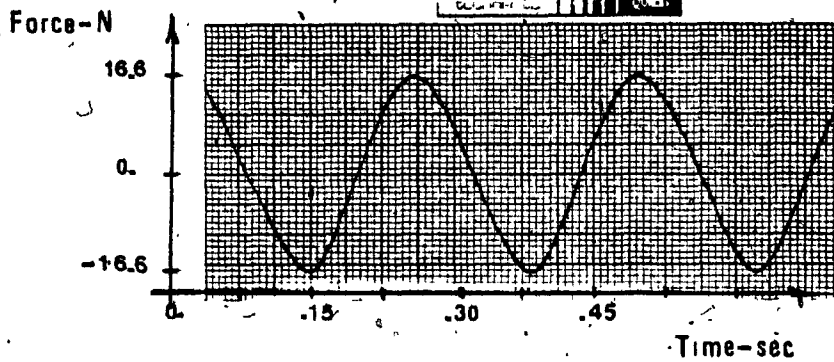


(b) Output Waveform-Servoalve Dither Added to the System.

Fig. 7.7. Output Waveform for the Closed-Loop Force Servo System at an Input Frequency Signal of 0.1 Hz. (a) No Dither Used, (b) Servoalve Dither Added to the System.



(a) Output Waveform-No Dither Used.



(b) Output Waveform-Servo Valve Dither Added to the System.

Fig. 7.8. Output Waveform for the Closed-Loop Force Servo System at an Input Frequency Signal of 4.0 Hz. (a) No Dither Used; (b) Dither Added to the System.

5. )  
Figs. 7.9 and 7.10 show the closed-loop frequency response plots for reference signals equivalent to  $\pm 7.7$  lbf and  $\pm 3.3$  lbf respectively. In both cases, servovalve dither was used. No significant improvement of system performance can be observed due to the application of dither.

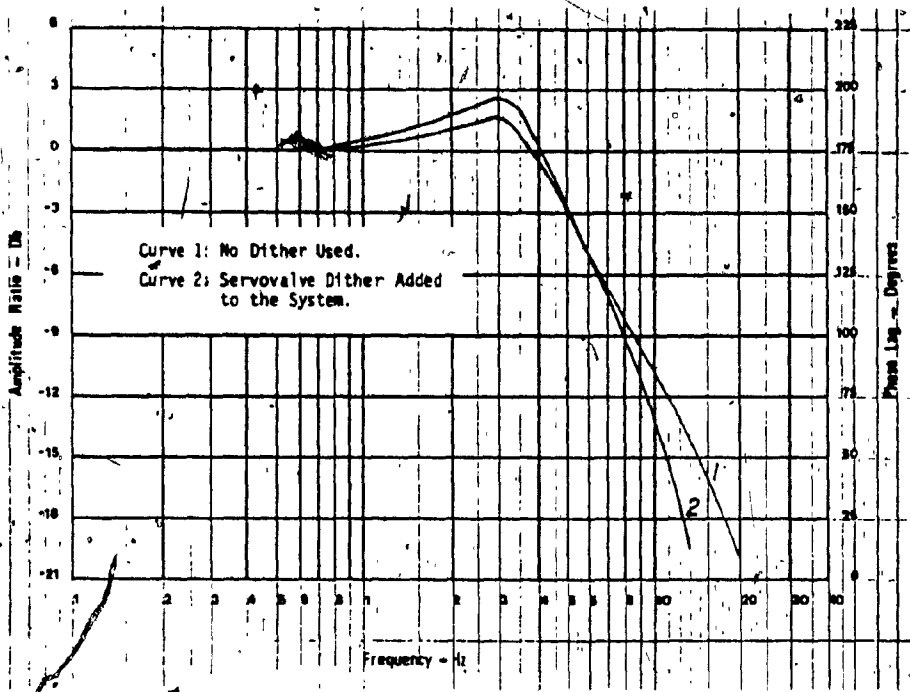


Fig. 7.9. Effects of the Servovalve Dither on the Amplitude Response. Reference Signal equal to  $\pm 7.7 \text{ lb}_f$ .

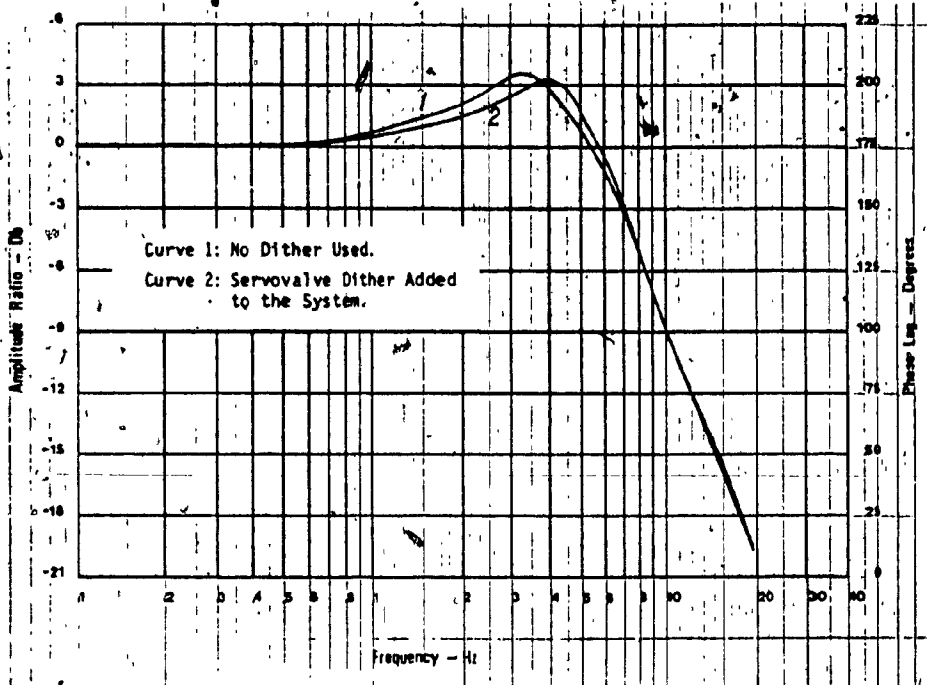


Fig. 7.10. Effects of the Servovalve Dither on the Amplitude Response. Reference Signal equal to  $+3.3 \text{ lb}_f$ .



**7.4.5. Effects of the Servo Valve Linear Variable Differential Transformer on the System Performance Characteristics**

When the servovalve LVDT is included in the system, the block diagram of Fig. 7.2 is modified as shown in Fig. 7.11.

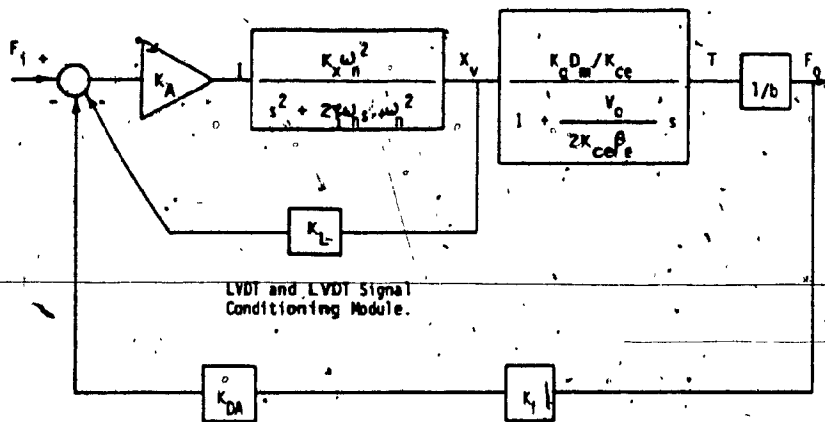


Fig. 7.11. Block Diagram of the Force Servo System with a Secondary Feedback.

Solving the inner feedback loop, the block diagram shown in Fig. 7.12 yields:

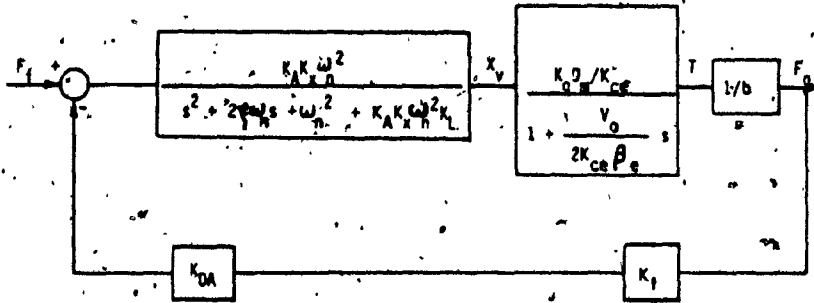


Fig. 7.12. Simplified Block Diagram.

From Fig. 7.12 a transfer function for  $F_o$  and  $F_i$  is obtained:

$$F_o = \frac{\frac{K_A K_X}{(s/\omega_n)^2 + (2\zeta/\omega_n)s + 1 + K_A K_X K_L} \cdot \frac{K_q D_m / K_{ce}}{1 + V_0 / 2K_{ce} \beta_e s} \cdot 1/b}{1 + \frac{K_A K_X}{(s/\omega_n)^2 + (2\zeta/\omega_n)s + 1 + K_A K_X K_L} \cdot \frac{K_q D_m / K_{ce}}{1 + V_0 / 2K_{ce} \beta_e s} \cdot 1/b \cdot K_{DA} K_f} \quad (7.14)$$

Let us simplify this equation by defining:

$$\begin{aligned} \tau_m &= V_0 / 2K_{ce} \beta_e \\ K_2 &= K_A K_X \cdot K_q D_m / K_{ce} \cdot 1/b \\ K_3 &= K_2 K_{DA} K_f \end{aligned}$$

$$\text{hence, } \frac{F_o}{F_i} = \frac{K_2}{\left[ \frac{(s/\omega_n)^2 + (2\xi/\omega_n)s + 1 + K_A K_X K_L}{(1 + \tau_m s)} \right] + \frac{K_3}{\left[ \frac{(s/\omega_n)^2 + (2\xi/\omega_n)s + 1 + K_A K_X K_L}{(1 + \tau_m s)} \right]}} \quad (7.15)$$

Further simplifications give:

$$\frac{F_o}{F_i} = \frac{K_2}{\left[ \frac{(s/\omega_n)^2 + (2\xi/\omega_n)s + 1 + K_A K_X K_L}{(1 + \tau_m s)} \right] + K_3} \quad (7.16)$$

If a step function of amplitude  $F_i = A$  is applied to the system, the steady-state value for  $F_o$  is:

$$F_o = \lim_{s \rightarrow 0} \left( s \cdot \frac{F_o(s)}{F_i(s)} \cdot \frac{A}{s} \right) = \frac{A K_2}{1 + K_A K_X K_L + K_3} \quad (7.17)$$

Fig. 7.13 shows the effects of the servovalve LVDT on system performance as predicted by theory. Curve (1) shows the closed-loop amplitude response, obtained from Eq. (7.12), for the overall system without including the servovalve LVDT feedback. Curve (2) shows the theoretical results, obtained from Eq. (7.17), when the servovalve LVDT feedback is added to the system. The values of coefficients used in Eqs. (7.12) and (7.17) are listed in Appendices A and B.

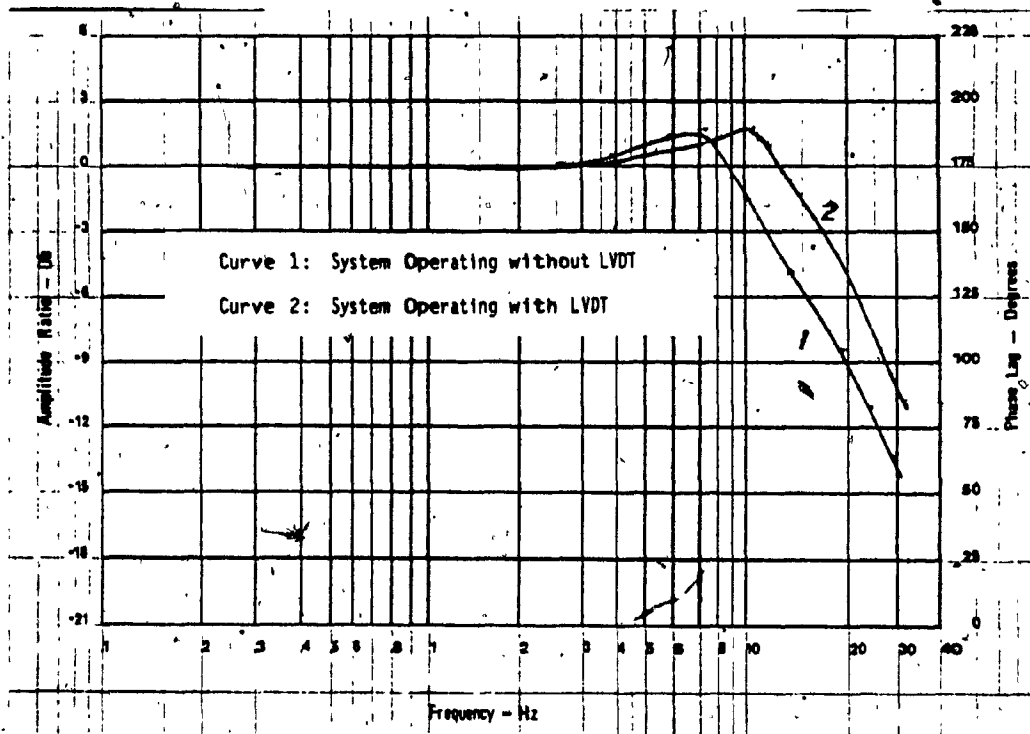


Fig. 7.13 Effects of Servovalve LVDT on the Amplitude Response. Theoretical Results.

Combining Eq. (7.16), Eq. (7.17) and the theoretical results shown in Fig. 7.13, the effects of the LVDT feedback on the system performance can be summarized as follows;

1. Eq. (7.16) shows that the characteristic equation of the closed-loop system is a third-order equation. Thus, the servoactuator remains a third-order system.
2. Eq. (7.17) shows that for the same servocontroller gain the steady-state value of the system gain with the servovalve LVDT is lower than the steady-state value of the system without LVDT. Therefore, in order to have the same overall system gain, the servocontroller gain must be increased when LVDT is used.
3. Fig. 7.13 shows that adding of the LVDT feedback increases the bandwidth of the system. In Fig. 7.14, Curve (1) shows the experimental closed-loop frequency response for the system without the LVDT, and Curve (2) shows the same frequency response when the LVDT was included in the circuit. In the latter case, as predicted by theory, a larger bandwidth was observed (12 Hz, compared with a bandwidth of 8.5 Hz for the system without the LVDT). An improvement in

the phase-lag was also obtained when the LVDT was included in the system.

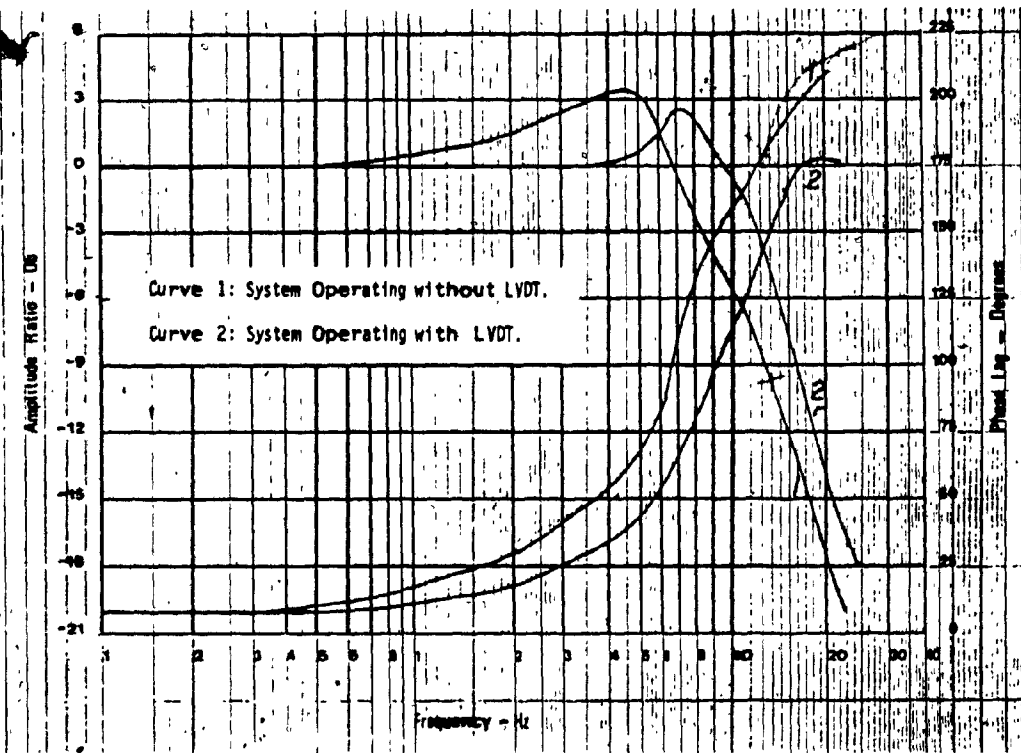


Fig. 7.14 Effects of Servovalve LVDT on the Closed-Loop Frequency Response. Experimental Results.

7.5. Summary and Discussion of Results

A study of a closed-loop force servo system has been presented. In order to carry out such a study, a theoretical analysis was developed and several experimental tests were performed.

The theoretical analysis gave a clear idea of how system performance was affected when the servovalve LVDT was used as second feedback. Another important result obtained from the theoretical analysis was that the whole system with or without the servovalve LVDT behaved as a third-order system.

Several steady-state and dynamic tests were carried out. Fig. 7.3 shows that the hydraulic motor torque and hydraulic motor pressure drop relationship depends on the motor shaft position. Figs. 7.9 and 7.10 show the servovalve dither effects on the system for command signals of  $\pm 7.7$  lbf and  $\pm 3.3$  lbf respectively. An improvement on system performance was observed for small command signals operating at low frequencies, Fig. (7.7).

Fig. 7.14 shows the effects of the servovalve LVDT on the overall system. A significant improvement in the system bandwidth as well as in the phase-lag is observed.

## CHAPTER 8

### CONCLUSION AND RECOMMENDATION FOR FUTURE WORK

Servo valve control of a hydraulic radial ball piston motor was investigated in this thesis. The design of a closed-loop force servo has been carried out including a review of the effect of servo valve external electronic feedback on system performance.

To facilitate this investigation, an experimental test stand was constructed. The experimental test stand used in this research is suitable for general use in evaluating the steady-state and dynamic characteristics of hydraulic motors with the following limitation: the load system used is not suitable to determine motor characteristics at low speeds due to low speed limitations of the loading pump. The evaluation of the motor characteristics in the stalled condition was performed by clamping the motor shaft.

The servo valve controlled hydraulic motor was studied in steady-state and dynamic conditions. For steady-state conditions the system was analyzed for unloaded and loaded motor conditions. The dynamic tests were carried with inertia load.

A digital simulation using the MIMIC language was



performed to assist in the planning of dynamic tests.

The steady-state characteristics with load show that, as expected, speed varies inversely with load. The assymetry with respect to direction of rotation which is apparent under load, would require compensation in critical control applications.

From the steady-state test results, several important conclusions can be drawn. The no load speed/current characteristics are symmetrical, an important quality in a motor to be used for control purposes. In addition, the low starting torque which indicates low static friction is necessary for applications involving high performance force loop configurations. As is the case with most hydraulic motors, the ball piston motor was difficult to control at low velocities. Sporadic pressure pulses were observed in the differential pressure across the motor for speeds below 370 rpm. Above this speed motion was smooth and predictable.

The evaluation of the motor torque characteristics with the motor shaft locked revealed that the pintle valve controlling the fluid to the motor chambers affected the results obtained. Several tests for different positions of motor shaft were carried out and the differences in the

results can be attributed to the pintle-rotor assembly of the motor which forms the valve controlling the fluid to the motor chambers. Step-input and frequency response tests indicated that for an open-loop servo configuration with a velocity command the valve controlled motor system is overdamped. Damping tends to increase with the amplitude of the input, a non-linear effect due to the dissipation of flow energy [1]. By using rigid piping for the hydraulic connections, a higher value for the bulk modulus was obtained and thus, a larger bandwidth of the system was observed. The rather low value of the bulk modulus was attributed to motor leakage.

The evaluation of the external electronic feedback of the servovalve was carried out using the servovalve in a closed-loop force servo. External electronic feedback can be used to compensate for some nonlinearities present in servovalves such as dead zone, torque motor hysteresis, spool stiction, etc. In this research, the external feedback was used with the purpose of improving the performance of the radial ball piston motor. The use of the servovalve external electronic feedback extended the bandwidth of the system. A decrease of the phase-lag was also observed.

Another method used in this project to correct the nonlinearities present in the motor was of using dither

signal. The use of servovalve dither improved the fidelity of the system response significantly for small command signals operating at low frequencies.

Based on the above, the hydraulic ball piston motor investigated in this work can be used in the following applications:

1. System operating at high speeds and low pressures. Because of the high leakage, these units are of low volumetric efficiency; as a result, their operating pressures is also low.
2. System where a minimum friction torque at starting is required. The nonlinear effects observed can be corrected by the use of external devices, such as the LVDT feedback used in this work.

For future investigation in the use of radial ball piston motors, the following suggestions are made:

1. Experimental investigation to determine the motor leakage effects on the apparent system bulk modulus should be performed.

2. A study of the motor speed versus motor leakage relationship should be carried out.
3. Experimental investigation to determine the behaviour of the hydraulic motor at low speeds for a constant loading torque should be performed.

## REFERENCES AND BIBLIOGRAPHY

1. Bell, R., and Cowan, P.:" The Performance of a High Speed Servomotor ", Second Fluid Power Symposium, 4th-7th January, Guildford, England; 1971.
2. Benedict, R.R.:" Electronics for Scientists and Engineers ", 2nd. Ed., Prentice-Hall Inc., Englewood Cliffs, N.J., 1976.
3. Blackburn, John, Reethof, Gerhard, and Shearer, J. Lowen:" Fluid Power Control ", the M.I.T. Press, Massachusetts , 1960.
4. Burrows, C.R., and Martin, D.J.:" The Dynamic Characteristics of an Electro-Hydraulic Servovalve ", Journal of Dynamic Systems, Measurements, and Control, p.395, December 1976.
5. Doebelin, Ernest O.:" Measurement Systems:Application and Design ", McGraw-Hill Book Company, New York, 1977.
6. Doebelin, Ernest O.:" System Dynamics: Modelling and Response ", Charles E. Merrill Publishing Co., Columbus-Ohio, 1972.

7. Doebelin, Ernest O.: " Dynamic Analysis and Feedback Control ", McGraw-Hill Book Company, New York, 1962.
8. Dorf, Richard C.: "Modern Control Systems ", Addison-Wesley Publishing Company, Massachusetts, 1980.
9. Fox, Harry W.: " OP-AMP Applications Handbook ", TAB Books, No. 856, PA., June 1980.
10. Geoffrey, Gordon: " System Simulation ", Prentice-Hall Inc. , Englewood Cliffs, N.J., 1969.
11. Gill, K.F., and Schwarzenbach, J.: " System Modelling and Control ", Edward Arnold (Publisher) Ltd., London, 1978.
12. Glickman, Myron: " Transient Speed Analysis of a Servovalve Controlled Hydraulic Motor ", Proc. Natl. Conf. on Indl. Hydraulics, 16, 174, 1962.
13. Guillon, M.: " Hydraulic Servo Systems: Analysis and Design ", Plenum Publishing Corporation, New York, 1969.

14. Harinck, J.G.:" The Design and Commercialization of Ball Piston Pumps and Motors ", Proceedings of the 27th National Conference on Fluid Power, 1971.
15. Hestad, Erling:" Analysis and Design of Steering Force Control Servo ", ASME Winter Annual Meeting, November 16-20, Los Angeles-California, 1969.
16. Hibi, A., and Ichikawa, T.:" Measurement Method of Starting Torque of Hydraulic Motors ", Hydraulic Pneum. Mech. Power, 21,252,pp. 434-9, December 1975.
17. Hibi, A., and Ichikawa,T.:" Mathematical Model of the Torque Characteristics for Hydraulic Motors ", Bulletin of the JSME, Vol. 20, No. 143, pp. 616-21, May 1971.
18. Hougen, Joel O.:" Measurement and Control Applications for Practicing Engineers ", Cahners Books, Boston-Mass., 1972.
19. Johnson, James E.:" Electrohydraulic Servo System ", Published by the Editors of Hydraulics and Pneumatics Magazine, Cleveland, 1978.

20. Johnson, K.L.:" Testing Method for Hydraulic Pumps and Motors ", Proc. 30th Nat. Conf. on Fluid Power (Philadelphia Civic Center), 28 pp. 331-370, Nov. 12-14 1974.
21. Keller, George R.:" Hydraulic System Analysis ", Published by the Editors of Hydraulics and Pneumatics Magazine, Ohio, 1974.
22. Klein, Edmun A.:" Hydraulic Motors ", Part 1, 2, and 3, Hydraulics and Pneumatics Magazine, Sept., Oct., 1970, July 1971.
23. Klimaszewski, R.A.:" Dynamic Consideration in the Application of Hydraulic Motors ", SAE paper 720768, Sept. 1972.
24. Klimaszewski, R.A.:" and Lonness, Kurt R.:" Discussion of Factors Affecting Dynamic Overspeed of Hydraulic Motors ", Proceedings of National Conference on Fluid Power, Volume 23, 1969.
25. Lewis, Ernest E., and Stern Hansjoerg:" Design of Hydraulic Control System ", McGraw-Hill Book Company Inc., New York, 1962.



26. McCloy, D., and Martin, H.R.:" The Control of Fluid Power ", Longman Group Limited, London, 1973.
27. Merritt, Herbert E.:" Hydraulic Control System ", John Wiley and Sons Inc., New York, 1967.
28. Morse, Allen C.:" Electrohydraulic Servomechanisms ", McGraw-Hill Book Company Inc., New York, 1963.
29. Nfemas, F.J.Jr.:" Understanding Servovalves and Using them Properly ", Part 1, 2, and 3, Hydraulics and Pneumatics Magazine, Oct., Nov., Dec. 1977.
30. Nikiforuk, P.N., Ukrainetz, P.R., and Tsai, S.C.:" Detailed Analysis of a Two-Stage Four-Way Electrohydraulic Flow-Control Valve ", J. Mech. Engng. Sci., Vol 11, No. 2, p. 168, 1969.
31. Nonnenmacher, G.:" Starting Characteristics of Hydraulic Motors ", First European Fluid Power Conference, 10-12 September 1973.
32. Oberg, E., Jones, P.D., and Horton H.L.:" Machinery's Handbook ", Twentieth Edition, First Printing, New York, 1975.

33. Ogata, Katsuhiko: " System Dynamics ", Prentice-Hall Inc., Englewood Cliffs, New Jersey, 1978.
34. Oshima, Yasujiro: " Electro-Hydraulic Components ", Trends in Control Components, M. Nalecz (Editor), North-Holland Publishing Company, 1974.
35. Pegasus Servovalves: " Two-Stages Series: Strong on Performance ", Koehring-Pegasus Division, PSV 279, Troy-Michigan.
36. Pegasus Servovalves: " Two and Three-Stage Series. Internal Operation ", Koehring-Pegasus Division, PSV 076, Troy-Michigan.
37. Planet Hydraulic Motors: " How Planet Hydraulic Motors Work ", Planet Products Corporation, Cincinnati, Ohio.
38. Rothbart, Harold A., Editor in Chief: " Mechanical Design and System Handbook ", McGraw-Hill Book Company, 1964.
39. Schiesser, W.E.: " The Effect of Fluid Mass on Frequency Response ", Control Engineering, February 1966.
40. Shigley, Joseph E.: " Mechanical Engineering Design", McGraw-Hill Kogakusha Ltd., Tokyo, 1972.

41. Shinnars, Stanley M.: "Modern Control System. Theory and Applications ", 2nd. Ed., Addison-Wesley Publishing Company Inc., Reading-Mass., 1978.
42. Shinsky, F.G.: " Process-Control System: Application/ Design/Adjustment ", McGraw-Hill Book Company, Second Edition, New York, 1974.
43. Stern, Hans, and Rauch, W.T.: " Ball Piston Pumps and Motors ", Proceeding of the National Conference on Industrial Hydraulic, Volume 7, pp. 89-99, 1958.
44. Stringer, John: " Hydraulic System Analysis: An Introduction", The McMillan Press Ltd., London, 1976.
45. Thayer, William J.: " Specification Standards for Electrohydraulic Flow Control Servovalves ", Moog Inc. Controls Division, East Aurora, N.Y., Technical Bulletin 117, 1962.
46. Thayer, William J.: " Transfer Function for Moog Servovalves ", Moog Inc. Controls Division, East Aurora, N.Y., Technical Bulletin 103, 1965.
47. Walters, R.: " Hydraulic and Electro-Hydraulic Servo Systems ", Illiffe Books Ltd., London, 1976.

APPENDIX A  
PEGASUS SERVOVALVE

- A1. Servovalve Coefficients
- A2. Servovalve Transfer Function
- A3. Servovalve Assembly Drawing

### A1. Servovalve Coefficients.

In the following, the coefficients for the servovalve which controls the hydraulic motor are calculated.

1. Flow coefficient,  $K_q$ . When the servovalve flow is given in terms of the spool displacement and the pressure drop across the actuator, the following equation is used:

$$Q_v = K_q X_v - K_c P \quad (A1)$$

where  $K_q$  is the flow gain coefficient and  $K_c$  is the flow/pressure coefficient. If the supply pressure remains constant and small variations in the load are observed, then the flow and spool displacement are related directly by the ratio,  $Q_v = K_q X_v$  where,

$$Q_v = C_d \pi D_s X_v \sqrt{P_s - P_L / \rho} \quad (A2)$$

and,  $D_s =$  spool diameter = 0.01267 m

$C_d =$  discharge coefficient = 0.61 [27]

$\rho =$  oil density = 860. Kg/m

The servovalve rated flow @ 1000 psi pressure drop

( $P_L = 0$ ) is 5 gpm or  $3.1583 \times 10^{-4} \text{ m}^3/\text{s}$ . The flow gain coefficient for these conditions is:

$$K_q(\text{rated flow}) = C_d \pi D_s \sqrt{0.6895 \times 10^7 / 860} \text{ m}^3/\text{s/m}$$

$$K_q = 2.174 \text{ m}^3/\text{s/m}$$

2. Maximum spool displacement,  $X_{v\max}$ .

$$X_{v\max} = Q_{\max}/K_q = 3.1583 \times 10^{-4} \text{ (m}^3/\text{s)} / 2.174 \text{ m}^3/\text{s/m}$$

$$X_{v\max} = 1.4528 \times 10^{-4} \text{ m}$$

3. Spool Displacement Gain,  $K_x$ , is defined as the slope of servovalve spool position/servovalve current plot.

$$K_x = X_v/I = 1.4528 \times 10^{-4} \text{ m}/100 \text{ mA}$$

$$K_x = 1.4528 \times 10^{-6} \text{ m}/\text{mA}$$

4. Pressure gain coefficient,  $K_p$ , is defined as the slope of the pressure gain curve. The curve for the valve employed in this project is shown in Fig. 2.21.

$$K_p = 0.8136 \times 10^6 \text{ N/m}^2/\text{mA} \text{ (118 psi/mA)}$$

5. Pressure/spool displacement coefficient,  $K_{px}$ .

$$K_{px} = K_p/K_x = 0.8136 \times 10^6 \text{ (N/m}^2\text{/mA)} / 1.4528 \times 10^{-6} \text{ m/mA}$$

$$K_{px} = 5.6002 \times 10^{11} \text{ N/m}^2\text{/m}$$

6. Flow/pressure coefficient,  $K_c$ .

$$K_c = K_q/K_{px} = 2.174 \text{ (m}^3\text{/s/m)} / 5.602 \times 10^{11} \text{ (N/m}^2\text{/m)}$$

$$K_c = 4.746 \times 10^{-12} \text{ m}^3\text{/s/N/m}^2.$$

In summary, the servovalve coefficients are:

$$K_v = \pi D_s = 0.03988 \text{ m}$$

$$K_q = 2.174 \text{ m}^3\text{/s/m}$$

$$x_{vmax} = 1.4528 \times 10^{-4} \text{ m}$$

$$K_x = 1.4528 \times 10^{-6} \text{ m/mA}$$

$$K_p = 0.8136 \times 10^6 \text{ N/m}^2\text{/mA}$$

$$K_{px} = 5.6002 \times 10^{11} \text{ N/m}^2\text{/m}$$

$$K_c = 4.746 \times 10^{-12} \text{ m}^3\text{/s/N/m}^2.$$

Rated Flow = 5 gpm @  $0.6895 \times 10^7$  N/m<sup>2</sup> (1000 psi)

Rated Current = 100 mA

## A2. Servovalve Transfer Function.

As was stated in Chapter 2, Section 2.3; two models for the servovalve transfer function were assumed. In the following, the way in which the two models were obtained is explained.

### 1. First Order Transfer Function.

A first order transfer function for the servovalve can be described by the following equation:

$$E(s) = Qv/K_0 I = 1/1 + \tau vs \quad (A3)$$

Since the actual frequency response for the servovalve is supplied by the valve manufacturer, the coefficients of the approximate transfer function can be determined by fitting the above equation to the known frequency response curve.

If a sinusoidally varying input current is applied to the servovalve, the amplitude ratio can be expressed as  $G(j\omega)$ . In this case the operator (s) is replaced by the



complex operator ( $j\omega$ ) which is the frequency of the sinusoidally varying input current.

The numerical value of the amplitude ratio or frequency response for any frequency is found by taking the absolute value of the complex function  $G(j\omega)$ .

In order to simplify further calculations, the square of the amplitude ratio shall be written:

$$|G(j\omega)|^2 = [1 + (\tau_v\omega)^2]^{-1} = F(\omega)^{-1} \quad (A4)$$

The actual values of  $F(\omega)$  are known for any frequency from the frequency response plot and therefore the numerical value of  $\tau_v$  can be obtained by fitting the above equation to the curve of the actual value of  $F(\omega)$  versus ( $\omega$ ). Thus, the coefficient  $\tau_v$  is found as follows :

$$|G(j\omega)|^2 = (1 + \omega^2\tau_v^2)^{-1}$$

or 
$$\tau_v^2 = [1 - |G(j\omega)|^2] / |G(j\omega)|^2\omega^2 \quad (A5)$$

For a - .3 db value, the frequency of the actual servovalve transfer function is equal to 60 Hz or 377 rad/s. But, - 3 db corresponds to an amplitude ratio equal to

0.707, thus:

$$\tau_v^2 = (1 - 0.501) / (0.501)(377)^2 = 7.00 \times 10^{-8} \text{ s}$$

$$\text{or } \tau_v = 2.64 \times 10^{-3} \text{ s}$$

Now, the servovalve transfer function can be expressed as:

$$G(s) = 1 / [1 + (2.64 \times 10^{-3})s] \quad (\text{A6})$$

The phase-lag was determined by using Eq.(A7) :

$$\phi = - \text{tg}^{-1} (\omega \tau_v) \quad (\text{A7})$$

A plot of the actual frequency response from manufacturer's data and frequency response based on Eqs. (A6) and (A7) is shown in Fig. A1(a).

## 2. Second-Order Transfer Function.

A similar procedure was followed to determine an approximated second-order transfer function of the servovalve.

Assume the transfer function has the form:

$$G(s) = 1 / \left[ (s/\omega_n)^2 + (2\xi/\omega_n)s + 1 \right]$$

Replacing  $s$  by  $j\omega$ :

$$G(j\omega) = 1 / \left[ (j\omega/\omega_n)^2 + (2\xi/\omega_n) + 1 \right]$$

$$|G(j\omega)| = 1 / \sqrt{\left[ 1 - (\omega/\omega_n)^2 \right]^2 + (2\xi/\omega_n)^2} = F(\omega) \quad (A8)$$

The actual values of  $F(\omega)$  are known for any frequency from the frequency response plot. Assuming numerical values for  $\xi$  and  $\omega_n$ , the curve given by Eq. (A8) is fitted by iteration to the curve of the actual value of  $F(\omega)$  vs  $\omega$ . Thus, The coefficients  $\xi$  and  $\omega_n$  are:

$$\xi = 0.8$$

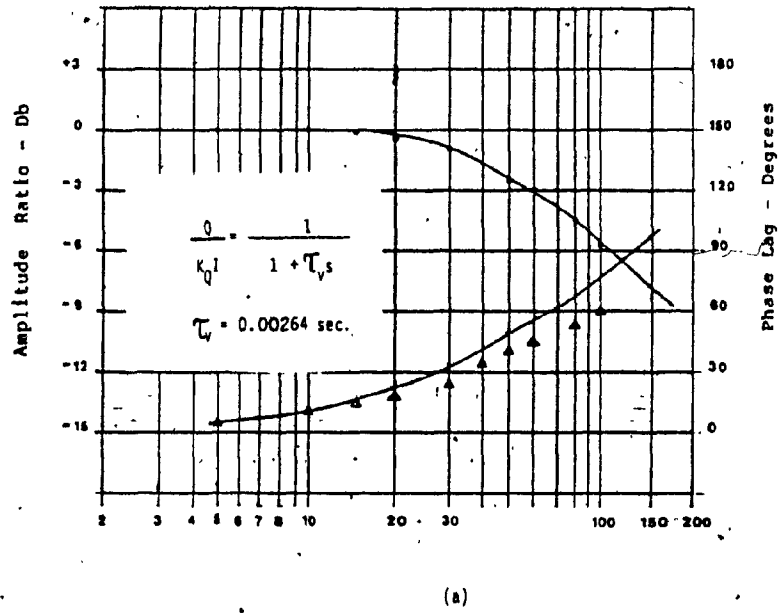
$\omega_n = 90$  Hz (565 rad/sec) and the second-order transfer function is represented by:

$$G(s) = 1 / \left[ (s/565)^2 + (2/565)s + 1 \right]$$

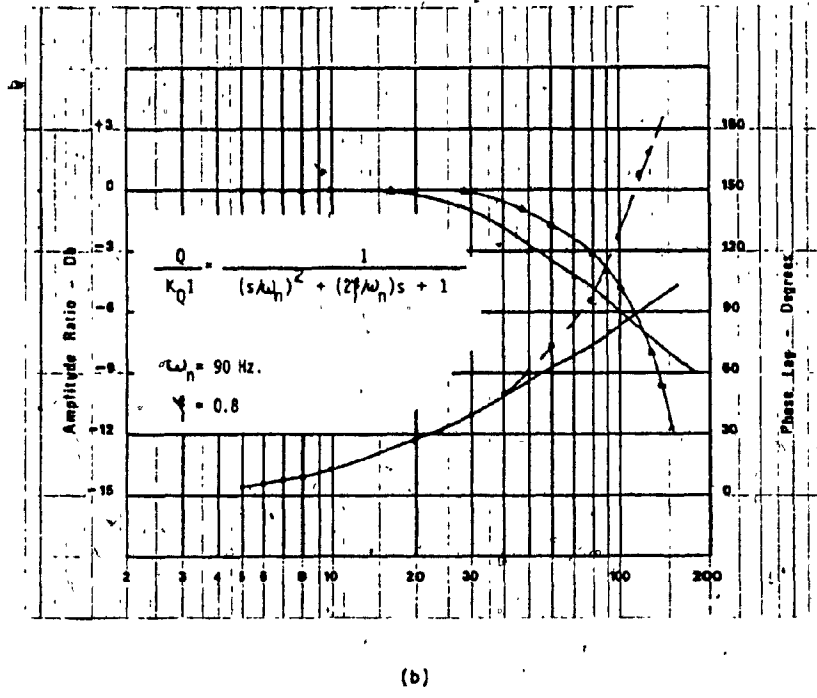
Fig. A1(b) shows a plot of the actual and approximated transfer function of the servovalve.

A3. Servovalve Assembly Drawing.

Fig. A2 shows a complete assembly drawing of the servovalve and servovalve Linear Variable Differential Transformer.



- Actual curves from manufacturer's data
- Amplitude Ratio computed points
- ▲ Phase Lag computed points.



- Actual curves from manufacturer's data
- ▲ Amplitude Ratio computed points
- Phase Lag computed points.

Fig. A1. Servovalve Frequency Response with First and Second-Order Transfer Function Fits. (a) First-Order Fit (b) Second-Order Fit.

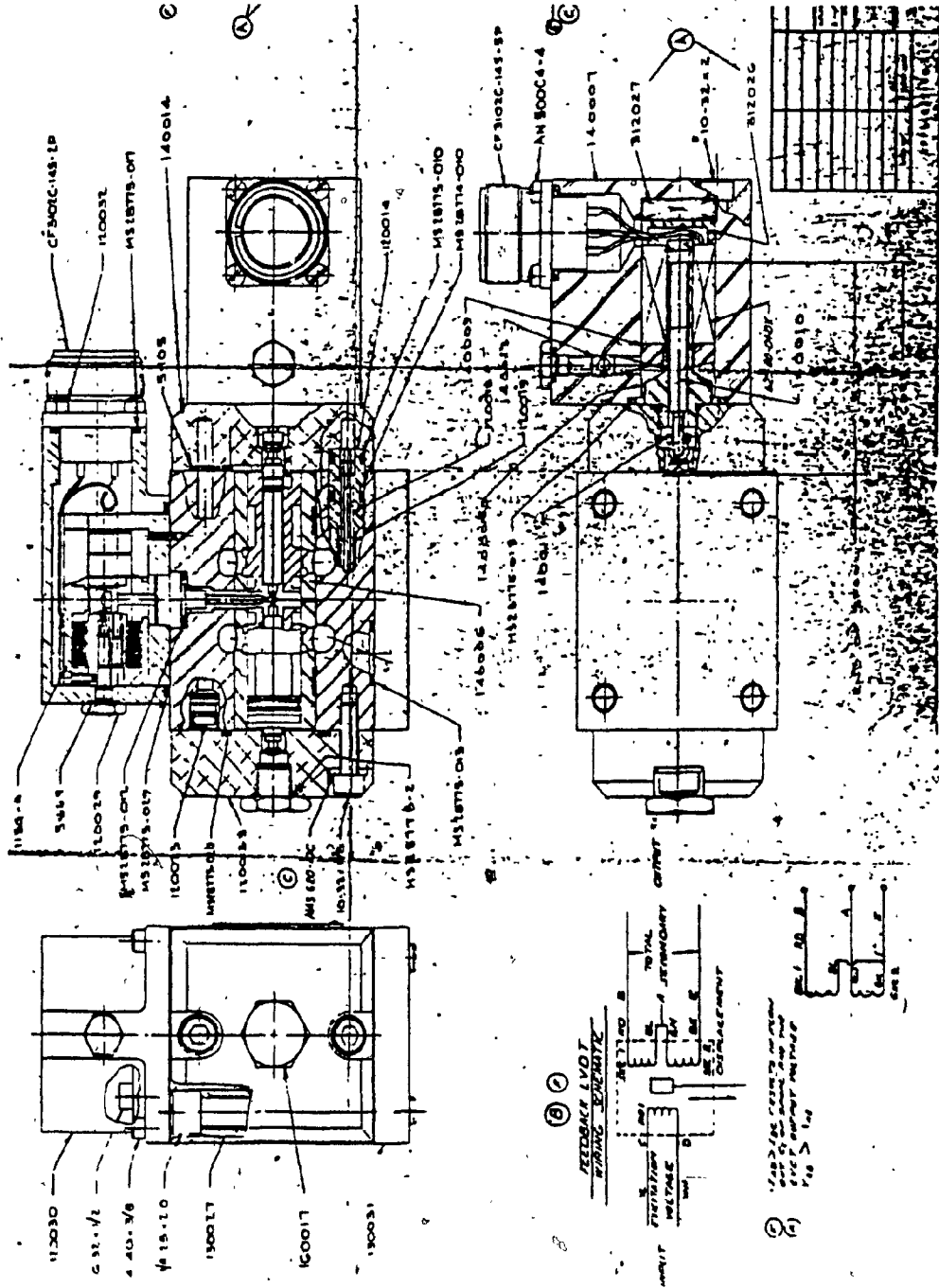


Fig. A2. Servovalve Assembly Drawing.

APPENDIX B

MIMIC MODEL OF THE OPEN-LOOP

SERVOVALVE CONTROLLED MOTOR

In the following, the MIMIC listing of the digital simulation is presented. The listing also includes the constants and parameters used as well as the results obtained. The latter are presented in the following order:

Fig. B1. Motor speed transient response for a current step function of 18 mA and inertial mass of 0.003 N-m-s .

Fig. B2. Pressure transient of the motor chamber for current step function of 18 mA and inertial mass of 0.003 N-m-s .

Fig. B3. Motor speed transient response for a current step function of 24 mA and inertial mass of 0.003 N-m-s .

Fig. B4. Pressure transient of the motor chambers for a step function of 24 mA and inertial mass of 0.003 N-m-s .

Fig. B5. Motor speed transient response for a current step function of 24 mA and inertial mass of 0.03247 N-m-s .

Fig. B6. Pressure transient of the motor chambers for a current step function of 24 mA and inertial mass of 0.03247 N-m-s .



MIMIC PROGRAM FOR AN OPEN LOOP VELOCITY SERVO SYSTEM

CONSTANTS AND PARAMETER GIVEN

```

1      CON(PI,KX,TAUV,XV0,KV,CD)
2      CON(ROW,PS,P0,BETA,V1,P10)
3      CON(V2,P20,DM,XVMIN,XVMAX)
4      CON(CTF,CL,OMEGA0,BM)
5      PAR(JL,IRL)

```

REFERENCE SIGNAL

```

6      IRT (IRL*100.)*T
7      IR  LIM(IRT,0.,IRL)

```

SERVOVALVE EQUATIONS

\* THIS SEQUENCE OF INSTRUCTIONS MODEL THE SERVOVALVE.  
 \* A FIRST ORDER RELATIONSHIP IS ASSUMED BETWEEN SPOOL  
 \* POSITION AND INPUT CURRENT, THE FLOW IS A FUNCTION  
 \* OF THE SQUARE ROOT OF THE PRESSURE DROP.  
 \*

```

8      XV (KX/TAUV)*INT(IR-IF,XV0)
9      IF  XV/KX
10     XVPOS FSW(XV0+XV,TRUE,TRUE,FALSE)
11     XVPOS1 NOT(XVPOS)
12     XVPOS QA 0.
13     XVPOS QD 0.
14     XVPOS1 QA CD*KV*(XV+XV0)*SQR((2./ROW)*(PS-P1))
15     XVPOS1 QD CD*KV*(XV+XV0)*SQR((2./ROW)*(P2-P0))
16     XVNEG FSW(XV0-XV,TRUE,TRUE,FALSE)
17     XVNEG1 NOT(XVNEG)
18     XVNEG QB 0.
19     XVNEG QC 0.
20     XVNEG1 QB CD*KV*(XV0-XV)*SQR((2./ROW)*(PS-P2))
21     XVNEG1 QC CD*KV*(XV0-XV)*SQR((2./ROW)*(P2-P0))
22     Q1 QA-QC
23     Q2 QD-QB

```

ACTUATOR CONDUITS

\* A DYNAMIC MODEL OF THE CONDUITS IS INCLUDED, THIS ELIMINATES  
 \* THE IMPLICIT RELATIONSHIP BETWEEN FLOW AND PRESSURE THAT  
 \* WOULD RESULT IF THE EFFECTIVE BULK MODULUS WAS NOT INCLUDED.  
 \*

```

24     P1T INT((BETA/V1)*(Q1-QM),P10)
25     P1  LIM(P1T,0.,PS)
26     P2T INT((BETA/V2)*(-Q2+QM),P20)
27     P2  LIM(P2T,0.,PS)

```

HYDRAULIC MOTOR

```

*
*
*
*
*
28      TM      DM*(P1-P2)-CTF*(P1-P2)
29      OM      DM*OMEGA+CL*(P1-P2)
*
*
*
30      OMEGA   (1./JL)*INT(TM-BM*OMEGA+OMEGA0)
*
*
*
31      DTMIN   0.005
32      DTMAX   0.005
33      DT       0.05
34      FIN(T,1.95)

```

\$DELETE

```

*
*
*
35      PLOT    RESULTS
36      PLO(T,OMEGA)
37      PLO(T,P1,P2)
      END

```

PI	KX	TAUV	XV0	KV	CD
.31416E+00	.14528E-05	.26400E-02	.72640E-06	.39880E-01	.61000E+00
ROM	PS	P0	BETA	V1	P10
.86000E+03	.10350E+08	0.	.51708E+09	.14749E-03	.51708E+07
V2	P20	DM	XVMIN	XVMAX	
.14749E-03	.51708E+07	.12260E-05	-.14528E-03	.14528E-03	
CTF	CL	OMEGA0	BM		
.53750E-06	.59384E-11	0.	.12000E-01		

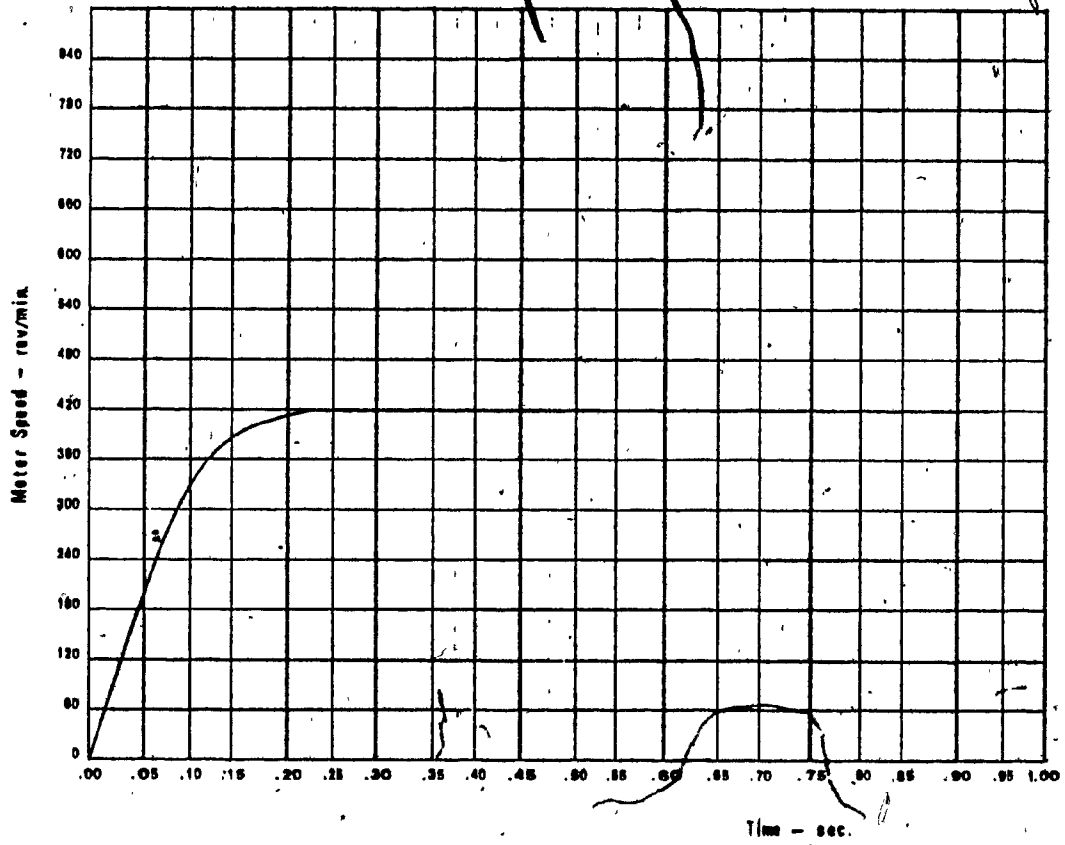


Fig. B1 .

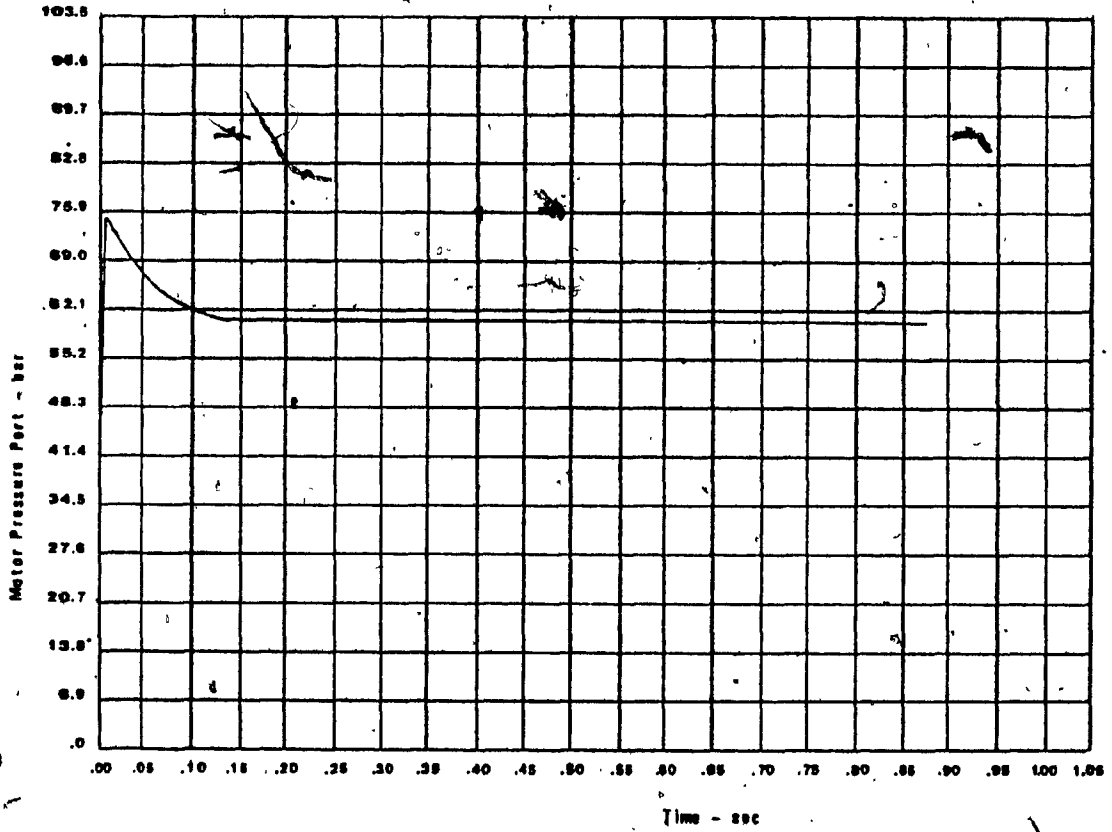


Fig. B2 .

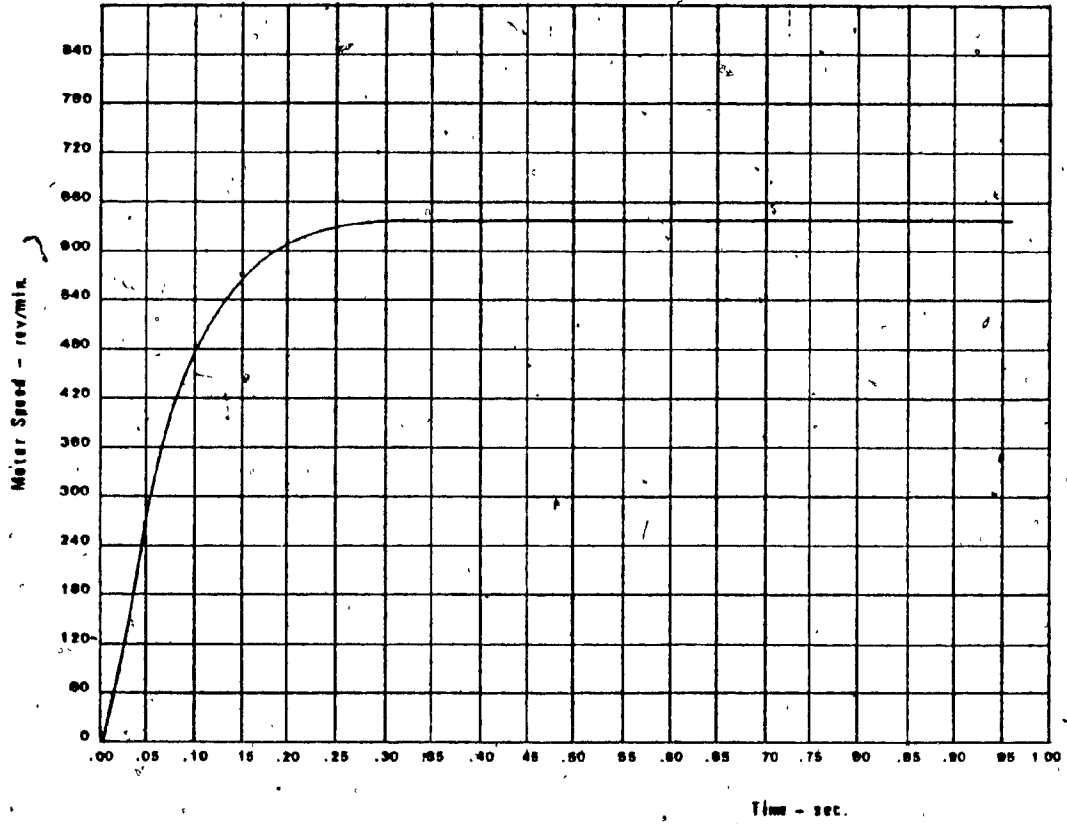


Fig. B3

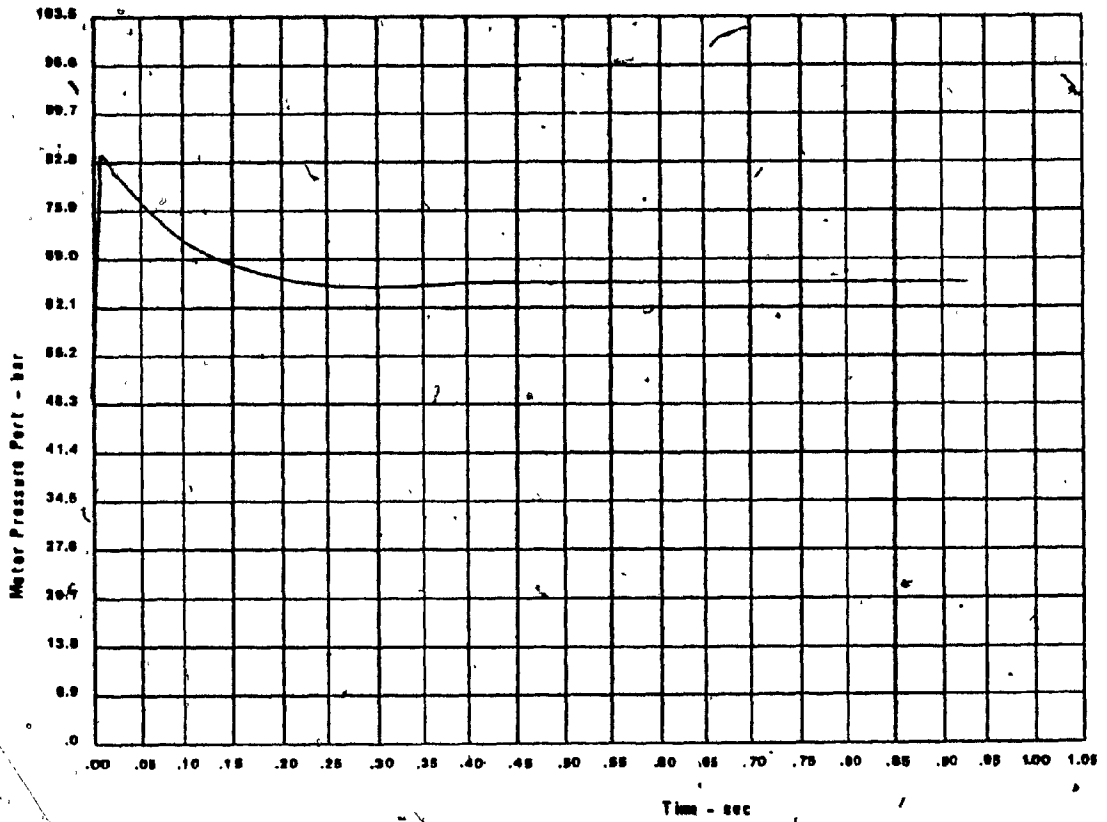


Fig. B4 .

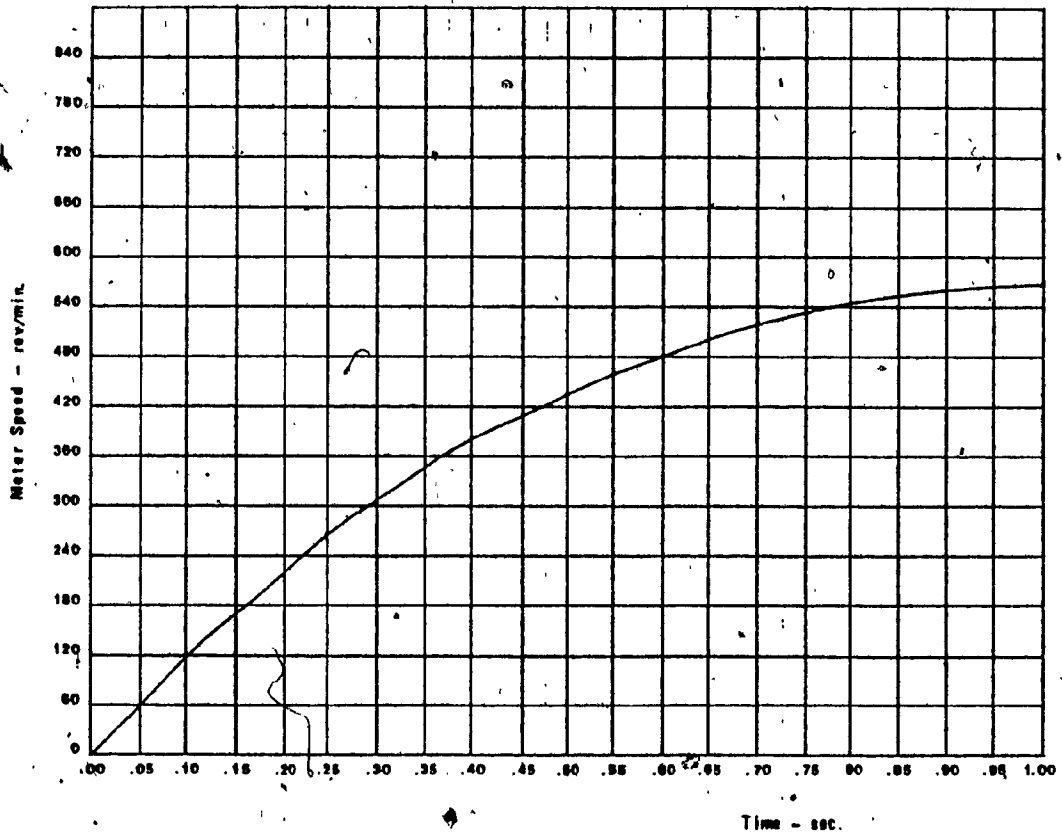


Fig. B5 .

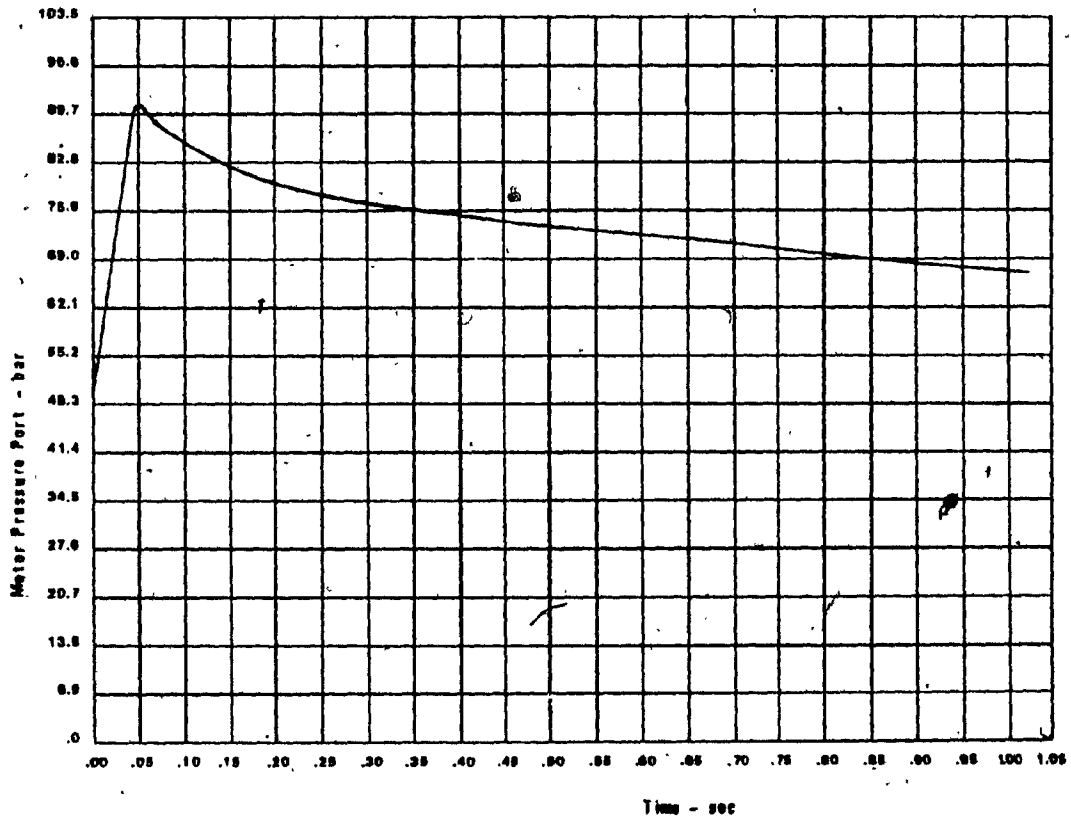


Fig. B6.



**APPENDIX C**

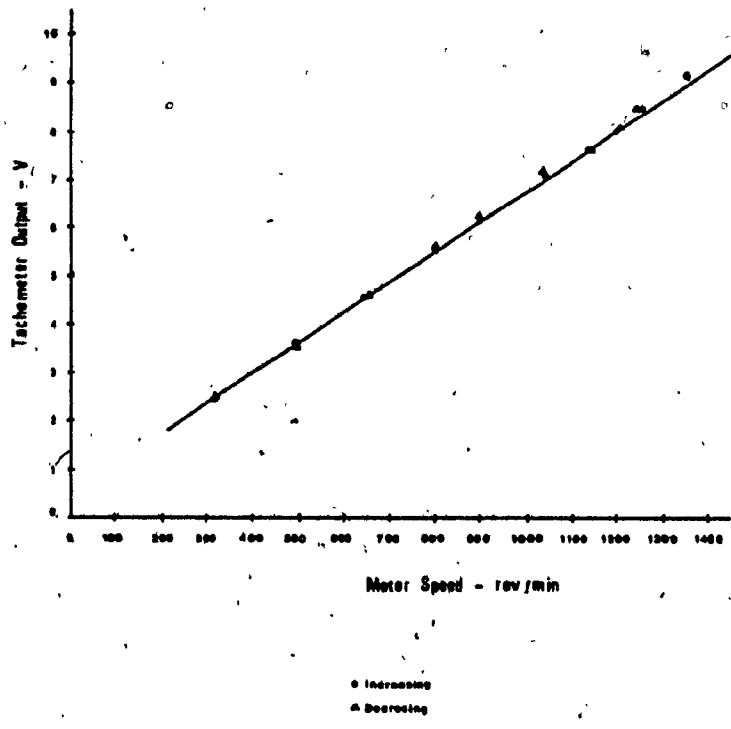
**AUXILIARY EQUIPMENT DESCRIPTION AND CALIBRATIONS**

Gear System. Two gears were used in order to obtain motor speed measurements. A gear was attached to the main shaft, while the another was connected to the tachometer shaft(see details in Figs. 3.1 and 3.2).- Both of them are manufactured by PIC, a Benrus Division, and the specifications are:

Gear Model	: 657-96
No. Teeth	: 96
Diametral Pitch	: 4.00 in.
Outside Diameter	: 4.083 in.
Pressure Angle	: 20

Tachometer. A DC tachometer was used as velocity transducer, with a ratio of 7 V/1000 rpm .The tachometer was manufactured by Servo TEK Products CO:(N.J.)

A calibration curve for the tachometer was obtained by using a stroboscope. Once the tachometer shaft through the gears was connected to the main shaft of the system, fluid was fed to the hydraulic motor .The motor shaft velocity was varied by the servovalve. Thus, for different motor shaft velocities, the curve shown in Fig. C1 resulted. From the curve ,a tachometer sensitivity of 6.7 V/1000 rpm was obtained.



Tachometer Sensitivity : 8.7 V/1000 rpm

Fig. C1. Tachometer Calibration Curve .

2

Pressure Transducer. A differential pressure transducer was used to obtain pressure measurements across the motor ports. The transducer, Model DP15T, was manufactured by Validyne Engineering Corporation. The DP15T pressure transducer is designed for low and medium pressure measurements of laboratory accuracy. In typical AC excited bridge circuits, the system delivers a full scale output of 35 mV per volt at 3000 Hz.

The pressure sensing element, Fig. C2, is a flat diaphragm of magnetic stainless, campled between case halves of the same material, in a symmetrical assembly. Pick off coils, embedded in the case halves, sense the diaphragm deflection. The embedded coils are covered with a non-magnetic stainless- layer, so that the presure cavity presents a completely stainless exposure to the working fluid. Vent valves facilitate complete liquid filling for dynamic measurements.

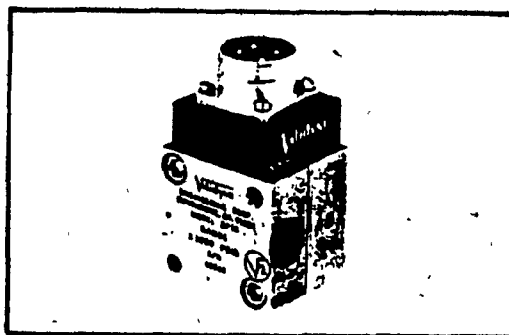


Fig. C2. Differential Pressure Transducer.

The transducer specifications are:

Range	:	3000 psid
Linearity	:	1/2 % F.S. best straight line
Hysteresis	:	1/2 % pressure excursion
Output	:	35 mV/V full scale nominal
Inductance	:	20 mh nominal, each coil.
Zero Balance	:	within 5 mV/V
Excitation	:	rated: 5 Vrms, 3 KHz to 5 KHz

Pressure Transducer Indicator. It is used to provide an accurate visual indication of the measured variable as well as providing an analog output. Excitation of 5 KHz sine waves is applied to the two inductance ratio arms of the transducer and the resulting output is amplified and demodulated using integrated circuit techniques. The DC output is obtained from an active filter circuit and gives a uniform response from steady-state to 1000 Hz. The Pressure transducer indicator used is also manufactured by Valydine Engineering Corporation, model C212. Fig. C3 shows a picture of the indicator, and its specifications are:

Power Requirements : 95-125 VAC 50 to 400 Hz  
at 5 watts.  
Output : 10 VDC  
Output Impedance : 10 ohms nominal  
Frequency Response : Selectable, 0-10, 0-50, 0-200,  
0-1000 Hz flat 10 %  
Ripple : less than 10 mV peak to peak  
Sensitivity : 15 mV/V transducer output  
minimum for full scale



Fig. C3. Pressure Transducer Indicator.

A calibration curve for the pressure transducer-transducer indicator combination was obtained using a dead-weight tester. The calibration curve was obtained as follows: the pressure line from the dead-weight tester was connected to the positive port of the pressure transducer, leaving the negative port open to the atmosphere. Then, various pressure levels were applied to

the transducer, and the output voltages from the transducer indicator were recorded. Negative readings were obtained by a similar procedure, but with the dead-weight tester pressure line connected to the negative port of the pressure transducer. The calibration curve is shown in Fig. C4.

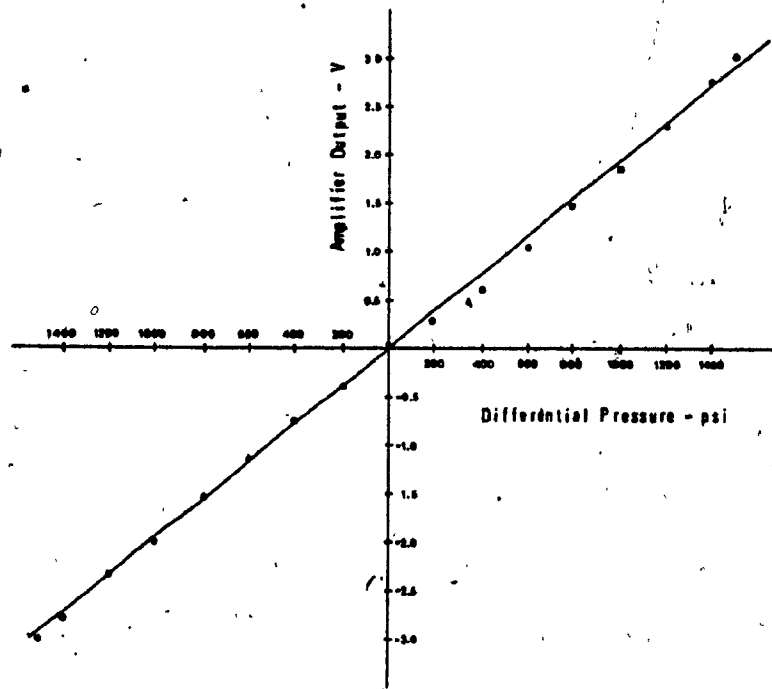


Fig. C4. Differential Pressure Transducer Calibration Curve.

Force Transducer. A strain gage load cell was used in this experiment as a force measuring device. A strain gage based transducer is a unit converting weight or force into an electrical output by virtue of the internal strain gage installation. The electrical output is then connected to bridge amplification instruments for indication.

Fig. C5 shows a picture of the load cell and its electrical diagram. This type of load cell is capable of both steady-state and dynamic load measurements.

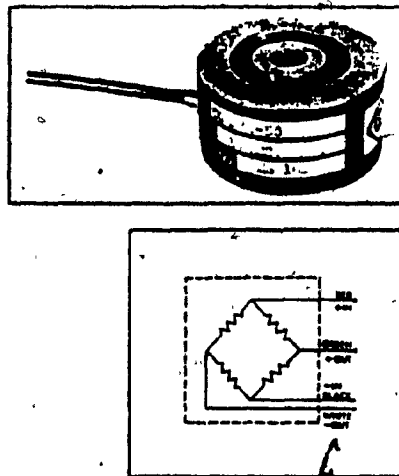


Fig. C5. Force Cell and its Electrical Diagram.



The force transducer used in this work is manufactured by Kulite Semiconductor Inc. model TC-2000 and the specifications are:

Range	: 100 lbs
Diaphragm Thickness	: 0.029 in
Nominal Deflection	: 0.0007 in
Natural Frequency	: 5.4 KHz
Overload	: 150 % of Rated Capacity
Operational Mode	: Tension and Compression
Rated Electrical Exc.	: 10 VDC/AC (rms)
Maximum Electrical Exc.	: 15 VDC/AC (rms)
Input Resistance	: 3000 ohms
Full Scale Output	: 75 mV (nom)
Output Resistance	: 1000 ohms
Non-Linearity	: 0.5 % FSO
Hysteresis	: 0.1 % FSO
Repeatability	: 0.1 % FSO
Resolution	: Infinite

Fig. C6 shows the load cell calibration curve which was obtained as follows: several steel discs weighed previously were used to load the force cell. A DC power supply was used to supply 10 volts to the four-arm wheatstone semiconductor bridge, integrally compensated for

thermal changes. Then, the load cell was loaded in a compression mode by the discs and the electrical output was recorded. Finally, the force cell was loaded in a tension mode recording the electrical output. Thus, the calibration curve shown in Fig. C6 resulted

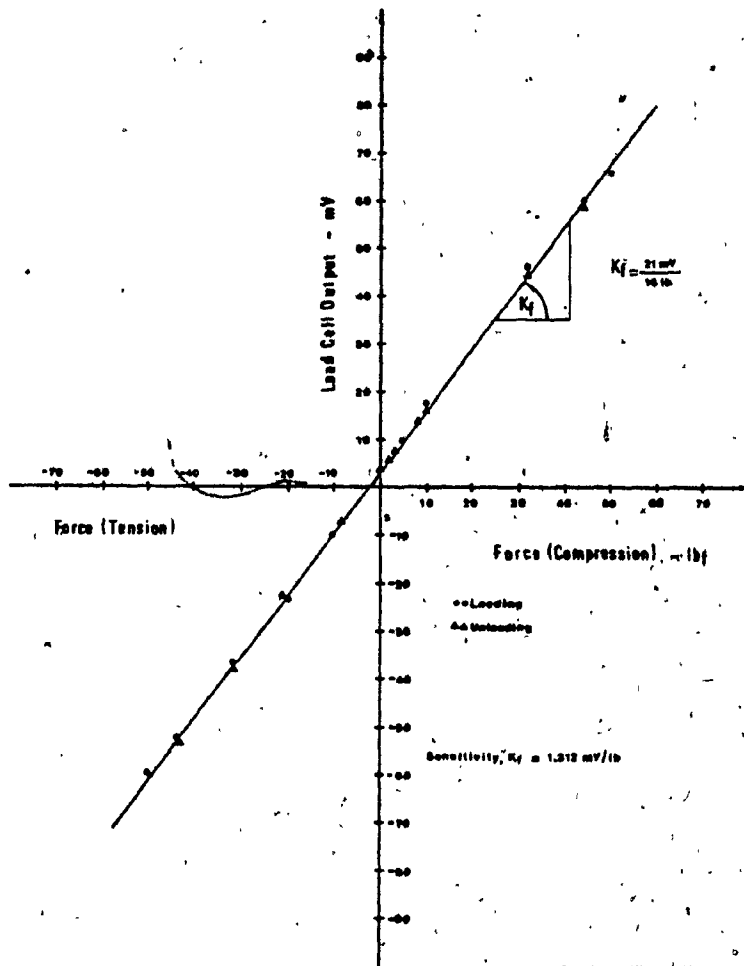


Fig. C6. Force Cell Calibration Curve.

